



ALMA MATER STUDIORUM
UNIVERSITÀ DI BOLOGNA

SCUOLA DI INGEGNERIA E ARCHITETTURA

**CORSO DI LAUREA MAGISTRALE IN
INGEGNERIA PER L'AMBIENTE E IL TERRITORIO**

WAVE CLIMATE IN THE SOUTHERN COAST OF MADEIRA ISLAND

Tesi di laurea magistrale in Idraulica Marittima

Relatore

Prof. Barbara Zanuttigh

Presentata da

Jacopo Venturi

Correlatore

Prof. Antonio Trigo-Teixeira

Prof. Diogo Mendes

Sessione III Febbraio 2024

Anno Accademico 2022/2023

INDEX

1	INTRODUCTION	4
1.1	ABOUT WAVE PROPAGATION FROM DEEP WATER TO SHALLOW WATER ON ISLANDS	4
1.2	AIMS	5
1.3	OUTLINE OF THE THESIS	5
2	HINDCAST DATA	5
2.1	INTRODUCTION	6
2.2	METOCEANVIEW DATASET	7
2.2.1	POINT NW	9
	Hs analysis	10
	Tp analysis	12
	Summer versus winter	14
2.3	COMPARISONS	18
2.3.1	NORTH WEST VERSUS SOUTH WEST	18
2.3.2	NORTH VERSUS SOUTH	19
2.3.3	NORTH VERSUS NORTH EAST	21
2.3.4	SOUTH WEST VERSUS SOUTH	24
2.4	SUMMARY	26
3	DEFINITION OF THE OFFSHORE BOUNDARY CONDITIONS	26
3.1	INTRODUCTION	27
3.2	NORTH WEST POINT	28
3.2.1	JOINT EMPIRICAL DISTRIBUTION OF Hs AND Tp	28
3.2.2	MONTHLY VARIATION ANALYSIS	34
3.2.3	EXTREME VALUES ANALYSIS	35
3.3	SUMMARY	44
4	SIMULATIONS	45
4.1	INTRODUCTION	45
4.2	SOFTWARE: STWAVE ON SMS	45
4.2.1	MODEL ASSUMPTIONS	46
4.2.2	EQUATIONS	46
4.3	BOUNDARY CONDITIONS	48
4.3.1	CHOICE OF HS	49

4.3.2	CHOICE OF TP.....	53
4.3.3	CHOICE OF DIR	54
4.4	BATHYMETRY	54
4.5	GRID RESOLUTION	57
4.6	RESULTS.....	59
4.6.1	SIMULATION WITH WAVES COMING FROM WEST	61
	Simulations 1 and 2	61
	Simulation 3.....	67
4.6.2	SIMULATION WITH WAVES COMING FROM SOUTH.....	71
	Simulation 6.....	71
	Simulation 7.....	74
	Simulation 8.....	76
4.6.3	COMPARISON: SIMULATION 4 VS SIMULATION 9	78
4.6.4	SIMULATION WITH WAVES COMING FROM NORTH: SIMULATION 5.....	83
4.7	TIDE.....	85
4.8	SUMMARY	87
5	COMPARISON BETWEEN DIFFERENT BATHYMETRIES.....	87
5.1	INTRODUCTION.....	87
5.2	BATHYMETRY WEB.....	88
5.2.1	BATHYMETRY MAP versus BATHYMETRY WEB	89
5.2.2	SIMULATION 4(Hs= 12 m, Tp= 20 s, Dir= 270°N).....	97
5.2.3	SIMULATION 9 (Hs= 8 m, Tp= 17 s, Dir= 202.5°N), waves from SSW.....	102
5.3	BATHYMETRY SURVEY SCATTERSET.....	106
5.3.1	BATHYMETRY SURVEY SCATTERSET versus BATHYMETRY MAP	106
5.3.2	SIMULATION 4 (Hs= 12 m, Tp= 20 s, Dir= 270°N) waves from W	112
5.3.3	SIMULATION 9 (Hs= 8 m, Tp= 17 s, Dir= 202,5°N).....	116
5.4	SUMMARY	120
6	CONCLUSIONS	120
7	LIST OF FIGURES	121
8	LIST OF TABLES	125
9	BIBLIOGRAPHY	126

1 INTRODUCTION

1.1 ABOUT WAVE PROPAGATION FROM DEEP WATER TO SHALLOW WATER ON ISLANDS

The study of wave climate plays a fundamental role in the design of engineering structures and projects aimed, among other things, at coastal protection from the energy and power of the sea.

In the development of these projects, reference must be made to a design wave with a certain return period. Therefore, a statistical study of offshore wave climate conditions is necessary, followed by a study of how these offshore waves propagate from deep water to shallow water and then break on the coast.

The study of offshore wave conditions is typically conducted through statistical analysis of available data. Hindcast data are usually used, particularly those related to significant wave height, peak period, and wave direction offshore. These data can often be found on the web, provided by various organizations responsible for collecting and organizing this information.

Once the offshore wave climate conditions are defined, the focus shifts to how the conditions in the area being analyzed allow the waves to propagate towards the coast. On the ocean surface, waves can travel long distances without significant changes in their conditions. Wave transformation begins when certain bottom conditions are reached, i.e. when the water depth becomes less than half the wavelength of the wave itself.

The factor that most influences the propagation of waves from deep to shallow water is therefore the bathymetry. Clearly, each type of coastline presents different characteristics in terms of bathymetry. Islands, in particular, often have a narrow irregular continental platform, which means that waves can propagate from deep to shallow water with minimal changes until they approach the coast. Additionally, the shape of the island creates the so-called shadow effect, preventing waves from certain directions from reaching certain portions of the coast.

The same offshore wave climate conditions can thus translate into a distribution of wave conditions that vary along the island's coast, even in very close positions. Therefore, a particularly careful analysis of the bottom depth is necessary, as any inaccurate or imprecise assessments in this regard can lead to significant errors in wave propagation and, consequently, incorrect evaluations in coastal protection studies or projects.

Clearly, the accuracy of the results in a study like the one presented here also relies on the reliability of the data used as input. Especially when dealing with small islands like Madeira, it is possible that the available Hindcast data have been developed using models that cannot take into account the influence of the island itself, which can, in turn, lead to errors in conducting studies of this kind.

1.2 AIMS

The area of interest for this thesis is the island of Madeira, specifically the southwest coast. The main purpose of this work is to provide a significant contribution to the understanding of the wave climate of this island. The focus will primarily be on three key aspects:

- Definition of offshore wave conditions around the island.

Using Hindcast data related to significant wave height, peak period, and wave direction available at five points offshore the coast of Madeira, the wave climate conditions have been defined at multiple locations offshore the island. This includes both average and extreme values, with an assessment of how seasonality can influence these conditions.

- Propagation of wave conditions from deep to shallow waters on the southwest coast

Through the use of specialized software, the study of wave climate conditions has been employed to evaluate how different offshore conditions can propagate towards the coast. This allows an observation of how these conditions may propagate differently depending on the underwater depth profile.

- Assessment of the influence of bathymetry accuracy on wave propagation

A comparison was made regarding how the results of wave propagation from deep to shallow waters could vary based on the accuracy of the bathymetry data used in the software. Three different sources of bathymetric data were selected to input into the software, and the differences in terms of final results were showed.

1.3 OUTLINE OF THE THESIS

This thesis comprises 6 chapters: following this introduction (Chapter 1), Chapter 2 presents the Hindcast data related to the five offshore points of Madeira Island, highlighting similarities and differences among the various points. Subsequently, in Chapter 3, a study is conducted regarding the persistent relationship between the three parameters of Hindcast data, namely significant wave height, peak period, and wave direction, followed by an analysis of extreme values.

Chapter 4 then introduces the nine simulations carried out, explaining the choices of boundary conditions and presenting the results of each, emphasizing both similarities and differences among them. Chapter 5 focuses on the study of the influence of bathymetry on the results. Three types of bathymetry are presented, demonstrating how the simulation results can vary depending on the chosen bathymetry.

Chapter 6 is then dedicated to the conclusions.

2 HINDCAST DATA

Study of the deep-water wave climate based on hindcast data.

2.1 INTRODUCTION

The second chapter of this thesis focuses on gathering and analysing the necessary data to characterize the wave climate in the deep waters of Madeira island, with the aim of studying how the island interacts with the wave propagation in that area of the Atlantic Ocean. It is expected that, in the absence of islands, the wave characteristics do not vary too much from one point to another in the hindcast grid close to the island. The Hindcast wave data will be used as the offshore boundary conditions to study wave propagation in the presence of Madeira Island.

The required data for this study include hindcast data for significant wave height (referred to as H_s), peak period (referred to as T_p), and mean wave direction (referred to as Dir). The hindcast data were provided by the website Metoceanview (MetOceanView).

Metoceanview Hindcast data is available worldwide with a certain distance between the grid points, covering a vast range of locations beyond the European coast.

It is immediately necessary to make a clarification regarding the use of Hindcast data as a tool to assess the wave climate in the deep water of an area like that of interest in this study. Remembering that hindcast data do not derive from direct measurements in the field but from the application of numerical models by those involved in managing these data, in a portion characterized by the presence of an island of small size like Madeira could lead to some errors in evaluating similarities and differences between the points analyzed and therefore between the wave climate.

Taking for example the study "estudo do clima de agitacao maritima ao longo da costa sudoeste da Madeira" carried out by WL | delft hydraulics, a study with objectives similar to those of this thesis had been specified how the Hindcast data that had been provided, studied and then analyzed, could lead to incorrect evaluations because the accuracy of the model used in the development of the Hindcast data themselves, was not able to take into account the influence of the island of Madeira itself (delf hydraulics, 2007).

The study just mentioned had therefore dealt both with finding data related to the measurement of H_s , T_p and Dir near buoys, and had dealt with making adjustments in the models used to eliminate the possibility of drawing incorrect conclusions.

In any event, these issues were not necessary in the present study because, as shown by the file provided by Metoceanview itself "Hs verification metrics against satellite estimates from 1991-2017", (MetOceanView, 2023) the precision used by the Metoceanview models is sufficient to take into account the influence of the island of Madeira.

This document provides, among other things, BIAS and RMSE values for cells of 0.25 degrees of latitude and longitude in the vicinity of the Madeira Island. It can be seen that in the area where the points where the Hindcast data have been made available are located, there are average values of $BIAS = -0.2$ m and $RMSE = 0.4$ m.

Below is a presentation of the dataset used to conduct this study, as well as an analysis of the wave climate at various points off the island of Madeira. This analysis is conducted by comparing H_s and T_p , coupled to the Dir , at points where data are available, using appropriately constructed Polar

Diagrams, both taking into account the whole year and studying the seasonality of the analyzed values.

2.2 METOCEANVIEW DATASET

Metoceanview provides Hindcast data for points around the world with a grid resolution of 0.5 degrees of longitude and latitude. A request was made to obtain hindcast data for the nearest points to Madeira. For the purpose of this thesis, and specifically for this second chapter, five points situated in deep water were selected for analysis. Figure 2.1 shows the locations of the five points.

POINT	LAT (°N)	LON (°E)
NW	33	342,5
N	33	343
NE	33	343,5
SW	32,5	342,5
S	32,5	343



Figure 2.1, Madeira Island, location of the five points where Hindcast data have been analysed: North East, North, North West, South West, and South.

Hs, Tp, and Dir data were available for those stations from 01/01/1979 to 05/03/2022 at 3-hour intervals, resulting in a total of 126,159 values of Hs, Tp, and Dir per station (Table 2.1). Wave direction is measured from the north in clockwise direction.

Dir (°N)	Tp (s)	Hs (m)	Date	Time (h)
297,4	14,99	3,766	01/01/1979	24
297	14,91	3,608	01/01/1979	3
296,7	14,77	3,448	01/01/1979	6
296,7	14,54	3,27	01/01/1979	9
296,8	14,07	3,09	01/01/1979	12
297,1	13,77	2,93	01/01/1979	15
297,4	13,58	2,812	01/01/1979	18
297,6	13,39	2,736	01/01/1979	21

297,6	13,17	2,644	02/01/1979	24
297,8	12,73	2,53	02/01/1979	3
298,1	12,43	2,408	02/01/1979	6
298,9	12,25	2,282	02/01/1979	9
300,1	12,09	2,156	02/01/1979	12
301,3	11,92	2,034	02/01/1979	15
302,5	11,58	1,914	02/01/1979	18
303,7	11,28	1,802	02/01/1979	21
304,8	11,05	1,698	03/01/1979	24
305,8	10,83	1,6	03/01/1979	3
306,2	10,58	1,514	03/01/1979	6
306,2	10,4	1,438	03/01/1979	9
305,8	10,23	1,372	03/01/1979	12
304,1	10,03	1,328	03/01/1979	15
300,2	9,91	1,332	03/01/1979	18
295,2	9,87	1,406	03/01/1979	21
298,4	9,82	1,486	04/01/1979	24

Table 2.1, Example of wave Hindcast parameters provided by MetOceanView between 1/1/1979 and 4/1/1979 at 3-hour intervals at the North point.

For the polar diagrams, the Windroses PRO software (WindRoses PRO) was utilized. This program is capable of visually representing both the frequency and directional distribution of a specific variable. It was used to graphically display the trend of the available Hindcast data, allowing for the examination of the most important directions to consider at each point in terms of frequency of occurrence and significant values.

The software requires, first of all, information regarding the direction, and then the variable to be analysed, in this case Hs or Tp.

There is also a tool within this program, which allows the user to apply a filter depending on the date (or even the time) related to the data that have been entered. This is useful if it is required to study seasonality and the relative variations in terms of Hs, Tp or Dir that occur considering a certain period of the year rather than another.

This tool was used in this study to evaluate the variations of Hs and Tp passing from summer, considered as every day of all months from June to August, to winter, considered as the set of all days from December to February.

This software provides the ability to analyse the distribution of directions along with their corresponding Hs both graphically and analytically.

Graphically, it provides polar graphs that display values along with their frequencies and directions. Analytically, it provides statistics on how these values are distributed, both within their own intervals and across 8 or 16 directions.

In this chapter, the results obtained for the North West point are presented in detail and discussed. Subsequently, these results will be compared to the results obtained for the points N, NE, SW, and S, which will be individually reported on annex A.

2.2.1 POINT NW

Point North West is located at a latitude of 33 degrees N and a longitude of 342.5 degrees E, Figure 2.2.



Figure 2.2, Madeira Island, location of the North West point.

To better perform the analyses, both Hs and Tp data for this point have been divided into 16 classes of Dir, each one with a directional interval (or bin) of 22.5 °, as shown in Figure 2.3.

This subdivision will also be used when conducting further analysis within this study.

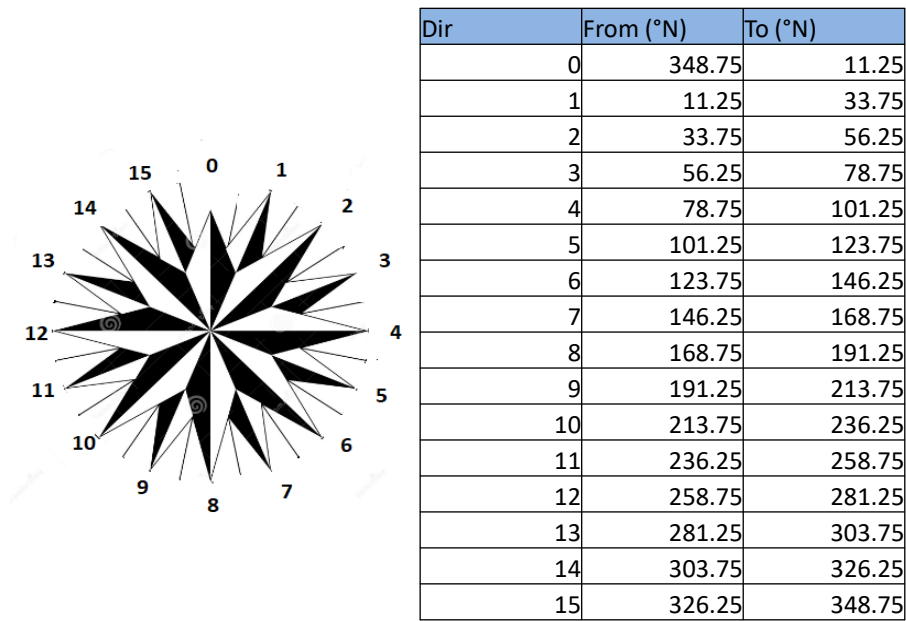


Figure 2.3, Classification of data into 16 directions for analysis.

Hs analysis

A Polar Diagram regarding Hs has been obtained, Figure 2.4. It is noticeable that the vast majority of waves come from the North West quadrant, with most of the largest waves also originating from this direction.

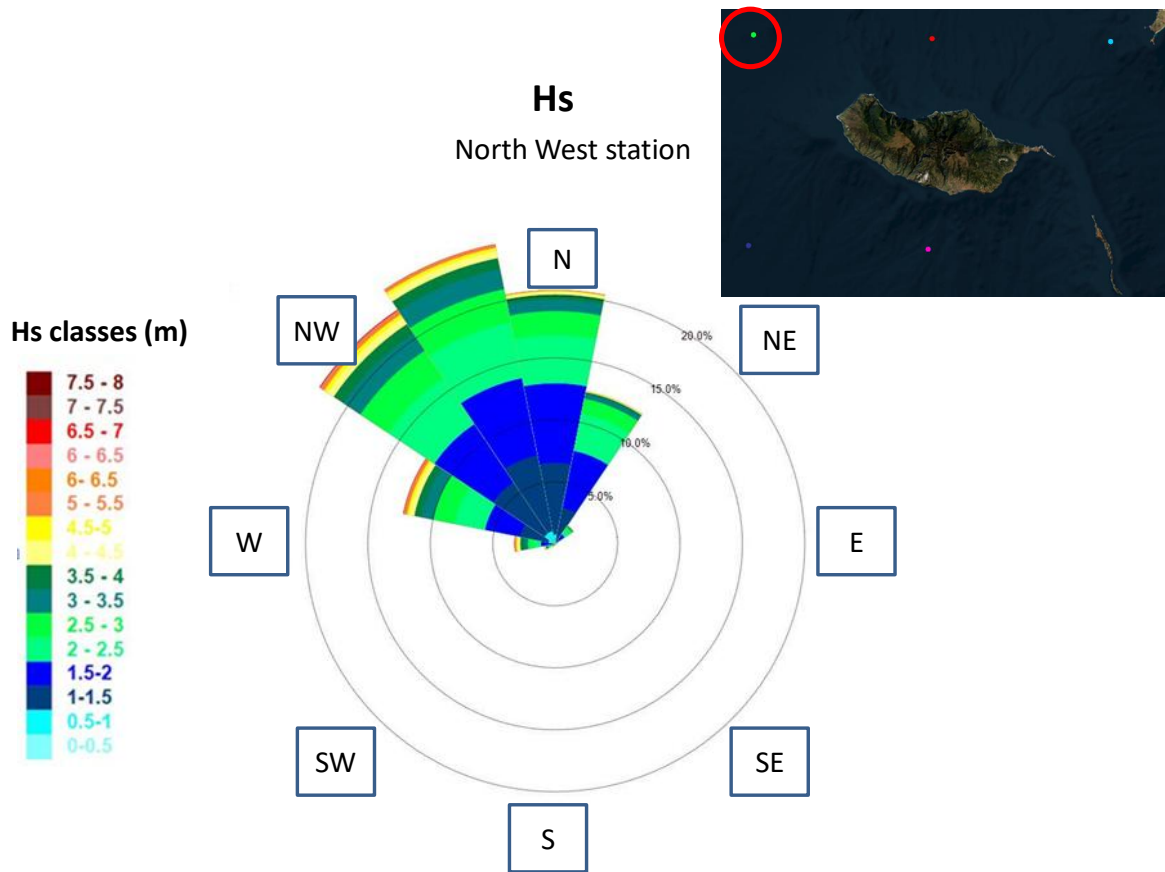


Figure 2.4, Polar diagram of Hs, North West point.

The polar diagram of Figure 2.4 is also presented in Table 2.2.

The table provides a breakdown of the number of waves within specific intervals for each of the 16 directions. It becomes evident that the vast majority of Hs is in the range between 1 m and 3 m. Additionally, it is remarkable that there are some values exceeding even the class of 6-7 m, particularly coming from the North and north-westerly directions.

	Hs (m)	0- 0.5	0.5- 1	1- 1.5	1.5- 2	2- 2.5	2.5- 3	3- 3.5	3.5- 4	4- 4.5	4.5- 5	5- 5.5	5.5- 6	6- 6.5	6.5- 7	7- 7.5	>7.5
Dir(°N)																	
348.75-11.25	0	914	7306	8122	4892	2440	1178	527	259	106	50	11	18	11	1	2	
11.25-33.75	0	257	3475	5923	3834	1557	507	204	67	36	14	3	1	2	0	0	
33.75-56.25	0	46	445	687	573	337	119	21	19	1	1	0	0	0	0	0	
56.25-78.75	0	9	77	68	87	42	9	2	0	0	0	0	0	0	0	0	
78.75-101.25	0	3	14	39	28	12	4	0	0	0	0	0	0	0	0	0	
101.25-123.75	0	0	11	21	22	5	1	0	0	0	0	0	0	0	0	0	
123.75-146.25	0	1	6	32	19	11	0	0	0	0	0	0	0	0	0	0	
146.25-168.75	0	0	7	32	37	5	1	0	0	0	0	0	0	0	0	0	
168.75-191.25	0	2	17	34	44	10	4	5	2	1	0	0	0	0	0	0	
191.25-213.75	0	5	13	51	60	38	18	6	6	6	4	4	0	0	0	0	
213.75-236.25	0	22	23	62	86	66	40	29	21	26	22	6	2	1	1	0	
236.25-258.75	0	73	95	182	217	210	146	92	56	45	20	12	6	5	0	0	
258.75-281.25	2	164	490	783	709	601	441	349	222	160	91	70	25	18	6	10	
281.25-303.75	1	701	2901	3635	3113	2202	1248	727	458	274	169	118	66	39	22	19	
303.75-326.25	2	1282	6263	7142	5586	3388	2084	1188	727	411	230	130	121	58	47	23	
326.25-348.75	0	1297	7856	8045	5761	3450	2093	1157	697	361	207	99	49	22	10	6	

Table 2.2, Number of sea states for each class of Hs and Dir based on the wave hindcast data provided by MetOceanView between 1/1/1979 and 4/1/1979 at 3-hour intervals at the North-West point.

Tp analysis

Regarding Tp, Figure 5 shows the analogous Polar Diagram, which remains consistent with the direction information depicted in Figure 2.5.

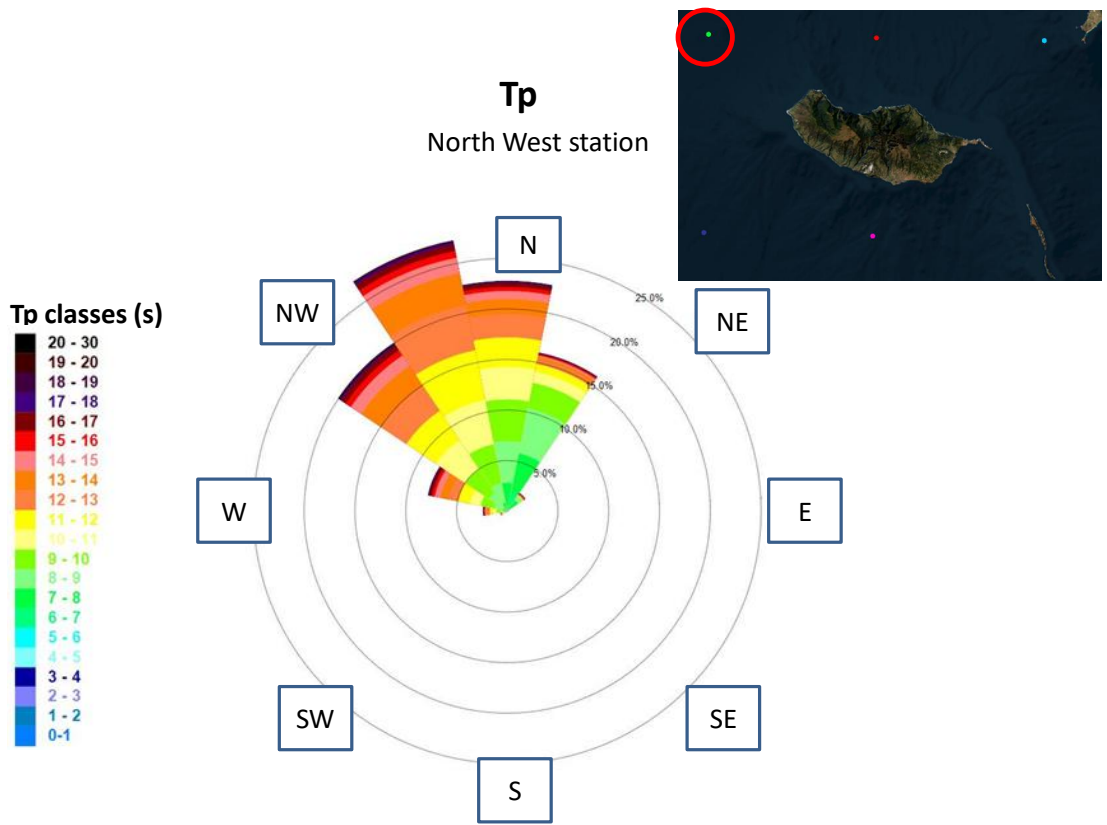


Figure 2.5, Polar Diagram for Tp, North West point.

Table 2.3 complements this by presenting the number of waves falling within specific Tp intervals. It becomes apparent that the vast majority of waves have a Tp falling into the 2-4 seconds class.

Classes (s)	Counts
0 - 1	5
1 - 2	2062
2 - 3	10969
3 - 4	10051
4 - 5	15
5 - 6	160
6 - 7	931
7 - 8	2759
8 - 9	4450
9 - 10	4802
10 - 11	4325
11 - 12	4332
12 - 13	3620
13 - 14	2669
14 - 15	1412
15 - 16	717
16 - 17	661

17 – 18	159
18 – 19	171
19 – 20	61
20 – 30	60
Total	31304

Table 2.3, wave count in Tp classes, North West point.

Summer versus winter

In Figure 2.6, the Hs distribution of winter and summer is compared. It is noticeable that the difference in terms of direction is not particularly pronounced, except for the fact that in summer there are significantly more waves coming from the North. However, the main distinction is that during winter there are larger waves.

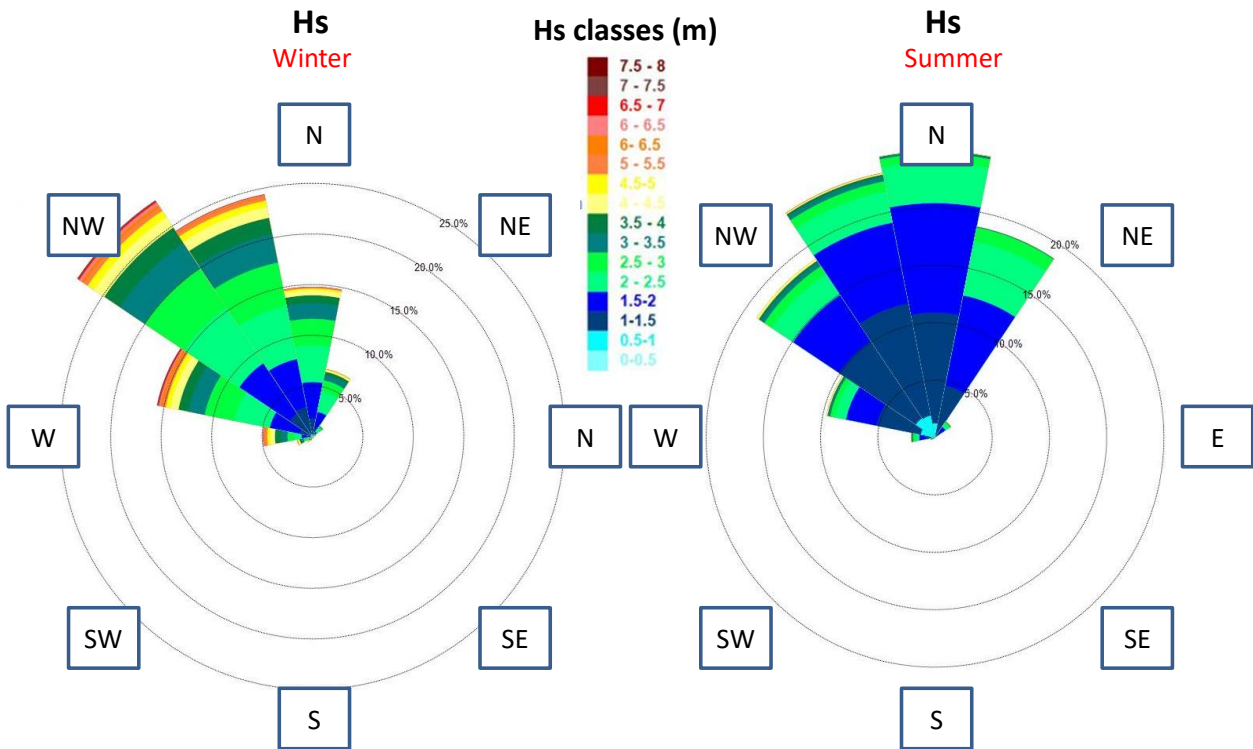


Figure 2.6, Comparison of Polar Diagram for Hs between Winter and Summer, North West point

Similar observations can be made when comparing the winter and summer Polar Diagram for Hs, as it is displayed in Figure 2.7.

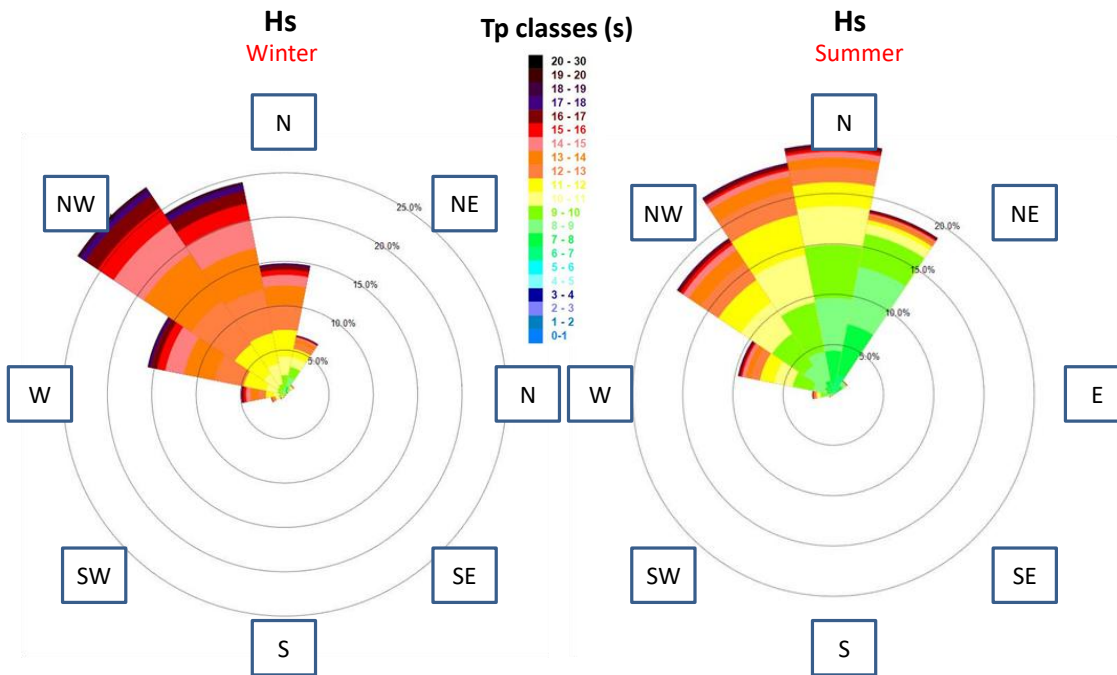


Figure 2.7, comparison of Polar Diagram for Tp between Winter and Summer, North West point

Then, similarly to what has been done in the study "ANÁLISE CLIMATOLÓGICA DA AGITAÇÃO MARÍTIMANA COSTA SUL DA MADEIRA" carried out by the Instituto Hidrográfico, Figure 2.8 illustrates the graphs displaying the maximum, minimum, and average values for Hs during winter (Figure 2.8.a) and summer (Figure 2.8.b) (Rita Esteves).

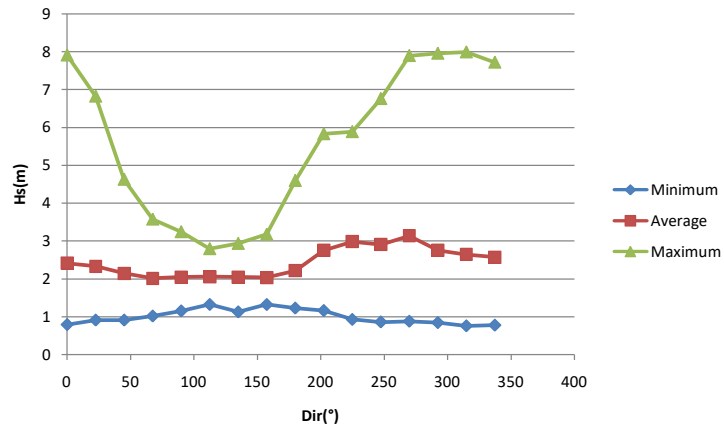
It is specified that while the study mentioned above used graphs of this type to study the variability of average and maximum values within the various months of the year, in this case clearly the variability is expressed as a function of the different wave directions, with the comparison between the different seasons that emerges simply by comparing the lower part (where there is the graph relating to the summer) and the upper part (where there is the graph related to winter) of the figure.

It is evident that there are substantial differences between the maximum and minimum values, indicating a wider range of wave heights. Conversely, during winter, although the absolute values of Hs are larger, the trend appears more linear, resulting in smaller percentage differences between the maximum and minimum values.

It is also interesting that, as it concerns waves coming from East (Dir 100-150 m), while winter displays values that are quite conform to other directions, apart from smaller maximum values, in summer there are no waves coming from this direction.

Minimum, maximum and average Hs values for each direction

a) WINTER



Hs

b) SUMMER

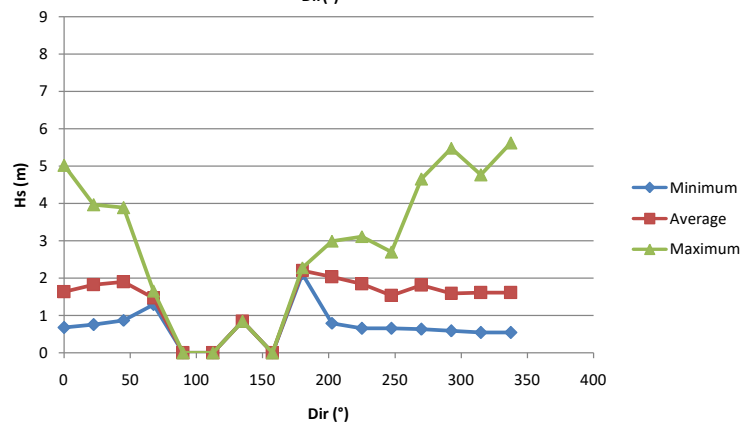


Figure 2.8, comparison of minimum, maximum, and average Hs values for each direction between: a) Winter; b) Summer. These graphs were generated as output following data processing by WindRosesPro, North West point.

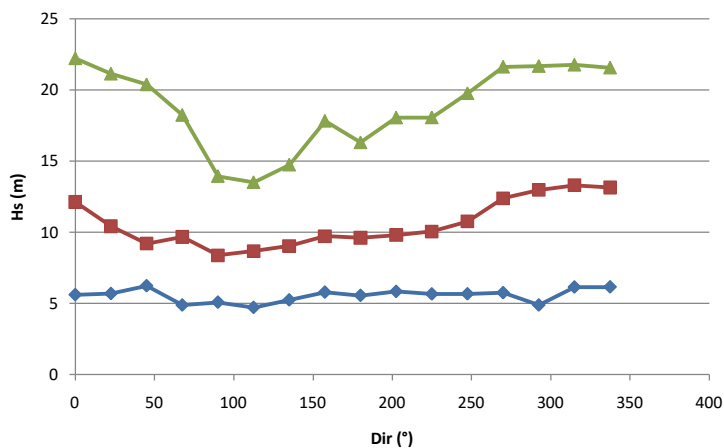
Similarly, Figure 2.9 shows the maximum, minimum, and average values for Tp during winter (Figure 2.9.a) and summer (Figure 2.9.b). It is apparent that there are significant variations between the maximum and minimum values, reflecting a broader range of wave periods. In contrast, the winter period exhibits a more linear trend, resulting in smaller percentage differences between the maximum and minimum values, despite having overall longer wave periods.

These observations suggest that in summer, wave conditions vary more dramatically, with larger differences between extreme values, while winter experiences a more constant pattern, despite having higher values.

Minimum, maximum and average Tp values for each direction

a) WINTER

Tp



b) SUMMER

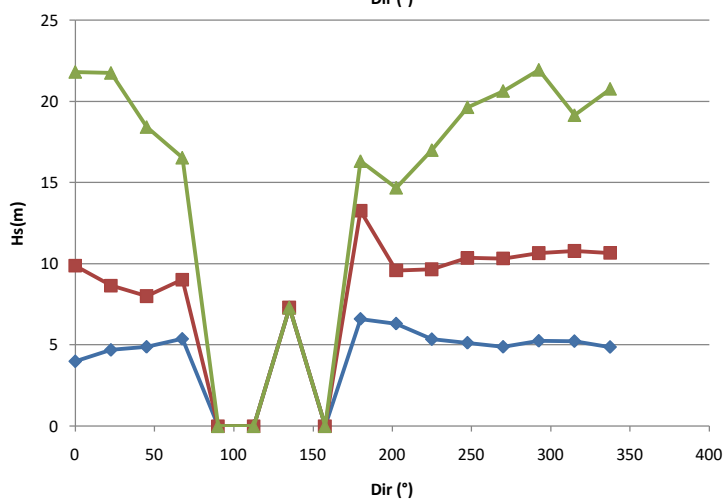


Figure 2.9, comparison of minimum, maximum, and average Tp values for each direction between: a) Winter; b) Summer. These graphs were generated as output following data processing by WindRosesPro, North West point.

2.3 COMPARISONS

The following pairs of points will now be compared

- North West versus South West
- North versus South
- North versus North East
- South West versus South

2.3.1 NORTH WEST VERSUS SOUTH WEST

The comparison between point North West and point South West(Figure 2.10) is now presented.

This comparison will serve as the basis for defining the similarities and differences between the waves in the western part of the island. Further details will be provided in subsequent chapters, where this analysis will be used to examine extreme wave values and determine the initial conditions for simulating wave propagation from the western side of the island.



Figure 2.10, Madeira Island, location of the North West point and the South West point

As it is evident from Figure 2.11, which displays the polar diagram of H_s , both values and directions are similar for the North West and South West points, as expected. However, one main difference is that the North West point shows more waves coming from the NE when compared to the South West point. This result supports the existence of a shadow area caused by the island. Considering the positions of the points, waves originating from the NE cannot reach the South West point, whereas this effect is not present at the North West point.

Based on this comparison, it can be concluded that on the West side of the island, aside from the variations in waves coming from the NE, the wave climate remains similar between the North West

and the South West point. Therefore, any evaluations made regarding Hs at a specific point on the West side can be applied to other points on the same side of the island.

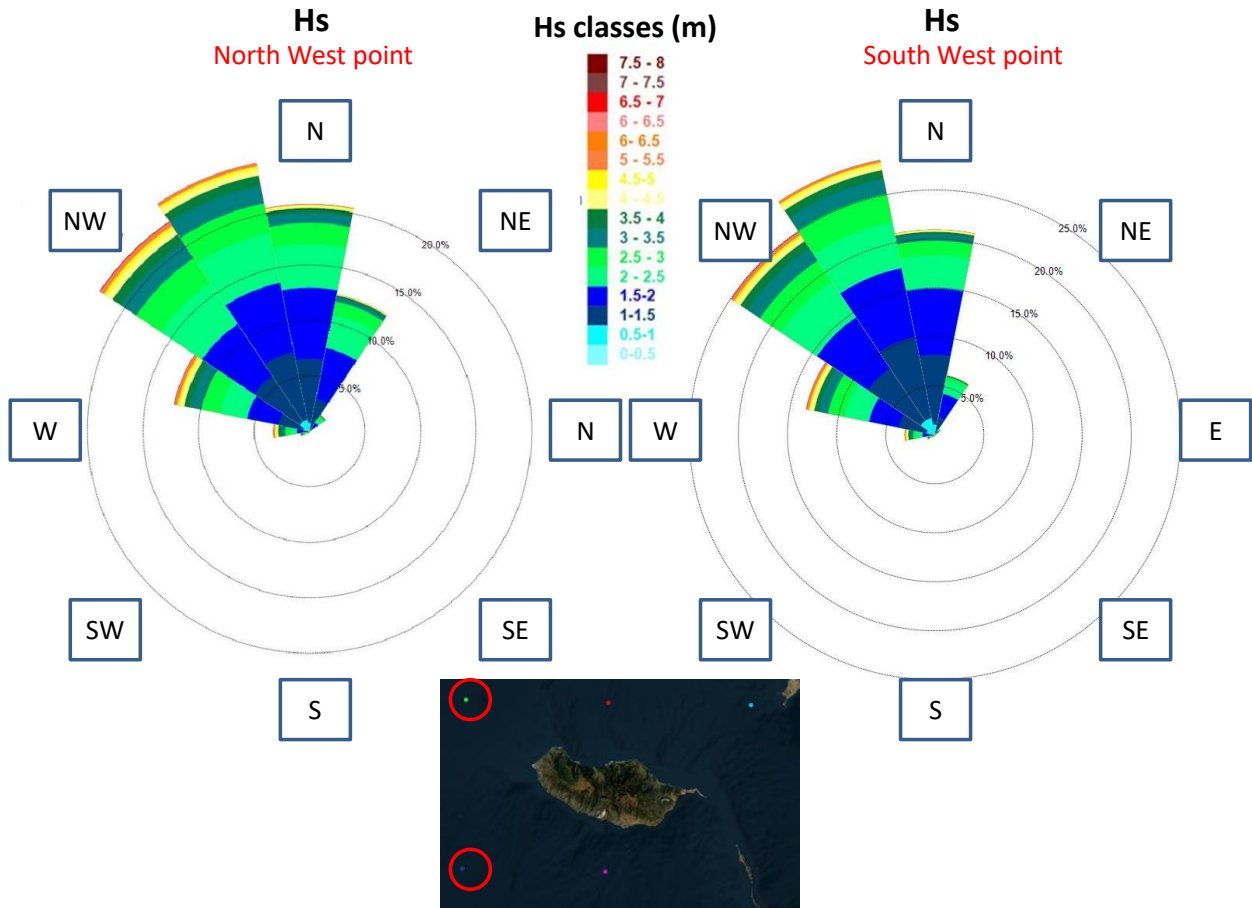


Figure 2.11, comparison of Polar Diagrams with Hs between the North West point and the South West point.

2.3.2 NORTH VERSUS SOUTH

The comparison between the North and South points provides an excellent demonstration of the shadow effect due to their locations on opposite sides of Madeira Island, which is possible to notice on Figure 2.12.



Figure 2.12, Madeira Island, location of the North point and the South point

As mentioned above, the software used to create these polar diagrams allows you to decide whether you want to divide H_s or T_p into 8 or 16 classes of directions. The polar diagrams related to the points covered by this comparison have been divided into 8 classes, unlike what was done for the previous points, so as to be able to emphasize more the difference in terms of waves coming directly from the North.

Dividing the waves into direction classes with a wider range allows you to better see the difference in terms of waves coming from the north, which in fact can be seen from Figure 2.13.

This figure illustrates the comparison of the polar diagrams of H_s values at the two points. There are two main differences: firstly, there is a decrease in the percentage of waves coming from the North when moving from the North point to the South point, dropping from over 40 percent to slightly more than 15 percent.

Secondly, the presence of yellow and orange portions (representing values of H_s above 4-5 m) in the polar diagrams relative to the North point, as well as a practically total absence of these colours in the one relative to the South point, suggests that waves having certain values of H_s are observable only in the North point and not in the South point.

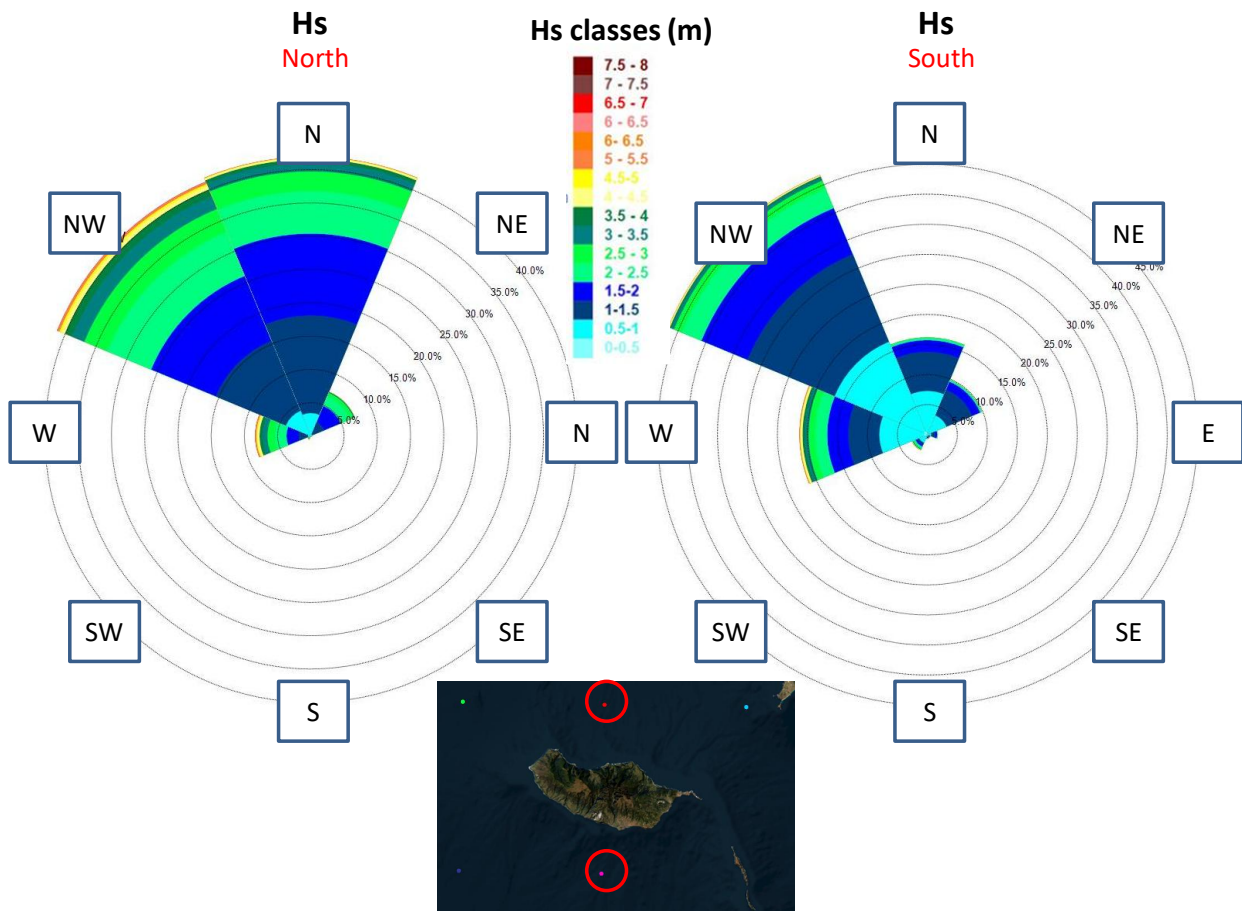


Figure 2.13, comparison polar diagrams with Hs values between the North point and the South point.

This comparison once again demonstrates the shadow effect that was previously introduced, which refers to the "shield" created by the island. This effect is responsible for reducing Hs values and altering the direction of the waves.

2.3.3 NORTH VERSUS NORTH EAST

It is now presented the comparison between the North point and the North East point, whose positions are shown in Figure 2.14.

As in the comparison between the North and South points, also in this case it has been decided to use 8 classes of directions instead of 16.



Figure 2.14, Madeira Island, location of the North point and the North East point

The comparison of the direction distribution with H_s values in Figure 2.15 reveals that although the difference in terms of H_s values is negligible, there are some variations among the main directions, particularly in waves coming from the North West.

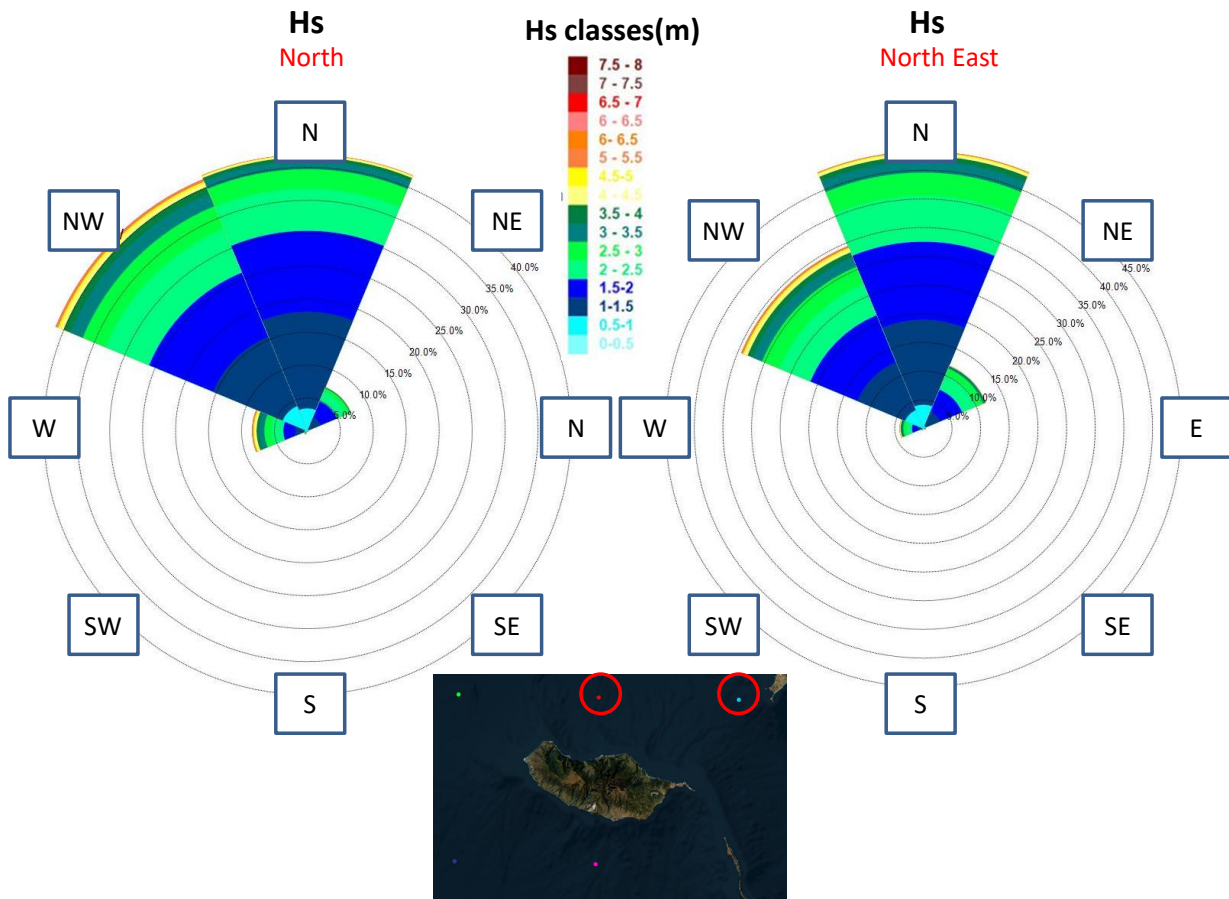


Figure 2.15, Comparison of direction distribution with Hs values between the North point and the North East point.

This is likely due to the positioning of the North East point, showed in Figure 2.16, which is close to the Porto Santo island that interferes with the wave propagation to this point.

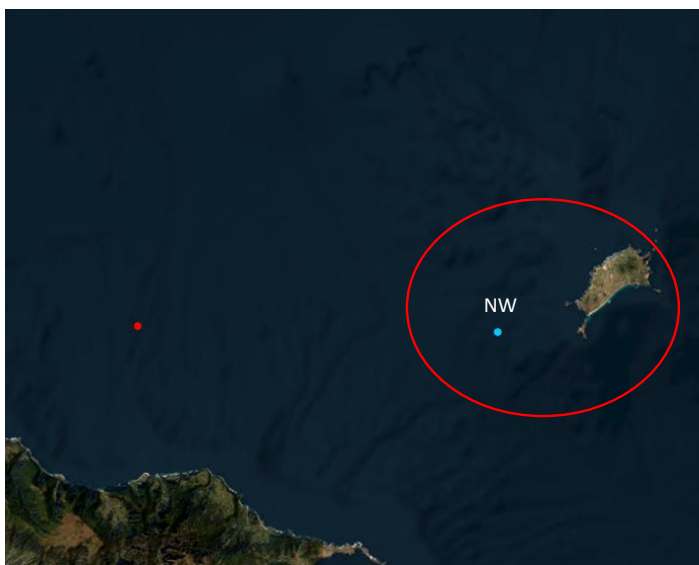


Figure 2.16, location of the North East point.

2.3.4 SOUTH WEST VERSUS SOUTH

The characteristics of the South side of the island are now being examined through the comparison between the South West and South point, whose positions are depicted in Figure 2.17.



Figure 2.17, Madeira Island, location of the South West and the South point

The polar diagrams with H_s values, as illustrated in Figure 2.18, highlights a significant decrease in H_s values when transitioning from the South West point to the South point. Additionally, there is a noticeable change in the direction distribution, with a decrease in the number of waves coming from the North as one moves from the South West point to the South point. This can once again be attributed to the shadow effect created by Madeira Island.

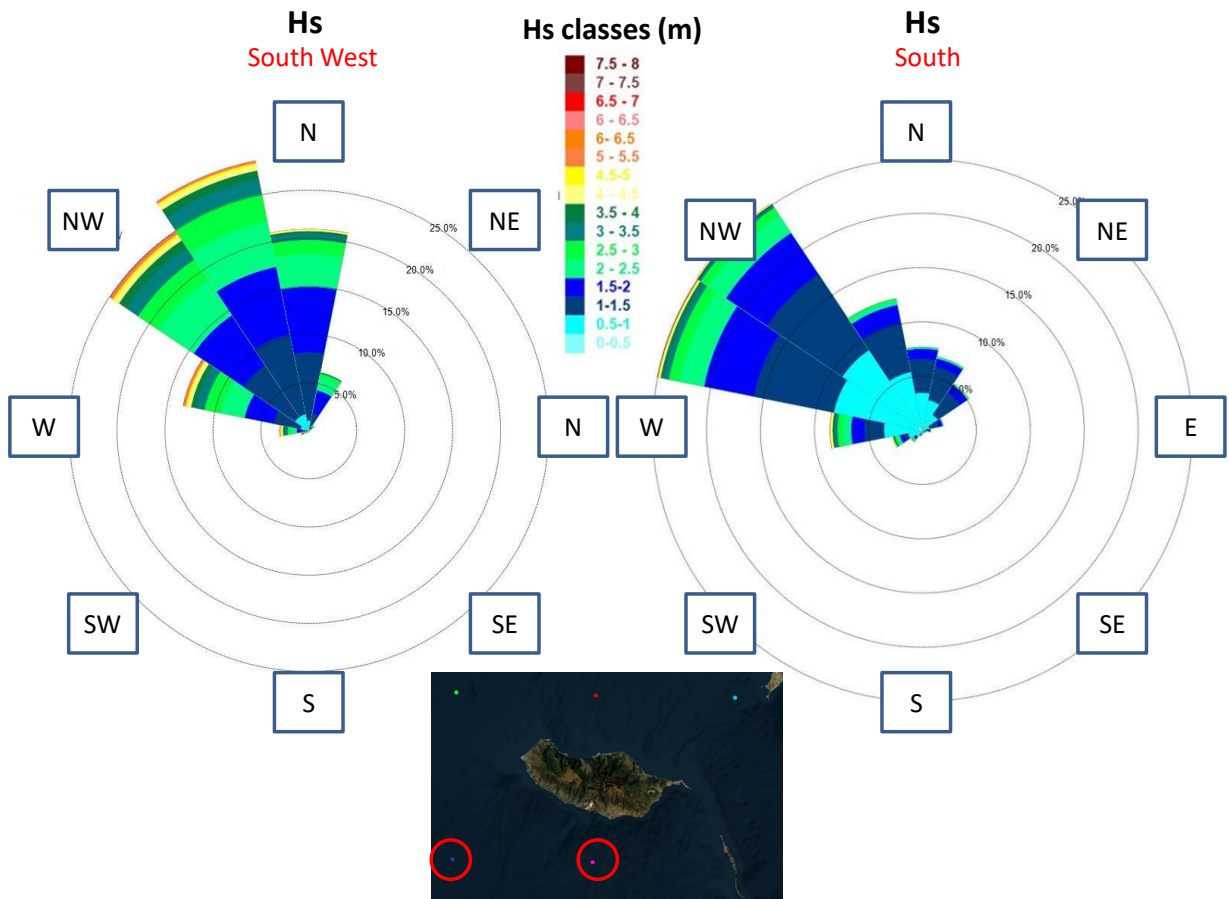


Figure 2.18, comparison of direction distribution with Hs values between the South West point and the South point.

Based on this comparison, it can be concluded that on the South side of the island, the evaluations made at a single point cannot be extended to all other points on the side, unlike what was possible on the West side. This aspect will be further discussed in Chapter 4, particularly when determining the boundary conditions for simulations propagating waves from the South.

2.4 SUMMARY

The analyses pursued in this chapter have provided a significant contribution to the understanding of the wave climate offshore of the Madeira Island. The dataset made available by Metoceanview has allowed for a focus on the characteristics of the different sides of the island, particularly the west side as well as the south and north sides, in order to highlight variations and similarities among them. Below, the most important conclusions that were possible to draw from this second chapter are summarized point by point:

- Waves coming from the North, and more generally from the third quadrant, tend to be more significant both in terms of H_s and in terms of occurrence frequency compared to those coming from the South, as shown in Figure 2.4
- The comparison conducted between the waves recorded in summer and winter has allowed us to observe tangible seasonal differences, especially concerning H_s values (Figure 2.6).
- The comparison among the various points carried out in paragraph 2.3 has shown the clear presence of the shadow effect: the presence of the Madeira Island represents a significant factor in the propagation of wave conditions recorded by the MetOceanView dataset within the ocean. It is important to add that this is also a clear indication that the Hindcast data used were obtained with models capable of accounting for the presence of the island (see discussion in paragraph 2.1).
- Another conclusion that can be drawn from the findings in section 2.3 pertains to the wave climate conditions on the west and south sides of the island: section 2.3.1 has demonstrated that conditions on the west side can be considered relatively constant along the entire side, whereas section 2.3.4 has shown that conditions on the south side are significantly more variable when moving from the South to the Southwest point.

3 DEFINITION OF THE OFFSHORE BOUNDARY CONDITIONS

NW, SW AND S POINTS: H_s AND T_p RELATIONSHIP, MONTHLY VARIATION, EXTREME VALUES ANALYSES

3.1 INTRODUCTION

In the second chapter wave data was analysed in five hindcast grid points around the Madeira Island. The present analysis is now reduced to three grid points since, as mentioned, one of the aims of this thesis is to identify the waves that, after propagation, can reach the southwest coast of Madeira, more specifically the area between Ponta do Pargo and Funchal (Figure3.1).



Figure 3.1, Madeira Island, South West coast, area of interest from Ponta do Pargo to Funchal.

To accomplish this task, additional statistics were calculated on the data points closest to the area of interest . The three points of interest are the North West, South West, and South points (Figure3.2).

With the Hindcast data relating to these points, analyses were carried out on the trend of H_s as a function of T_p and vice versa, on changes in H_s within the various months of the year and with regard to extreme events. The variables H_s , T_p , and Dir were already analysed in the previous chapter.



Figure 3.2, Madeira Island, closest points to South West coast where Hindcast data were available: North West, South West and South

For each of these three points, the additional statistics consist of:

- Tables displaying the bivariate empirical distribution of H_s and T_p .
- Creating box plots to illustrate the monthly variations.
- Analysing extreme values to determine the H_s for a given return period.

In this chapter, the additional statistical analyses performed for the North West point will be presented, while those for the South West and South points are provided in Annex B.

3.2 NORTH WEST POINT

It is reminded that the North West point covered by this paragraph is located with respect to the island of Madeira as shown in Figure 2.2 in Chapter 2.

As mentioned, the analysis will be conducted first with regard to the relationship between H_s and T_p , then move on to the study of the variability in terms of seasonality of H_s values, and finally the analysis of extreme values will be conducted to establish the H_s corresponding to a certain number of years of return period.

3.2.1 JOINT EMPIRICAL DISTRIBUTION OF H_s AND T_p

The primary objective of this paragraph is to illustrate the (highest frequency) most probable T_p for a wave with a given H_s . This information will be of interest for the subsequent chapter where wave propagation will be conducted. In those simulations, when considering a specific H_s with a

designated return period, the corresponding T_p needs to be input as well, and it will be determined using the study conducted in this paragraph.

In addition, the figures that will be presented include tables that demonstrate an important physical limit in deep water imposed by wave breaking. This limit is defined by equation 3.1 (Holthuijsen, 2007)

$$\frac{2\pi H_s}{gT_0^2} < \frac{1}{15} \quad (3.1)$$

Where

T_0 =mean wave period

The ratio between the T_0 present in the equation just presented and the T_p to which reference is made in this study, varies depending on the type of waves considered.

Since the T_0 data are not available, the relationship persisting between T_0 and T_p for regular waves was used, as in equation 3.2 (Y.Goda, 2000)

$$T_p \cong T_0 * 1,2 \quad (3.2)$$

Equation 3.1 then becomes

$$\frac{2\pi H_s 1,2^2}{gT_p^2} < \frac{1}{15} \quad (3.3)$$

Then putting all the constants to the right of the equation, the following expression is reached

$$\frac{H_s}{T_p^2} < \frac{g}{15 * 2\pi * 1,2^2} \cong 0,072 \quad (3.4)$$

Histograms will be utilized in this paragraph to illustrate this relationship between H_s and T_p . These histograms will illustrate that for small H_s values, corresponding T_p values exceeding a certain threshold in accord to equation 3.4 cannot be observed.

To perform this aims, all 126,159 values of H_s and T_p have been classified into intervals of 0.5 m for H_s and 1 s for T_p . Subsequently, a table as shown in Figure 3.3, was created.

The majority of values fall within the range of 8 to 14 s for T_p , accounting for more than 75% of the data. Similarly, the range of 1 to 2 m for H_s represents over 50% of the values. The bin (or class) with the highest number of values corresponds to 1,5-2 m of H_s and 11-12 s of T_p . This column (T_p) and row (H_s) contain the highest number of values.

Furthermore, the bottom left part of the histogram confirms the previously mentioned limitation imposed by wave steepness. In this area, only values of 0.00% are observed, indicating the absence of waves with steepness exceeding the threshold in accord to Equation 3.4. This pattern is consistent across all histograms like Figure 3.3, and it will not be repeated.

Hs vs Tp

North West point

bin	tot
>0,5%	>5%
>1%	10%
>3%	20%
>5%	30%

Hs (m)	Tp (s)																TOT
	<4	4--5	5--6	6--7	7--8	8--9	9--10	10--11	11--12	12--13	13--14	14--15	15--16	16--17	>17		
0--0,5 m	0,00%	0,00%	0,00%	0,00%	0,00%	0,00%	0,00%	0,00%	0,00%	0,00%	0,00%	0,00%	0,00%	0,00%	0,00%	0,00%	0,00%
0,5--1 m	0,00%	0,00%	0,01%	0,10%	0,71%	0,84%	0,62%	0,37%	0,23%	0,21%	0,26%	0,15%	0,10%	0,11%	0,07%	3,78%	
1--1,5 m	0,00%	0,03%	0,16%	0,62%	2,05%	4,15%	5,01%	3,93%	2,76%	1,64%	1,10%	0,61%	0,34%	0,40%	0,23%	23,03%	
1,5--2 m	0,00%	0,00%	0,14%	0,95%	2,14%	2,83%	3,54%	4,46%	5,21%	4,23%	2,32%	0,83%	0,38%	0,34%	0,25%	27,61%	
2--2,5 m	0,00%	0,00%	0,02%	0,34%	1,12%	1,64%	1,64%	1,99%	3,10%	4,08%	3,39%	1,41%	0,49%	0,39%	0,25%	19,86%	
2,5--3 m	0,00%	0,00%	0,00%	0,04%	0,30%	0,68%	0,89%	0,96%	1,38%	1,94%	2,40%	1,58%	0,60%	0,42%	0,21%	11,39%	
3--3,5 m	0,00%	0,00%	0,00%	0,00%	0,07%	0,23%	0,40%	0,52%	0,71%	0,90%	1,26%	1,02%	0,59%	0,36%	0,18%	6,25%	
3,5--4 m	0,00%	0,00%	0,00%	0,00%	0,01%	0,06%	0,18%	0,28%	0,37%	0,50%	0,61%	0,55%	0,39%	0,31%	0,16%	3,41%	
4--4,5 m	0,00%	0,00%	0,00%	0,00%	0,00%	0,01%	0,07%	0,13%	0,23%	0,27%	0,34%	0,31%	0,24%	0,25%	0,14%	2,01%	
4,5--5 m	0,00%	0,00%	0,00%	0,00%	0,00%	0,00%	0,02%	0,10%	0,11%	0,14%	0,19%	0,17%	0,13%	0,15%	0,11%	1,13%	
>5 m	0,00%	0,00%	0,00%	0,00%	0,00%	0,00%	0,01%	0,05%	0,13%	0,20%	0,25%	0,25%	0,20%	0,23%	0,20%	1,52%	
TOT	0,00%	0,03%	0,33%	2,05%	6,40%	10,46%	12,39%	12,79%	14,24%	14,11%	12,11%	6,89%	3,46%	2,96%	1,77%	100,00%	

Figure 3.3, Joint distribution Tp and Hs, North West point.

Additionally, a histogram has been created to depict the relationship between Tp on the X-axis and the percentage of Hs on the Y-axis. The histogram utilizes different colours to represent various class of Hs (Figure 3.4).

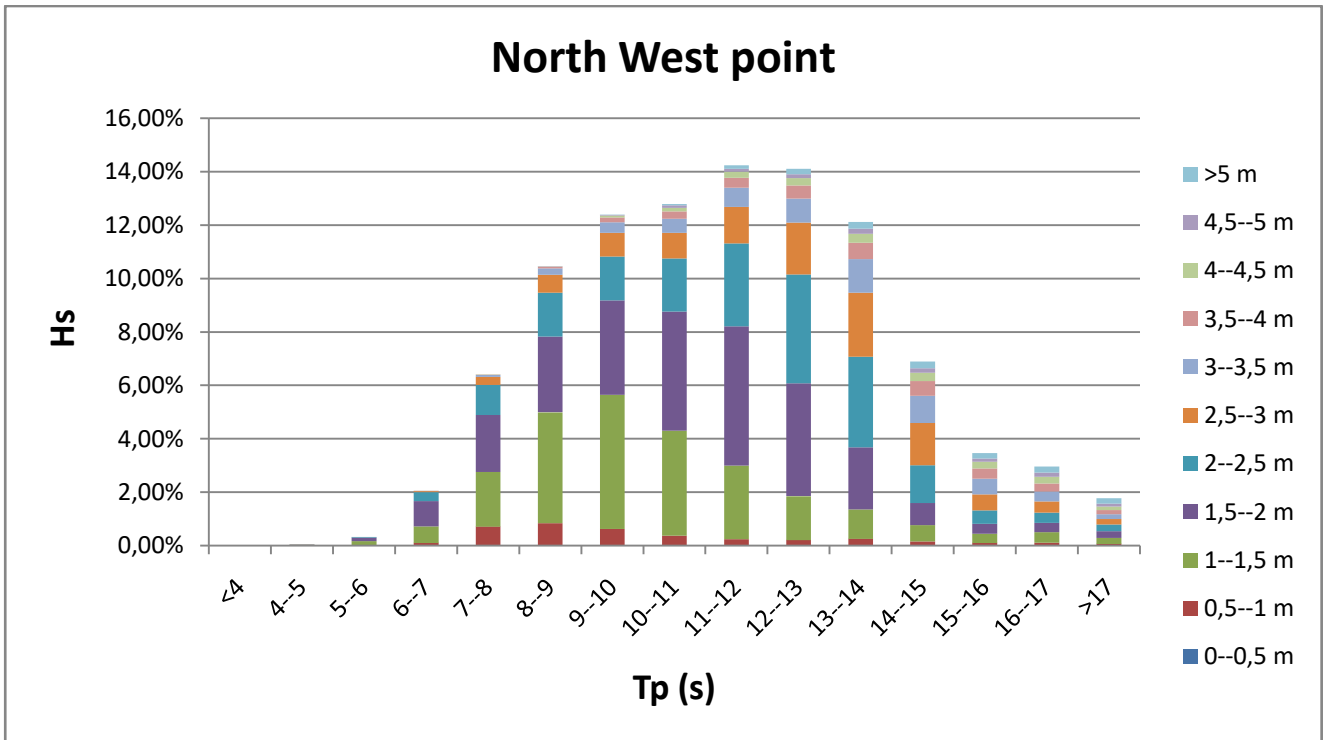


Figure 3.4, Histogram illustrating the relationship between T_p and H_s , North West point. For each T_p class, the percentage of waves with a period falling within that class is displayed, and for each bar, the colours represent the H_s classes that make up the respective bar.

Then, based on the division of the data into 16 directions as described in the previous chapter, the directions with more than 10 percent of the data were selected for specific analysis. In Table 3.1, these directions are highlighted in red.

Dir	Direction(°N)	# Data	Data(%)
0	0	25837	20,48
1	22,5	15880	12,587
2	45	2249	1,783
3	67,5	294	0,233
4	90	100	0,079
5	112,5	60	0,048
6	135	69	0,055
7	157,5	82	0,065
8	180	119	0,094
9	202,5	211	0,167
10	225	407	0,323
11	247,5	1159	0,919
12	270	4141	3,282
13	292,5	15693	12,439
14	315	28682	22,735
15	337,5	31110	24,659

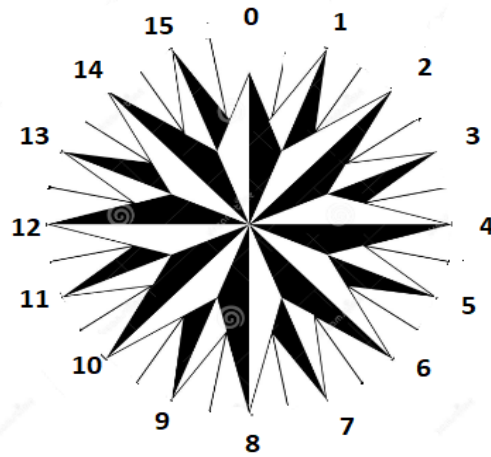


Table 3.1, % of data per each direction, North West point.

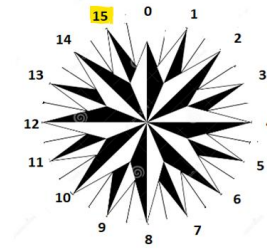
All the analyses for the five directions displayed similar results, i.e. that the values are distributed in a similar manner to the overall dataset.

Due to space constraints, only the results related to direction 15 (337.5°N), containing nearly a quarter of the total data, are presented, Figure 3.5.

a)

Hs vs Tp

North West point, direction 15



bin	tot
>0,5%	>5%
>1%	10%
>3%	20%
>5%	30%

Hs (m)	Tp (s)																TOT
	<4	4--5	5--6	6--7	7--8	8--9	9--10	10--11	11--12	12--13	13--14	14--15	15--16	16--17	>17		
0--0,5	0,00%	0,00%	0,00%	0,00%	0,00%	0,00%	0,00%	0,00%	0,00%	0,00%	0,00%	0,00%	0,00%	0,00%	0,00%	0,00%	0,00%
0,5--1	0,00%	0,00%	0,01%	0,05%	0,70%	0,95%	0,85%	0,46%	0,26%	0,19%	0,21%	0,09%	0,10%	0,15%	0,06%		4,09%
1--1,5	0,00%	0,00%	0,03%	0,13%	0,98%	3,22%	6,35%	5,68%	3,81%	2,36%	1,42%	0,55%	0,24%	0,31%	0,25%		25,33%
1,5--2	0,00%	0,00%	0,02%	0,14%	0,40%	1,02%	2,38%	5,12%	6,17%	5,33%	3,10%	1,05%	0,44%	0,33%	0,29%		25,82%
2--2,5	0,00%	0,00%	0,00%	0,04%	0,13%	0,42%	0,80%	1,76%	3,39%	4,82%	3,94%	1,75%	0,67%	0,51%	0,29%		18,53%
2,5--3	0,00%	0,00%	0,00%	0,01%	0,06%	0,13%	0,36%	0,77%	1,47%	2,26%	2,62%	1,85%	0,78%	0,57%	0,26%		11,13%
3--3,5	0,00%	0,00%	0,00%	0,00%	0,01%	0,06%	0,20%	0,37%	0,88%	1,04%	1,50%	1,22%	0,72%	0,49%	0,25%		6,73%
3,5--4	0,00%	0,00%	0,00%	0,00%	0,00%	0,02%	0,10%	0,19%	0,38%	0,50%	0,68%	0,65%	0,51%	0,46%	0,24%		3,72%
4--4,5	0,00%	0,00%	0,00%	0,00%	0,00%	0,00%	0,05%	0,09%	0,21%	0,27%	0,35%	0,42%	0,33%	0,31%	0,21%		2,23%
4,5--5	0,00%	0,00%	0,00%	0,00%	0,00%	0,00%	0,01%	0,05%	0,07%	0,13%	0,18%	0,21%	0,13%	0,18%	0,20%		1,16%
>5	0,00%	0,00%	0,00%	0,00%	0,00%	0,00%	0,00%	0,03%	0,07%	0,14%	0,17%	0,20%	0,24%	0,23%	0,20%		1,28%
TOT	0,00%	0,00%	0,05%	0,37%	2,27%	5,83%	11,09%	14,53%	16,71%	17,03%	14,17%	7,99%	4,15%	3,55%	2,26%		100,00%

b)

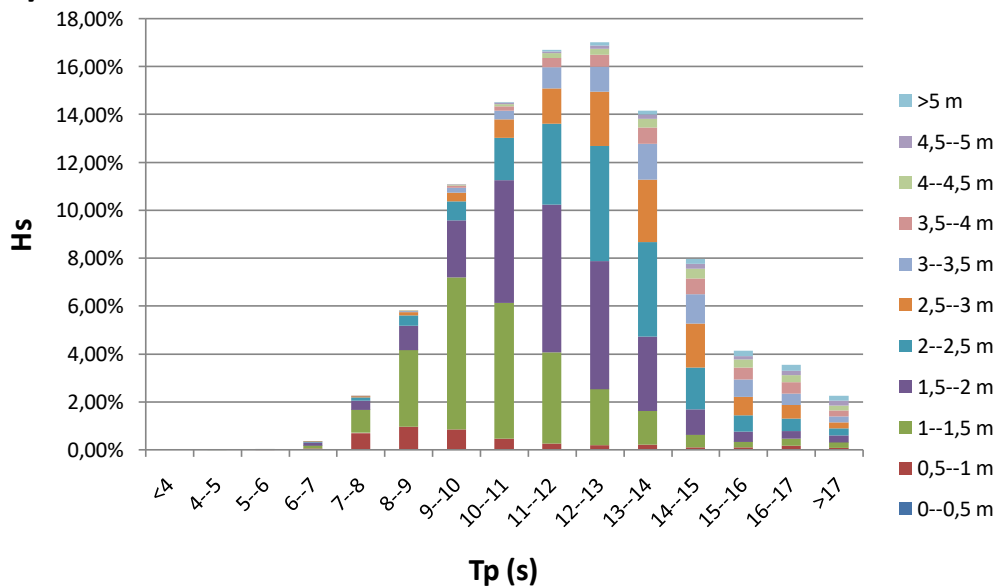


Figure 3.5, North West point, direction 15 (337.5 °N): a) Joint distribution Tp and Hs; b) Histogram illustrating the relationship between Tp and Hs, North West point. For each Tp class, the percentage of waves with a period falling within that class is displayed, and for each bar, the colours represent the Hs classes that make up the respective bar.

3.2.2 MONTHLY VARIATION ANALYSIS

Subsequently, using the software 'Rstudio' (Rstudio) box plots as in Figure 3.15 were created to visualize the variability of Hs values for each month.

These plots show the median(blue line), the 25th and 75th percentile(upper and lower part of the “box”).

Furthermore, the black lines, named “whiskers” represent the 25th and 75th percentiles, respectively decreased and increased by 1,5 times the interquartile range, i.e. the distance between 25th and 75th percentiles.

This makes it easier to identify outliers within the dataset. The outliers, red in Figure 3.15, represent those points that, with respect to the sample as a whole, assume values that may not belong to the probability distribution that represents the sample under examination. In other words, the outliers of a data sample are those elements that deviate significantly from the main distribution.

These graphs are constructed to determine the months in which it is most suitable to work on coastal construction projects. If a month exhibits significant variations compared to its average, it indicates a higher likelihood of finding severe conditions when working during that month.

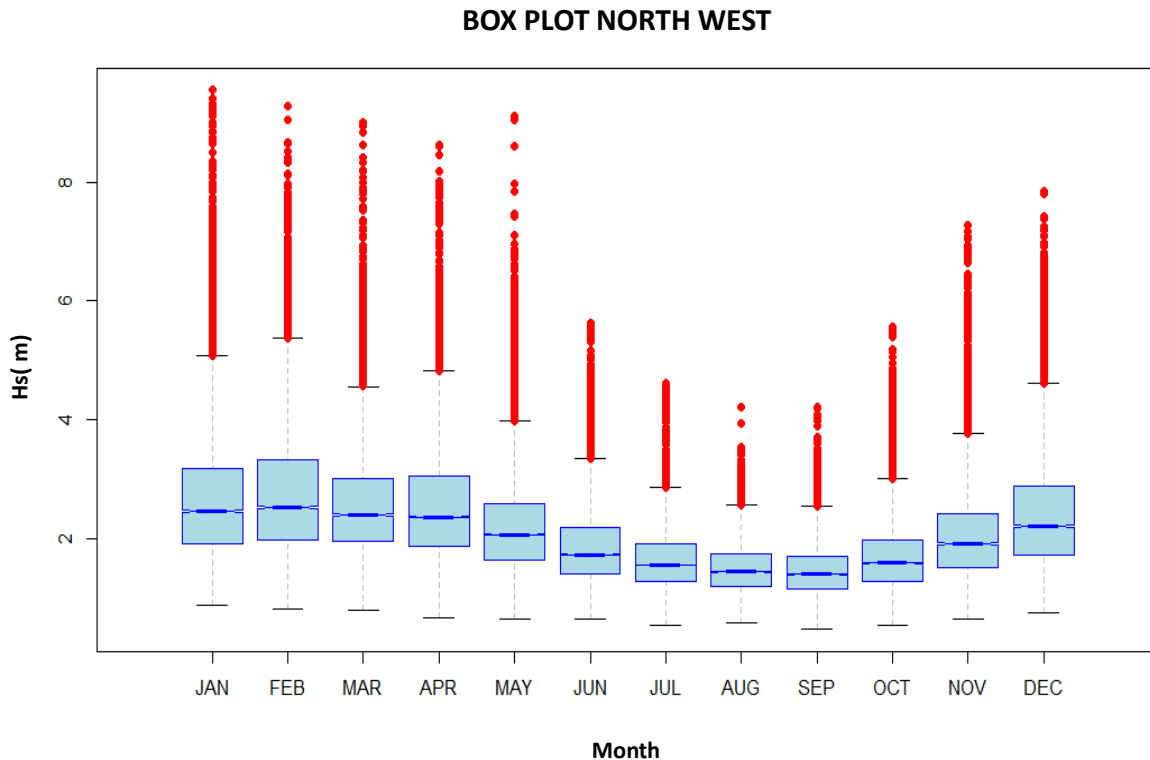


Figure 3.6, Box plot showing the monthly variability in terms of Hs. Red points: outliers; Black lines: “whiskers”, Blue lines: median; upper side of the box: 75th percentile; lower side of the box: 25th percentile. North West point.

Figure 3.6, showing the monthly variability in terms of Hs for the North West point, clearly shows greater variations in the winter months, where significantly more outlier points are observed. However, it can be said that the variability within these variations is within the normal range.

3.2.3 EXTREME VALUES ANALYSIS

The extreme values analyse has been conducted.

This type of analyses are made in order to establish the Hs value for a given return period.

In this study it has been reported the Hs of 10, 20, 50 and 100 year of return period, with particular attention to the Hs of 100 years of return period, since, as it will be seen in the next chapters, all the simulations will be made taking into account 100 years of return period.

The extreme values analyses were conducted following the Method of Annual Maximums (MAM). The choice of how to conduct this type of analysis could have fallen on other methods. For example, the already mentioned "Estudo do clima de agitacao maritima aolongo da costa sudoeste de Madeira" has used the Peak Over Threshold (POT) method (delf hydraulics, 2007).

The decision on the most appropriate method for conducting extreme values analyses should take into account the specific conditions of both the area being considered, the purpose of the study and the data sample available. In this study the method of annual maximums was chosen since the

simplicity of which it is characterized is supported by the motivations of the study and the sample of data available.

Referring to the manual “Waves in Oceanic and Coastal Waters“ which states” One advantage of this approach is that basic support is provided by the extreme-value theory and that only the highest value in a year needs to be considered (thus reducing any numerical simulation effort to only a few storms). A serious disadvantage is that generally not enough years of observations or Hindcast are available to estimate the parameters of the distribution and hence the return period with reasonable reliability” (Holthuijsen, Waves in Oceanic and Coastal Waters, 2007).

The number of years in which the Hindcast data with which this study was conducted are available are considered sufficient (43) and therefore the disadvantage mentioned in the manual "Waves in oceanic and coastal waters" is not reflected in this case, and therefore the Method of Annual Maximum is adequate for the application.

STEPS

It follows an explanation of the procedure regarding MAM followed to perform the extreme values analyse (see L.H. Holthuijsen, Waves in Oceanic and Coastal Waters. Delft University of Technology and UNESCO-IHE, 2007, p. 98-100 and Y. Goda, Random seas and design of maritime structures. Yokohama National University, 2000, p. 377-413), and then the results will be shown. (Holthuijsen, Waves in Oceanic and Coastal Waters, 2007, p. 98-100; Y.Goda, 2000, p. 377-413)

- 1) Extract the maximum value for each year.
- 2) Arrange the maximum values in descending order
- 3) Deciding which probability distribution had the best fit with the yearly maximum values sample.

In particular it has to be established whether to use the distribution of

- Gumbel, having the following cumulative distribution formula

$$F(x) = \exp\left(-\exp\left(-\left(\frac{x-\mu}{\alpha}\right)\right)\right) \quad (3.5)$$

With μ and α respectively location and shape parameter and x random variable, in this case H_s .

Or

- Weibull, having the following cumulative distribution function (CDF)

$$F(x) = 1 - \exp\left(-\left(\frac{x}{\beta}\right)^\alpha\right) \quad (3.6)$$

With β and α are respectively scale and shape parameters, and x random variable, in this case H_s .

To establish the best fit it is necessary to

- i. Find the parameters of each CDF (μ and α for Gumbel CDF and β and α for Weibull CDF).

This can be done either with Maximum Likelihood Estimation (MLE) method or with the Momentum method (MM).

Both methods have been applied, using the software “R” that gave the parameters of the CFD functions as output.

After finding 4 pair of parameters (2 pairs for each CDFs using MLE and MM) it is possible to

- ii. Compare the CDF curve with the non exceeding probability of the sample in exam, which is given by the formula below

$$F(x) = 1 - \frac{i}{N + 1} \quad (3.7)$$

Where “i” is the position of every single value after being ordered from the highest to the lowest, and N is the total number of data values in the series.

In this way the biggest values will have $i=1$ and the highest non exceeding probability, and the lowest will have $i=N$, and the highest non exceeding probability.

- 4) Running Pearson test in order to check if the CDF chosen with the relative parameters actually represents a good fit.
- 5) Using the relationship between non exceeding probability $F(x)$ and return period R_p (view point “iv” of the following equations) to obtain values of H_s for a given return period.

The analytical steps followed (for the Gumbel CDF) are:

- i. $F(x) = \exp\left(-\exp\left(-\left(\frac{x-\mu}{\alpha}\right)\right)\right)$
- ii. $w = \frac{x-\mu}{\alpha}$
- iii. $w = -\ln\left(-\ln\left(\frac{1}{F(x)}\right)\right)$
- iv. $\frac{1}{T} = P(X \geq Xt) = 1 - P(X \leq Xt) = 1 - F(Xt)$
- v. $F(Xt) = \frac{T-1}{T}$
- vi. $Wt = -\ln\left(-\ln\left(\frac{T}{T-1}\right)\right)$
- vii. $Xt = \mu + \alpha * Wt$

The H_s values for 10, 20, 50 and 100 years of return period(i.e X_{10} , X_{20} , X_{50} and X_{100})will be showed.

RESULTS

1) MAXIMUM H_s VALUES FOR EACH YEAR

Table 3.2 shows the yearly maximum H_s values for North West point for every year from 1979 to 2022.

Year	Hs max (m)
1979	9.3
1980	5.6
1981	6
1982	9.2
1983	7.2
1984	6
1985	7.7
1986	7.4
1987	8.8
1988	6.2
1989	8
1990	9.5
1991	9
1992	5.9
1993	7.1
1994	6.3
1995	6.6
1996	8.6
1997	8.1
1998	9.3
1999	9.3
2000	5.9
2001	7.7
2002	6.5
2003	9.1
2004	5.2
2005	7
2006	6.5
2007	6.4
2008	7.5
2009	8.8
2010	7.7
2011	6.8
2012	4.7
2013	8
2014	6.7
2015	9.2
2016	6.6
2017	6.2
2018	8.6
2019	6.1

2020	7.2
2021	6.3
2022	5

Table 3.2, Maximum Hs values for every year from 1979 to 2022, North West point.

2) ORDER THE YEARLY MAXIMUM VALUES FROM LARGEST TO SMALLEST

Table 3.3 shows the maximum values ordered from largest to smallest with the respective order number “i”

i	Hs max (m)
1	9.5
2	9.3
3	9.3
4	9.3
5	9.2
6	9.2
7	9.1
8	9
9	8.8
10	8.8
11	8.6
12	8.7
13	8.1
14	8
15	8
16	7.7
17	7.7
18	7.6
19	7.5
20	7.5
21	7.2
22	7.2
23	7.1
24	7
25	6.8
26	6.7
27	6.5
28	6.6
29	6.5
30	6.5

31	6.4
32	6.3
33	6.3
34	6.2
35	6.2
36	6.1
37	6
38	6
39	5.9
40	5.9
41	5.6
42	5.2
43	5
44	4.7

Table 3.3, yearly maximum values arranged in descending order, with their respective order number "i", North West point.

3) DETERMINE WHICH CDFS WITH THEIR RESPECTIVE PARAMETERS BEST DESCRIBE THE DATA SAMPLE

The parameters found with "Rstudio" are reported in Table 3.4 for both Gumbel and Weibull CDF.

CDF	GUMBEL		WEIBULL	
	μ (location)	α (shape)	β (form)	α (shape)
MLE	6.64396	1.18584	6.17027	7.85097
MM	6.52176	1.04218	4.60712	7.981075

Table 3.4, Gumbel and Weibull parameters obtained using MLE and MM, North West point.

Then, Gumbel and Weibull cumulative distribution functions (CDFs) have been plotted on a graph as in Figure 3.7 to assess the goodness of fit. Additionally, the non-exceeding probability of the sample, $F(x)$, has been included. The comparison between the curves indicates that the Gumbel curve exhibits a better fit than the Weibull distribution in terms of both shape (the trend of the curves) and discrepancy (the distance between the sample points and the curves). This analysis suggests that the Gumbel distribution provides a more accurate representation of the population of H_s max compared to the Weibull distribution.

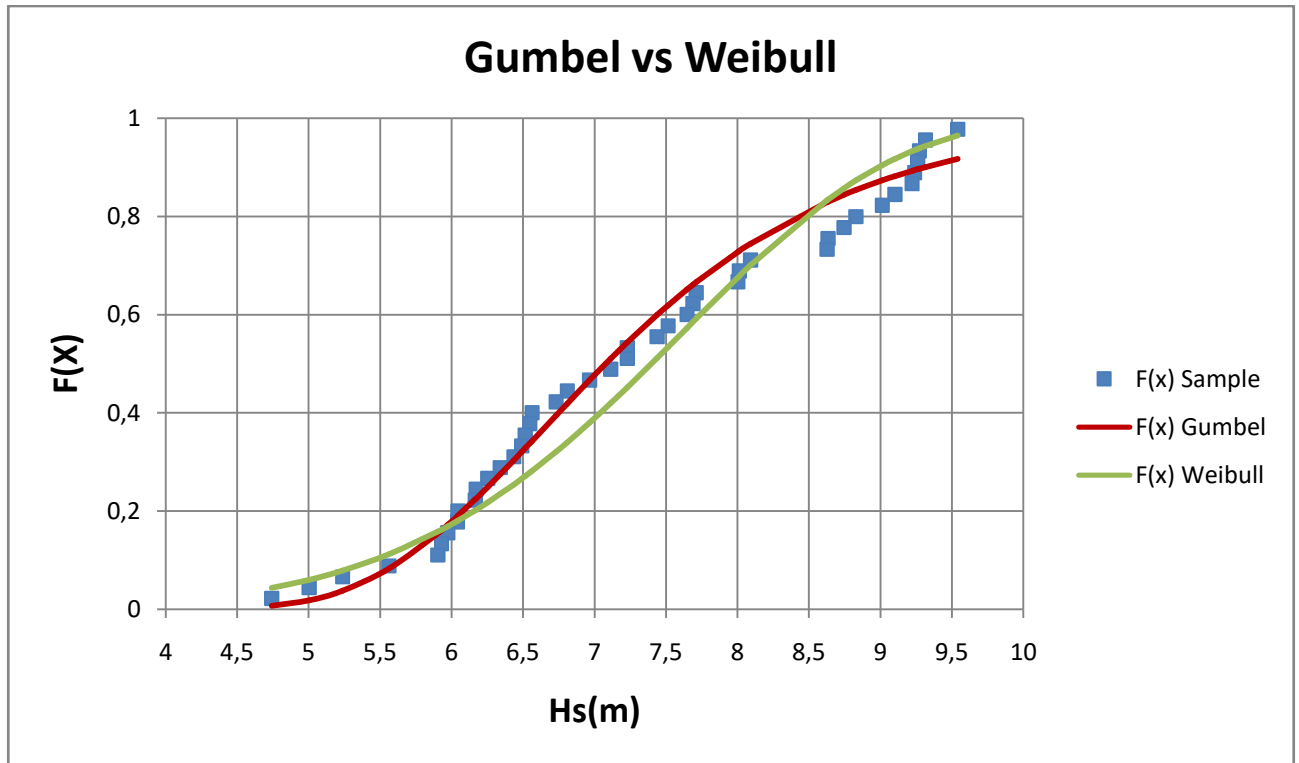


Figure 3.7, Plot comparing frequency distribution relative to the sample of data under consideration with both the Gumbel and Weibull curves to determine which curve provides a better fit to the data, North West point.

The parameters used to create the CDF curves were obtained using MLE method; in fact, Figure 3.8 illustrates the Gumbel CDF curve generated using the parameters derived from both the MLE and Momentum Method, alongside the sample non-exceeding probability. The comparison shows that the CDF curve based on the MLE parameters provides the best fit to the data, in this case in terms of discrepancy rather than shape. This indicates that the MLE method successfully captures the underlying distribution of the data, resulting in a more accurate representation of the non-exceeding probability compared to the Momentum Method.

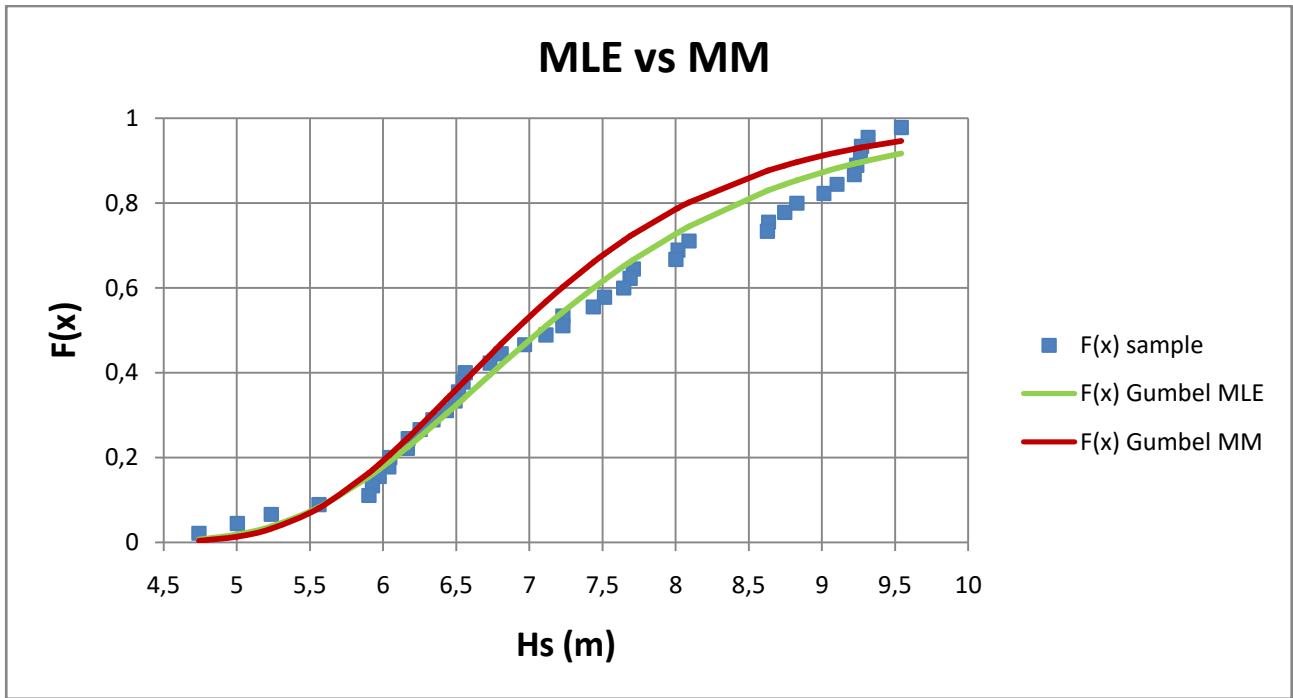


Figure 3.8, Plot comparing the CDFs fitted to the data sample using both MLE method and MM , in order to determine which method provides better parameters for fitting the data, North West point.

4) PEARSON TEST

The Pearson Test was conducted, which resulted in a value of Pearson correlation coefficient of 0.814, corresponding to a p value of $1.78e-10$.

Remember that the Pearson test is a statistical test that allows you to arrive at two possible conclusions: sustain or reject the hypothesis that the frequency distribution relative to the sample of data under consideration is the same theoretical frequency distribution that is being considered, in this case the Gumbel distribution.

Sustaining or rejecting the hypothesis depends on the comparison between the p value and the critical value function of a tolerance threshold, which is often 0,05, value that was taken as a reference in this study.

If $p > 0,05$ the hypothesis that there is no difference between the distributions can be rejected, while the hypothesis that there is a difference can be accepted.

If $p < 0,05$, the hypothesis that there is no difference is sustained.

In this case, it is clear that $p < 0,05$, so the conclusion is that there is no reason to say that the data sample under consideration does not follow a Gumbel distribution having the parameters set out in the previous paragraph.

5) RESULTS

In Table 3.6, values of H_s corresponding to return periods of 10, 20, 50, and 100 years are presented. Following the reasons explained in this chapter, these values have been calculated using the Gumbel distribution, with parameters determined using MLE method. The methodology used to obtain the results presented in Table 3.6 is summarized in Table 3.5.

CDF	GUMBEL
CDF equation	$F(x) = \exp\left(-\exp\left(-\left(\frac{x-\mu}{\alpha}\right)\right)\right)$
μ (location parameter)	6.643964
α (shape parameter)	1.185836
Hs equation	$H_{S_{R_p}} = \mu + \alpha * -\ln\left(\ln\left(\frac{R_p}{R_p - 1}\right)\right)$

Table 3.5, CDF used with relative parameters and equation to calculate the Hs values corresponding to a given Return Period, North West point.

Return Period(years)	Hs(m)
10	9.3
20	10.2
50	11.3
100	12.1

Table 3.6, Hs values corresponding to return periods of 10, 20, 50, and 100 years, calculated using the Gumbel distribution, with parameters determined using MLE method, North West point.

To conclude this analysis, the results obtained downstream of the extreme values analyses were compared with the similar values relating to the Hs for assigned return time reported on the Metoceanview website. Please note that the data provided by this website was used to carry out the analysis, and therefore the results should not be very different.

In fact, Table 3.7, which shows Hs values corresponding to 1, 5, 10, 50 and 100 years reported on the Metoceanview website, shows that the values of Hs that can be compared between Table 3.6, where there are the Hs calculated in this study, and Table 3.7, are very similar to each other.

	Return period [years]				
	1	5	10	50	100
significant height of wind and swell waves <i>m</i>	8,5	9,6	10,1	11,1	11,6

Table 3.7, Hs values corresponding to 1, 5, 10, 50 and 100 years of Return Period reported on MetoceanView website.

3.3 SUMMARY

In this chapter, further analyses have been conducted on the Hindcast data already examined in Chapter Two, with a focus on the three points closest to the southwest coast of the island of Madeira. These analyses will be of fundamental support in the next chapter, particularly in defining the boundary conditions for simulating wave conditions from offshore to the shoreline along the southwest coast of the island. Below are the key conclusions drawn from the analyses presented in this chapter:

- Section 3.2.1 illustrated the joint behaviour of Hs and Tp, highlighting firstly the presence of the physical limit in deep waters due to wave breaking (see equation 3.1), and secondly, it provided crucial insights into how Tp behaves with varying Hs, see Figure 3.3. This aspect will be essential in determining the Tp to be used in the boundary conditions of the simulations discussed in Chapter 4, as described in Section 4.3.2.
- The analysis of monthly variations conducted in Section 3.2.2 revealed more significant changes during the winter months. However, these variations were assessed to fall within a normal range, as depicted in Figure 3.6.
- The analysis of extreme values, carried out using the Method of Annual Maximum as described in Section 3.2.3, yielded the values of Hs with return periods of 10, 20, 50, and 100 years, as shown in Table 3.6. The Hs with a 50-year return period was found to be 11.3 meters, while the Hs with a 100-year return period was found to be 12.1 meters.

4 SIMULATIONS

Methodology and results of the simulations carried out to propagate wave conditions from deep water to the coast

4.1 INTRODUCTION

To carry out engineering projects, studies about the propagation of waves from offshore to inshore are commonly required.

Starting from the data in deep water, the propagation of waves towards the shallow water is often studied using specific software.

These software are able to perform simulations that propagate the deep water characteristics of the waves towards the shallow water and then towards the coast, following a series of assumptions and equations that are the basis of the software itself, in accordance with the bathymetry that presents the area being examined.

Recalling the studies carried out in chapters 2 and 3 and the related considerations and conclusions, in this chapter the data analyzed in the previous chapters will be used and inserted as boundary conditions of STWAVE, a software capable of propagating the offshore conditions of the waves towards the coast.

This chapter consists of a first part in which the operation of the software used is explained, in particular the equations that underlie it. The choices of the boundary conditions entered to complete the simulations carried out with STWAVE will then be justified.

The bathymetry used as a basis for the simulations will then be presented, as well as two other bathymetry with which a comparison will be conducted in chapter 5.

Finally, the results of 9 different simulations will be presented, each with a different trio of H_s , T_p and Dir , following the H_s variations in points and arcs, both along the entire area of interest, or the portion of the coast that goes from Ponta do Pargo to Funchal, and in specific parts of the coast, in order to illustrate how different conditions of deep water waves can propagate towards different parts of the coast

4.2 SOFTWARE: STWAVE ON SMS

As previously mentioned, all the simulations have been done using STWAVE, a software able to propagate waves condition from deep water to the coast, using deep water H_s , T_p and Dir as boundary conditions.

STWAVE is a numerical modelling software capable of simulating and analyzing wave transformation. It is commonly employed in studies aiming to comprehend wave behaviour and their interaction with coastal areas and structures. STWAVE is a component of SMS (Surface water-Modelling System), a software package developed by Acquaveo, able to perform surface-water simulations in a three dimensional environment.

STWAVE operates as a spectral wave model based on the wave action balance equation. In this paragraph, the equations that serve as the foundation for the software will be presented, following an explanation of the underlying assumptions.

4.2.1 MODEL ASSUMPTIONS

According to the manual of the software, (Acquaveo) the most important assumptions made while running the simulations with STWAVE are the following:

- Phase-averaged: The relative phases of the spectral components are random, and phase information is not tracked.
- Mild bottom slope and negligible wave reflection: Waves reflected from the shoreline or steep bottom features are neglected.
- Steady-state waves: STWAVE is suitable for wave conditions that change at a slower rate than the time it takes for waves to propagate across the domain.
- Linear refraction and shoaling: STWAVE does not consider wave asymmetry or other nonlinear wave features.
- Wave-current interaction is neglected

While the first four assumptions presented are made by the software itself, the decision not to take into account wave-current interaction was made manually.

4.2.2 EQUATIONS

STWAVE simulates, among other things, the refraction and shoaling due to the variation in seafloor depth, the breaking caused by depth and steepness, and the interaction between different waves that redistributes and dissipates energy in a growing wave field.

The main equation used in STWAVE is the wave dispersion relation, given by:

$$\omega^2 = gk * \tanh(kh) \quad (4.1)$$

where:

ω = angular frequency ($\frac{\text{rad}}{\text{s}}$)

g = gravitational acceleration ($\frac{\text{m}}{\text{s}^2}$)

k = wave number (m^{-1})

d = water depth (m)

This equation is iteratively solved to obtain the wave number K .

To account for shoaling and refraction, the wave celerity C , and group celerity C_g are computed as follows:

$$C = \frac{\omega}{k} \quad (4.2)$$

$$C_g = 0,5 * C * \left(1 + \frac{2kd}{\sinh(2kd)}\right) \quad (4.3)$$

The wave orthogonal direction is determined using the following equation

$$C_g \frac{Da}{DR} = - \frac{CK}{\sinh 2kd} * \frac{Dd}{Dn_0} \quad (4.4)$$

Where

a= wave orthogonal direction (normal to wave crest)

D= total derivative

R= coordinate in the direction of the wave ray

n_0 = coordinate normal to the wave orthogonal

The wave ray direction is the same as the wave orthogonal direction, as wave-current interactions are neglected.

Finally, the governing equation for steady-state conservation of spectral wave action along a wave ray accounting for wave-current interaction is

$$(C_g)_i \frac{\partial}{\partial x} \frac{C C_g \cos a E(\omega, a)}{\omega} = \sum \frac{S}{\omega} \quad (4.5)$$

Where

E=wave energy density divided by both ρ_w (density of water) and g

S= energy source and sink terms

So to explained what has just been reported, the wave spectrum is calculated by back tracing a wave ray for each component of frequency and direction of the spectrum.

The 2D wave spectra are set as input along the first column of the grid holding the simulation, i.e. on the offshore boundary. Derivatives of depth are estimated and substituted into the equations to calculate the wave orthogonal direction at the previous column.

The wave number(Equation 4.1) , wave celerities(Equation 4.2), group celerities(Equation 4.3), and wave ray angles (Equation 4.4)are then calculated in the previous column or row.

Finally, the energy is computed as a weighted average of energy between two adjacent grid points using the conservation of wave action along a ray (Equation 4.5)

The wave breaking criterion used in STWAVE is both function of wavelength and water depth.

$$H_{mo_{max}} = 0,1L \tanh kd \quad (4.6)$$

Where

$H_{mo_{max}}$ =maximum energy based zero moment wave height

L=wavelength

As it concerns bottom friction, STWAVE includes two formulations:

- JONSWAPP
- Manning's n

For this study, JONSWAPP formulation has been used, where the spectral energy loss due to bottom friction is given by

$$S_{bf} = -\frac{1}{C_g} C_f \frac{\sigma^2}{(\sinh kd)^2} E(f, a) \quad (4.7)$$

Where

f= wave frequency

C_f =friction coefficient

4.3 BOUNDARY CONDITIONS

As previously mentioned, in order to perform the simulations, STWAVE requires the 2D spectra as an input, i.e. H_s , T_p and Dir need to be specified in the first column of the grid holding the simulation.

Referring to the data collected and analyzed in the previous chapters, this paragraph deals with justifying the choice of boundary conditions for each of the simulations that have been launched.

4.3.1 CHOICE OF HS

The first decision to be made was to choose which H_s to use as a boundary condition for each of the simulations launched.

Referring to the discussions carried out in Chapter 2, it is clear that the value of H_s to be taken into account with regard to values in deep water, depends directly on which side of the island the waves are considered to come from, in particular the direction of the waves.

For this reason, the simulations were divided into packages depending on their direction.

As far as the directions are concerned, the subdivision already used in chapter 2 has been followed, i.e. the one shown in figure 2.3, where 16 different directions interspersed with 22.5° have been assigned a number from 0 to 15, with the North direction ($0^\circ N$) assuming the number 0, and the following directions clockwise assuming the following numbers, until you get to the direction corresponding to $337.5^\circ N$ to which corresponds the number 15.

The directions will be called from now on with the respective number.

It follows the description of the two packages in which simulations were divided.

Package 1:

This package includes the simulations propagating waves coming from direction 12 to 15, with also 0 direction to show the shadow effect of Madera discussed in Chapter 2(see paragraph 2.3). This package clearly contains all the simulations having waves coming from the fourth quadrant (West, North West and North), and it is summed up in Figure 4.1.

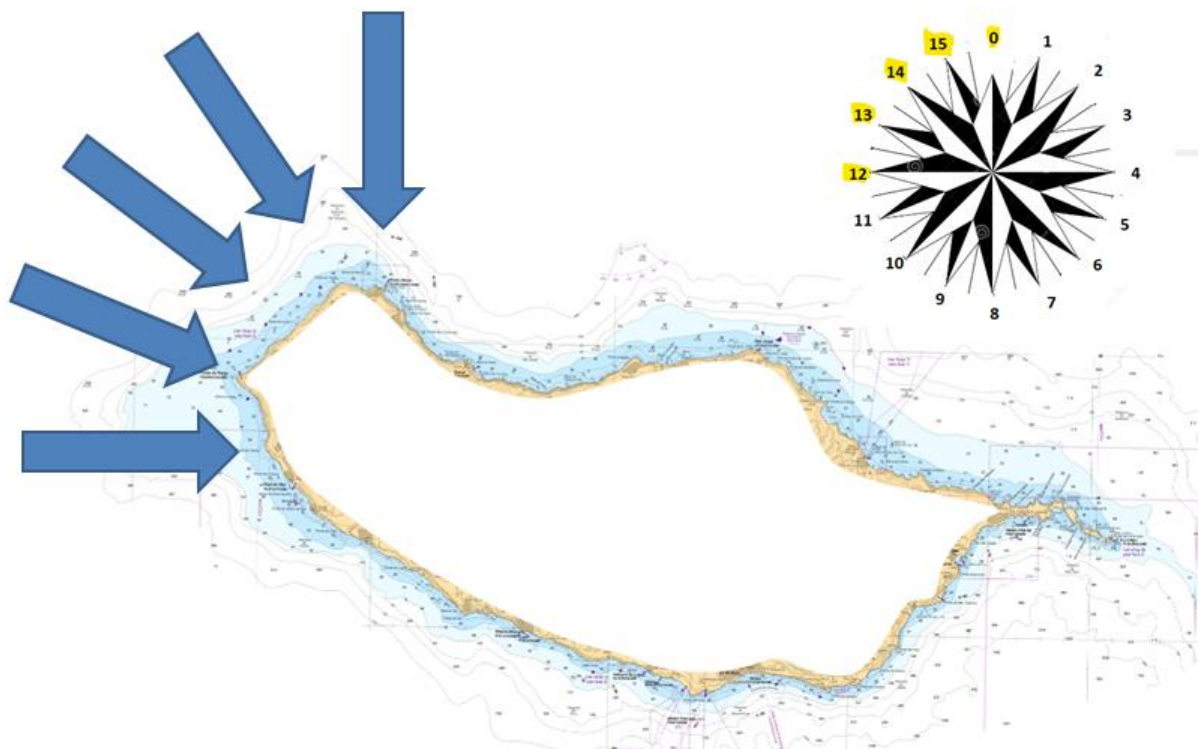


Figure 4.1, Madeira Island, Package 1 of simulations with waves coming from 12 to 15 direction, and 0.

It is reminded that, in line with the conclusions drawn from Chapter 2 in paragraph 2.5, wave climate conditions on the west side of the island can be considered almost constant. To support this hypothesis, the comparison between the direction distribution of North West and South West points is presented in Table 4.1 and Table 4.2, where directions having more than 10% of the whole amount of data are highlighted.

N Dir	Dir (°N)	N Data	Data(%)
0 (North)	0	25837	20.48
1	22.5	15880	12.587
2	45	2249	1.783
3	67.5	294	0.233
4 (East)	90	100	0.079
5	112.5	60	0.048
6	135	69	0.055
7	157.5	82	0.065
8 (South)	180	119	0.094
9	202.5	211	0.167
10	225	407	0.323
11	247.5	1159	0.919
12 (West)	270	4141	3.282
13	292.5	15693	12.439
14	315	28682	22.735
15	337.5	31110	24.659

Table 4.1 direction distribution, North West point.

N Dir	Dir (°N)	N Data	Data(%)
0 (North)	0	26434	20.953
1	22.5	7820	6.199
2	45	913	0.724
3	67.5	256	0.203
4 (East)	90	123	0.097
5	112.5	102	0.081
6	135	96	0.076
7	157.5	105	0.083
8 (South)	180	137	0.109
9	202.5	223	0.177
10	225	410	0.325
11	247.5	1140	0.904
12 (West)	270	3884	3.079
13	292.5	16877	13.378

14	315	31478	24.951
15	337.5	36109	28.622

Table 4.2, direction distribution, South West point.

These tables shows that the values are distributed in a very similar way, with the majority of the waves having a direction pointing at the coast of Madeira.

For this reason the same value of H_s will be used as the initial condition for all simulations in Package 1.

As it concerns the choice of this unique value of H_s , it is necessary to refer to extreme values analyse made in Chapter 3.

Table 4.3 and 4.4 display the values of H_s obtained after extreme value analysis for NW and SW points, respectively

NW	
RP(y)	Hs (m)
10	9.312531
20	10.16613
50	11.27102
100	12.09899

Table 4.3, Hs for 10,20, 50 and 100 years of return period, North West point.

SW	
RP(y)	Hs (m)
10	9.022242
20	9.858963
50	10.94201
100	11.75361

Table 4.4, Hs for 10,20, 50 and 100 years of return period, South West point

The decision has been to refer to H_s for 100 years of return period, since this value of return period is often used as reference for costal engineering projects. Given the need to take into account two values of H_s relative to 100 years of return time (one for the North West point and one for the South West point) an average was made between the two values, which was approximated to 12 meters, which was therefore the chosen value to be used as a boundary condition of H_s in deep water for all the simulations of package 1.

PACKAGE 2

This package includes all the simulations propagating waves coming from direction 8 to 11, i.e. it contains all the simulation considering waves coming from the third quadrant(South and South West). Figure 4.2 sums it up.

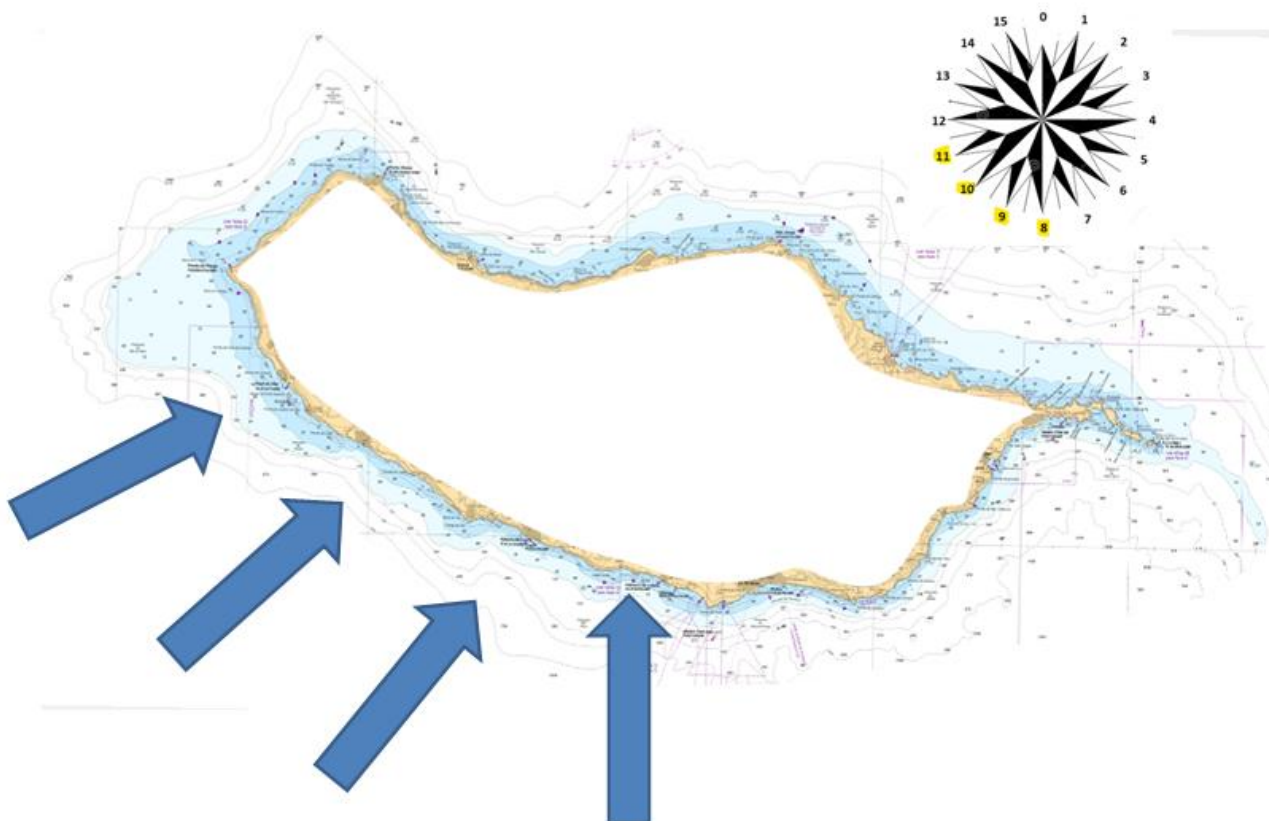


Figure 4.2, Madeira island, Package 2 of simulations with waves coming from 8 to 11 direction

As for package 1, the conclusions drawn on Chapter 2 need to be followed, i.e. that it is not possible to consider constant the deep water conditions off the south side of the island (see paragraph 2.5). For this reason, only the extreme values analysis regarding South point has been considered. The respective results are reported in Table 4.5.

South	
RP(y)	Hs (m)
10	6.902967
20	7.585989
50	8.470092
100	9.132602

Table 4.5, Hs for 10,20, 50 and 100 years of return period, South point.

Although one could think of simply considering the value of Hs relative to 100 years of return time (i.e. 9,13 meters), further considerations are necessary given the distribution of directions that South point presents (Table 4.6).

N Dir	Dir (°N)	N Data	Data(%)
0 (North)	0	9723	7.707
1	22.5	8742	6.929
2	45	6574	5.211
3	67.5	2541	2.014
4 (East)	90	1001	0.793

5	11.,5	485	0.384
6	135	386	0.306
7	157.5	340	0.27
8 (South)	180	432	0.342
9	202.5	768	0.609
10	225	1668	1.322
11	247.5	3617	2.867
12 (West)	270	10822	8.578
13	292.5	31621	25.064
14	315	31783	25.193
15	337.5	15656	12.41

Table 4.6, direction distribution, South point.

It is clear that there is a very low percentage of waves with direction towards the coast of Madeira; in fact, direction 8,9,10 and 11 corresponds to very low values of percentage of waves compared to the total.

This suggests that, of all the Hindcast data used to conduct the extreme values analysis, few of them represented waves that actually affected the southwest coasts of Madeira.

To take this fact into account, the extreme values analyse was conducted again, this time using only data relating to waves having directions belonging to the second and third quadrants (directions 4 to 12), obtaining the results displayed in Table 4.7.

RP(y)	Hs (m)
10	5.870314
20	6.495347
50	7.304387
100	7.910649

Table 4.7, Hs for 10, 20, 50 and 100 years of return period, obtained from extreme values analyse using only waves coming from 4 to 12 direction

So in conclusion, this procedure led to consider an Hs of one meter smaller. Considering the direction distribution displayed in Table 4.6, which demonstrate that more than half of the waves registered in this point have directions that do not head to the coast of Madeira, this seems a sustainable decision: always taking into account a return time of 100 years, the value of Hs chosen as a boundary condition for all simulations belonging to package 2 was that of 8 meters, an approximate value of the one displayed in table 4.7.

4.3.2 CHOICE OF TP

After having established the values of Hs to use, the second boundary condition to decide has been Tp.

To take this decision, it has considered the study presented in chapter 3 regarding the relationship between Hs and Tp. All the histograms displaying the trend of Tp as a function of Hs has been analyzed to decide which Tp to attribute to the values of Hs chosen for the simulations, i.e. 12 and 8 meters of Hs.

In particular, to decide the T_p corresponding to 8 meters (waves coming from the south) the histograms relating to the South and South West points were analyzed (see annex B), while for the choice of the T_p corresponding to 12 meters of H_s (waves coming from North West) the histograms relating to the relationship between H_s and T_p at the North West point, reported in Chapter 3, and in the South West point (see annex B) were analysed.

Following these histograms, the decision has been to use 17 s as T_p for simulations propagating waves with 8 m of H_s , and to use 20 s as T_p for simulations propagating waves having 12 m of H_s .

4.3.3 CHOICE OF DIR

The last boundary condition to be established was which direction to attribute to the waves considered in the simulations.

This decision was made by trying to evaluate as many wave directions as possible, in order to establish what were actually the offshore wave conditions corresponding to the most significant conditions on the coast, while trying to reduce as much as possible the number of simulations.

The decision was to take into account simulations having as offshore wave direction all the directions capable of reaching the southwest coast of the island of Madeira: directions from direction 8 (180 °N) to direction 15 (337.5 °N) were considered, i.e. 8 consecutive clockwise directions spaced by 22.5 degrees

Furthermore, a simulation propagating waves having direction 0 (0°N) was launched, in order to highlight again the shadow effect discussed in Chapter 2, trying to show how far the waves coming from the north were propagated in the southern part of the island

In this way, 9 different simulations were launched, and consequently the respective results were analyzed and compared with each other.

These 9 simulations are reported with the respective boundary conditions on Table 4.8.

N° SIMULATION	H_s (m)	T_p (s)	Dir	Dir (° N)
1	12	20	14	315
2	12	20	15	367,5
3	12	20	13	292,5
4	12	20	12	270
5	12	20	0	0
6	8	17	10	225
7	8	17	11	247,5
8	8	17	8	180
9	8	17	9	202,5

Table 4.8, simulation with respective H_s , T_p and Dir

4.4 BATHYMETRY

As mentioned before, after establishing the boundary conditions, i.e. the offshore values of H_s , T_p and Dir of the wave to be considered, STWAVE also needs the information about the bathymetry in the area where the waves are propagated in order to run the simulations.

As it will be shown in Chapter 5, the results of a simulation can considerably vary depending on the bathymetry, and it is therefore important to use a bathymetry that is at the same time as precise as possible and that covers the area necessary in order to complete the simulation.

For this study, 3 different sources were made available to derive a bathymetry for use in simulations:

- Bathymetry from a navigation map
- Bathymetry from the Web
- Bathymetry from a survey scatter set

As will be shown later, these three bathymetries possess varying degrees of accuracy. This aspect will be discussed in detail in Chapter 5, where it will be demonstrated how the bathymetry used to conduct a simulation and its corresponding accuracy can impact the simulation results.

The Navigation map, the Web and the survey scatter set provided the necessary information in order to create bathymetry with which simulations could be conducted.

The bathymetry from the navigation map was obtained manually creating a scatter set using the bathymetry lines in a scanned picture of the map, showed in Figure 4.3.

The bathymetry created using the scatter set is hereafter referred to as Bathymetry map.

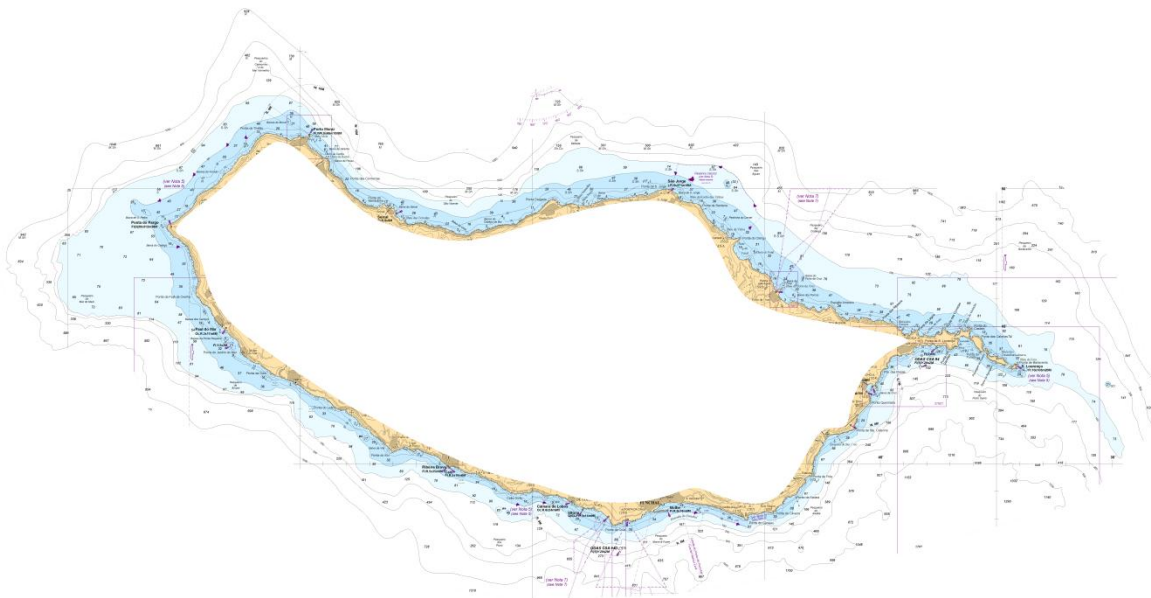


Figure 4.3, Madeira Island, navigation map used to manually create the scatter set with the depth.

As for the bathymetry coming from the web, a GeoTiff file was downloaded from the Web(Figure 4.4), which was converted with a STWAVE tool into a scatter set and consequently into a bathymetry that can be used in simulations

This scatter set and the consequential bathymetry is hereafter referred to as Bathymetry web.

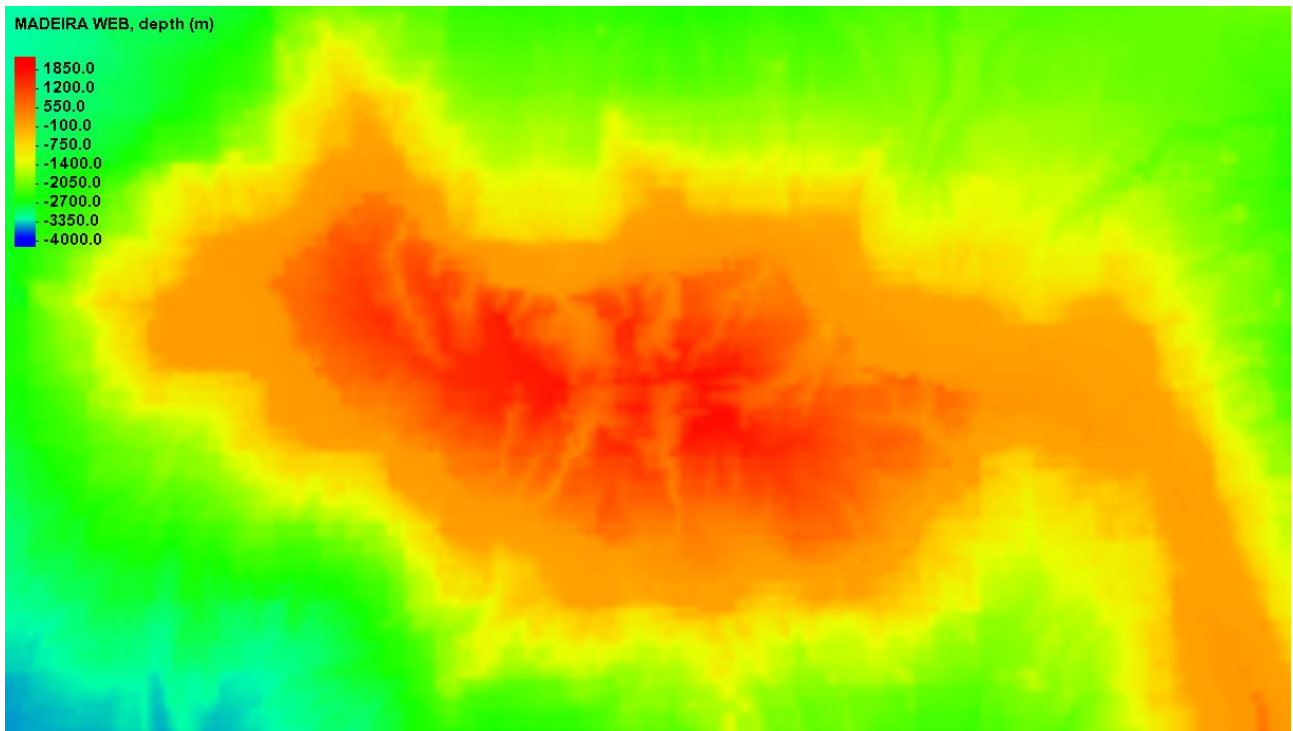


Figure 4.4, Madeira Island, Bathymetry downloaded from the Web, GeoTiff file.

Finally, information from a detailed survey carried out on the coasts of a portion of the southwest coast of Madeira was provided as a scatter set.

Covering this scatter set only a limited portion of the coast, it was necessary to join to this scatter set some points from the navigation map mentioned above.

The bathymetry obtained in this way, which is shown in Figure 4.5, will be called Bathymetry survey scatter set.

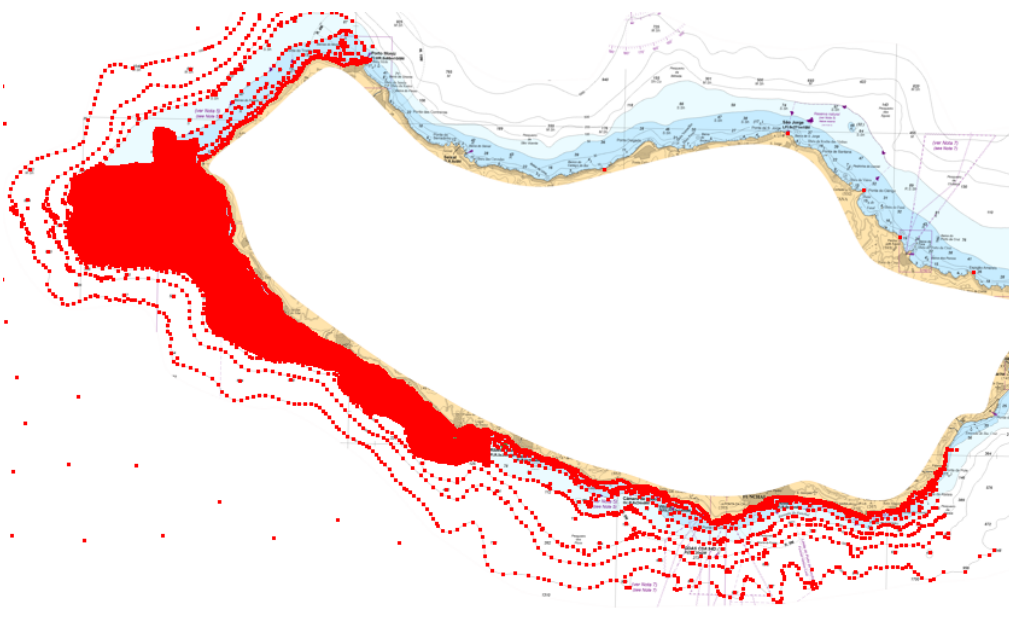


Figure 4.5, Madeira Island, survey scatter set merged with points of the Bathymetry Map in order to create the Bathymetry survey scatter set.

All the simulations whose results will be reported below in this chapter 4, have been obtained using the Bathymetry map as a basis.

Later, in Chapter 5, the simulations to which the most significant results corresponded, were launched again with both Bathymetry Web and Bathymetry survey scatter set as a basis.

4.5 GRID RESOLUTION

As previously mentioned, boundary conditions are specified on one side of the grid, and, by launching the simulation, these conditions propagate row by row, in accordance with, among other things, the depth corresponding to each cell of the grid, i.e. the bathymetry imported to the grid.

It is intuitive how the results of the simulations can certainly improve in terms of accuracy by increasing the number of cells that compose the grid.

At the same time, using grids with lots of cells can result in an unsustainable amount of time required to complete simulations.

While specifying the dimension of the cells composing the grid holding the bathymetry, both the previous factors need to be taken into account.

It has been tried to analyze the relationship between the improvement in terms of precision and the reduction of the size of the cells, with a consequent increase in the number of them, constituting the grid.

In fact, since each bathymetry has its own precision, increasing the number of cells may not always lead to the same improvements in terms of accuracy.

This analyse has been conducted running 4 simulations with same boundary conditions and the same bathymetry as basis, using different cell dimension each time: simulations leaning on grids having 100, 60, 40 and 10 meters as cell dimension have been run.

Then, an observation arc has been used to compare the results. Figure 4.6 displays the results obtained

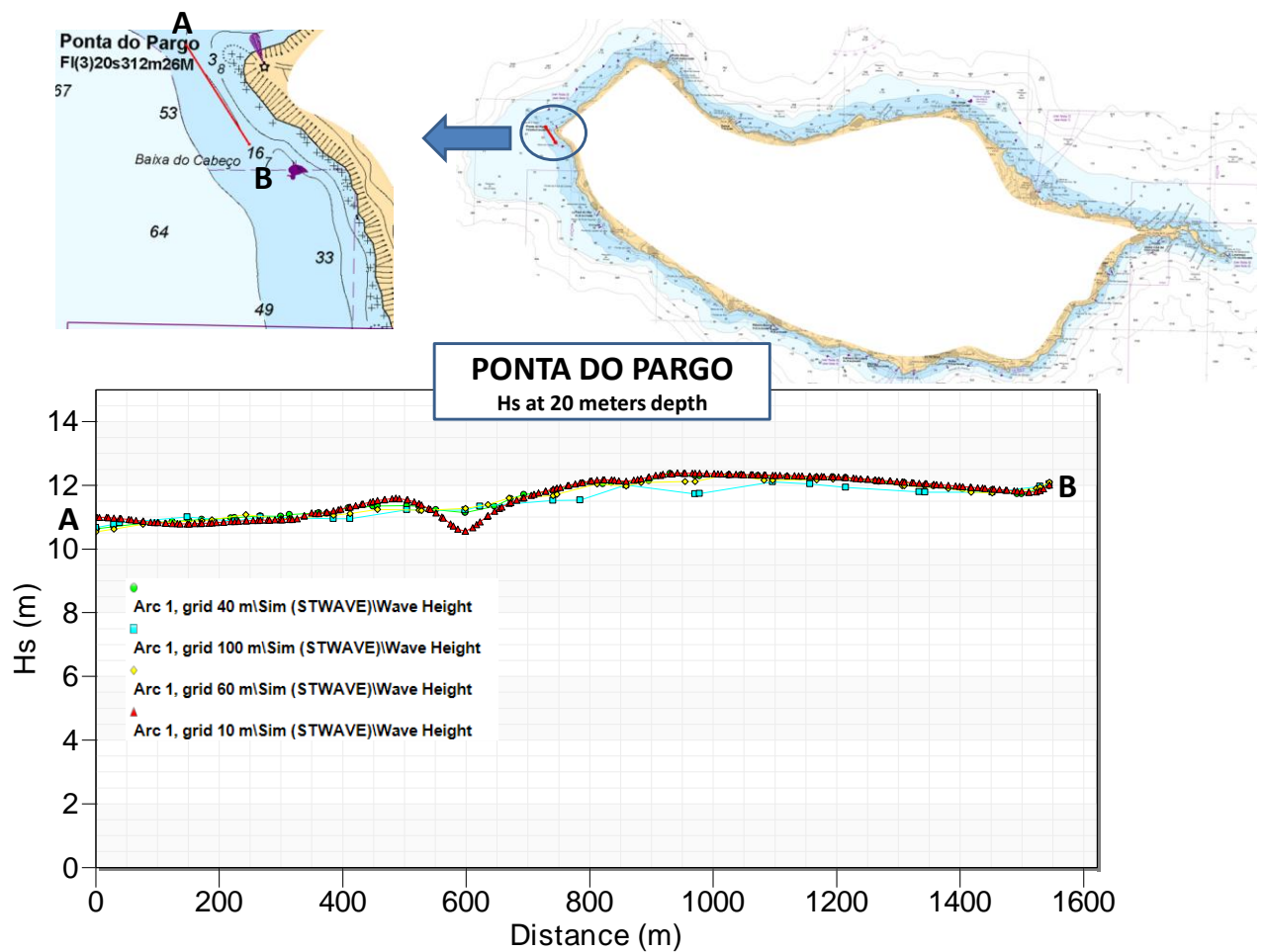


Figure 4.6, comparison of results obtained with 10, 40, 60 and 100 meters cells grid, Ponta do Pargo.

Looking at the different curves corresponding to different cells size, it can be said that the curve corresponding to the results of the simulation with cells of 100 meters is considerably distant from the rest of the curves, demonstrating a difference in results which, assuming increasing precision while increasing the number of cells, suggests the need to use smaller cells.

At the same time the discrepancy between the curves relative to 10 and 40 and 60 meters it is not so marked, except for a small portion of the graph.

Therefore, considering that a significant additional amount of time is required to carry out simulations with grids having cells of 10 meters compared to cells of 40 or 60 meters, it was established sufficient to use cells of 40 or 60 meters.

Then having to choose a number of cells in this range, it was decided to use cells with dimensions of 40 meters, given the negligible difference in time between carrying out simulations with 40 or 60 meters.

So, to conclude, the simulations that are presented below have been launched having Bathymetry map as a base on a Grid having cells of 40 meters.

4.6 RESULTS

The results are presented first of all by referring to six monitoring points, to provide a first idea of the trend of the results in several areas of the island, and then in detail for each simulation referring to 4 observation arcs.

The six points were chosen trying to cover the entire area from Ponta do Pargo to Funchal, thus interspersing the six points from approximately constant distances.

Figure 4.7 shows these six points: Ponta do Pargo and Ponta do Foja do Ovelja in the North West part, Hotel (Calheta) and Lugar de Baixo in the Central West and Cabo Girao and Funchal in the South part.

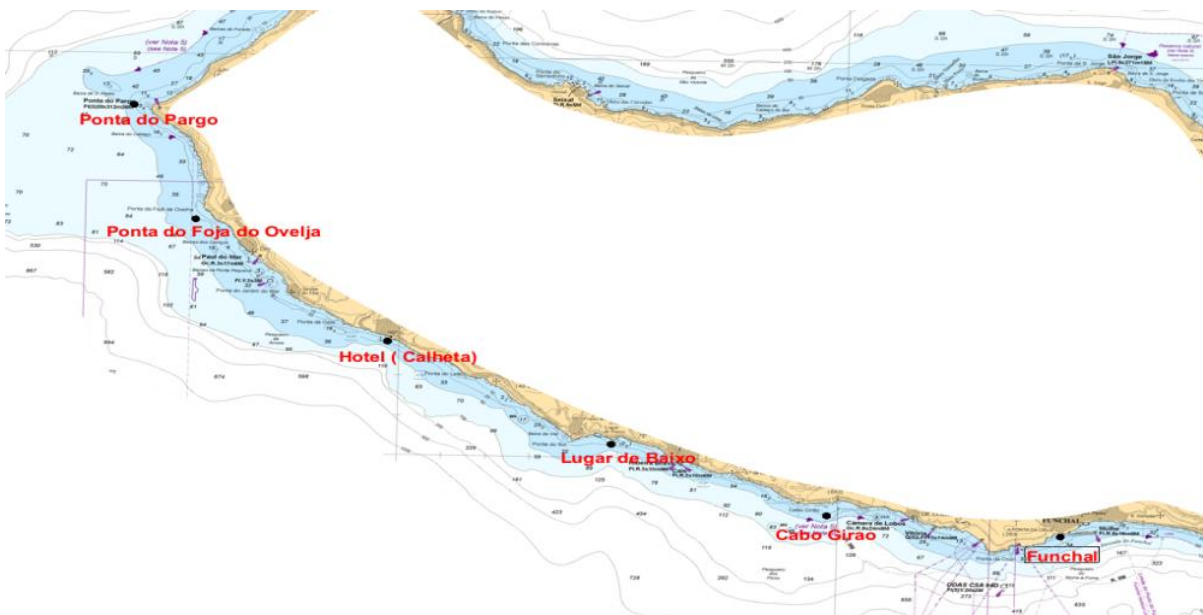


Figure 4.7, Madeira Island, 6 monitoring points: Ponta do Pargo, Ponta do Foja do Ovelja, Hotel (Calheta), Lugar de Baixo, Cabo Girao and Funchal.

Table 4.9 sums up the values of Hs in the six monitoring points presented in Figure 4.7.

position on the island	LOCATION	N° SIM	1	2	3	4	5	6	7	8	9
NW	Ponta do Pargo		10.61	9.75	10.86	11	9.67	10.6	10,08	4,98	7.75
NW	Ponta do Foja Ovelja		11.38	10.2	11.67	11.47	6.44	8.96	9	6,6	7.68
CW	Hotel (Calheta)		0.83	0.23	2.03	5.12	0.01	6.85	5.91	5,93	6.96
CW	Lugar De Baixo		0.41	0.02	4.18	7.28	0	6.37	6.27	6,65	6.15
S	Cabo Girao		0.57	0.03	3.33	8.7	0	8.46	8.62	8,73	8.45
S	Funchal		0	0	0.1	4.68	0	3.47	4.52	4,32	5.54

Table 4.9, Hs for every simulation in each of the monitoring points

Remembering that each simulation is characterized by one direction as in Table4.8

Looking at the results shown in the table, the following comments can be drawn:

- As for the two points situated in North-West part of the Island (Ponta do Pargo and Ponta do Foja Ovelja) the biggest Hs values are obtained from simulation 3 (offshore direction 292.5 °N) and simulation 4 (offshore direction 270 °N). In addition, in this area all simulations produce significant values of Hs, even simulation 5 (offshore direction 0°N).
- As for the central part of the stretch of the coast being studied, in the first point (Calheta) the highest Hs correspond to simulation 9 (offshore direction 202.5 °N), while for Lugar de Baixo it happens for simulation 4 (offshore direction 270).
Also, in this area the waves of simulation 1 (offshore direction 315 °N), simulation 2 (offshore direction 367.5 °N) and simulation 5 (offshore direction 0 °N) do not reach the coast with considerable values.
- As for the points situated in the south part of the Island, the biggest values of Hs are obtained with simulations with the waves coming from South, in particular simulation 9 (offshore direction 202.5 °N).
Also, as for the central part of the Island, the waves coming from North and North West are not relevant anymore, but still the waves coming from west are able to reach this part of the coast.

Subsequently, four observation arcs were created, to simultaneously evaluate the trend of Hs in a larger area. Observation arcs can provide more reliable results than monitoring points, as they show the trend of Hs in larger areas and not in individual points. The arcs were created following the bathymetry of 20 m depth contour. These 4 observation arcs are showed in Figure 4.8: Ponta do Pargo, Calheta, Lugar de Baixo and Funchal.



Figure 4.8, Madeira Island. Observation arcs at 20 m depth contour: Ponta do Pargo, Calheta, Lugar de Baixo and Funchal

The results of the simulations propagating waves from the northwest quadrant, i.e. simulations 1, 2 and 3, will first be presented. Then follow the results obtained for simulations 6, 7 and 8, which propagate waves coming from the south.

The results of simulation 4 (offshore direction 270 °N) and simulation 9 (offshore direction 202.5 °N), will then be presented together to present a comparison between a simulation propagating waves from the West and a simulation propagating waves from the South.

In addition, the results of simulation 5 (offshore direction 0 °N), will be presented to confirm the shadow effect produced by the island itself.

4.6.1 SIMULATION WITH WAVES COMING FROM WEST

As mentioned, the results of simulations propagating waves coming from West will be presented first, starting from simulations 1 and 2 (Table 4.10) and then following with simulation 3 (Table 4.11).

Simulations 1 and 2

N° SIMULATION	Hs (m)	Tp (s)	Dir	Dir (° N)
1	12	20	14	315
2	12	20	15	367,5
3	12	20	13	292,5
4	12	20	12	270
5	12	20	0	0
6	8	17	10	225
7	8	17	11	247,5
8	8	17	8	180
9	8	17	9	202,5

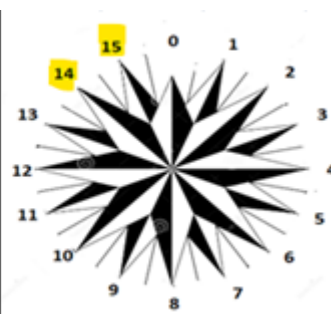


Table 4.10, simulations 1 and 2

Figure 4.9 shows simulation 1 (Hs=12 m, Tp=20 s, Dir=315°N), i.e. the Hs and the vectors representing the wave direction. It is clear how, moving down the south in the coast, lower values of Hs are found, with initial values of more than 8 m at the westernmost point, decreasing until they reach constant values below two meters.

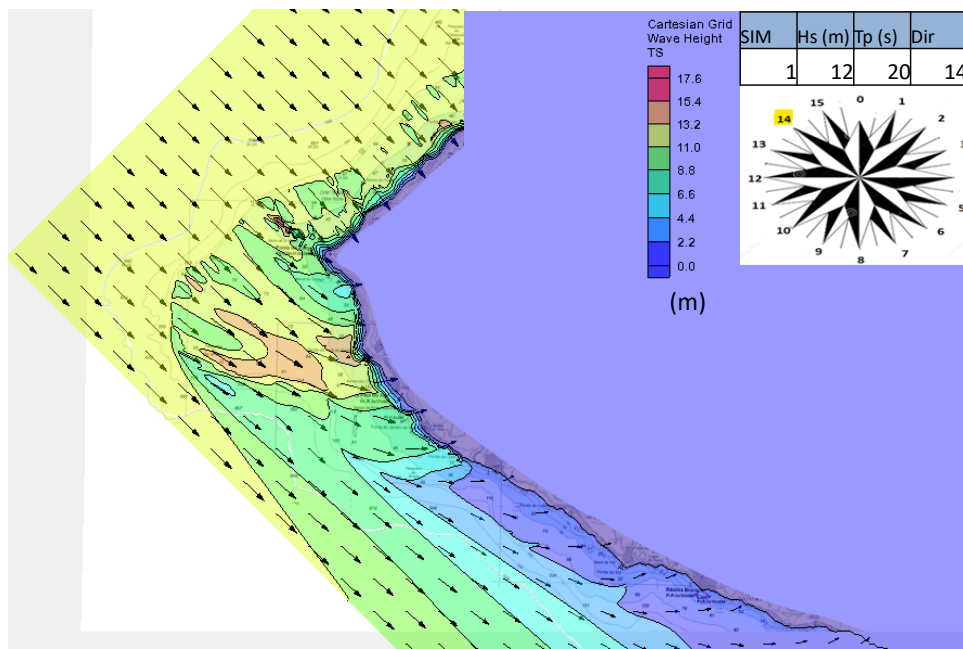


Figure 4.9, Madeira Island. South West part, Hs values and Dir, Simulation 1 (Hs=12 m, Tp=20 s, Dir = 315°N).

In figures 4.10 and 4.11 the Hs values on the observation arcs in front of Ponta do Pargo and Calheta are showed. In Ponta do Pargo the values of Hs vary from 6 to 11 m, with the lower values in the central part of the observation arc.

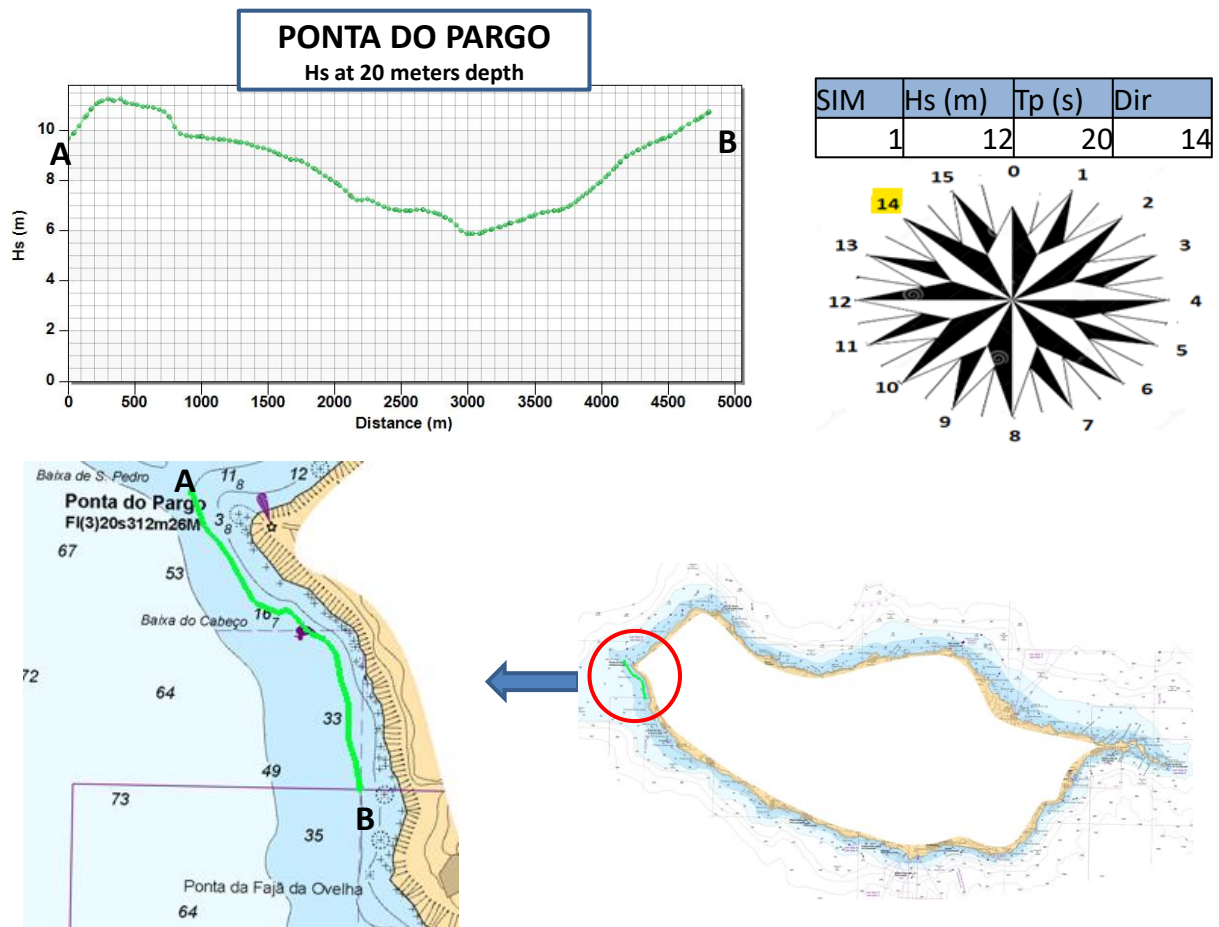


Figure 4.10, Madeira Island, Ponta do Pargo, Hs at 20 m depth, simulation 1 (Hs=12 m, Tp= 20 s, Dir= 315°N).

As it concerns Calheta, the values of Hs drastically decrease compared to the ones observed for Ponta do Pargo, with values between 4 and 0.5 m. This is fully in line with what might have been expected, as Calheta is located further down coast from Ponta do Pargo.

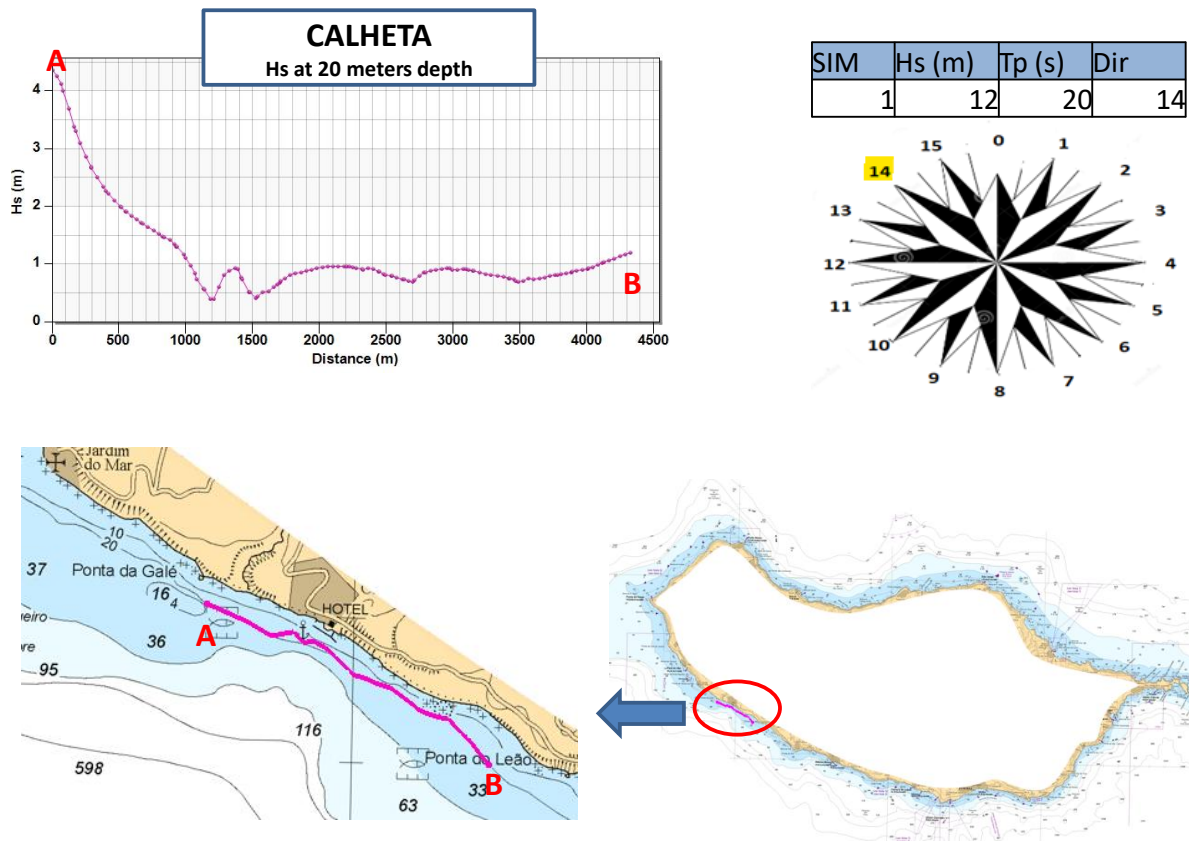


Figure 4.11, Madeira Island, Calheta, Hs variation at 20 meters depth, simulation 1 (Hs= 12 m, Tp= 20 s, Dir =315°N)

Similar results are obtained for simulation 2(Hs=12 m, Tp=20 s, Dir=337,5°N), where the waves reach the southernmost parts of the coast even with lower values (Figure 4.12).

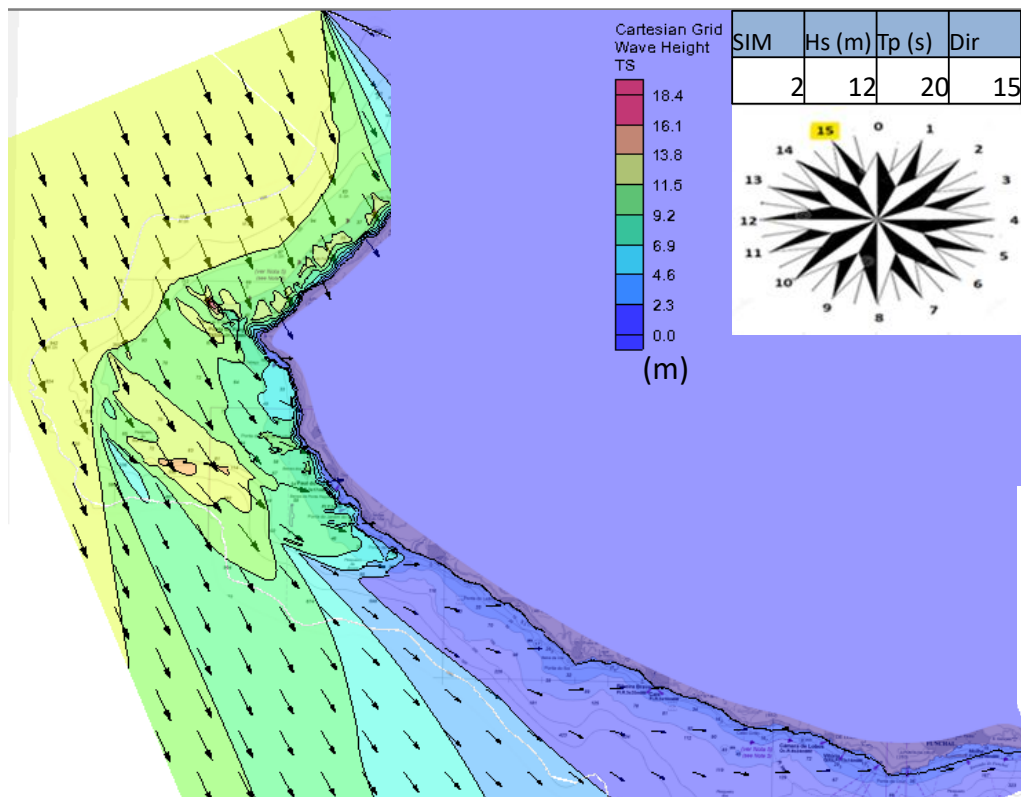
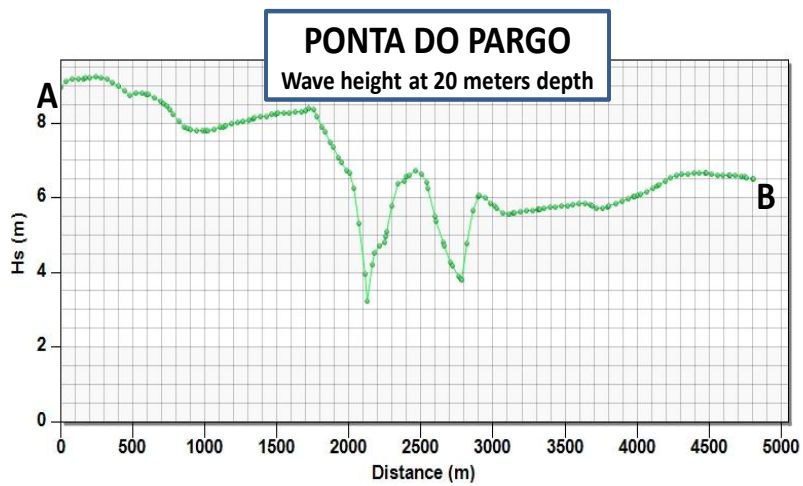


Figure 4.12, Madeira Island, South West part, Hs values and Dir, Simulation 2 (Hs =12 m, Tp =20 s, Dir= 337,5°N).

Figure 4.13 shows the trend of Hs on the observation arc in front of Ponta do Pargo: the values are significantly lower than those observed in Figure 4.10.



SIM	Hs (m)	Tp (s)	Dir
2	12	20	15

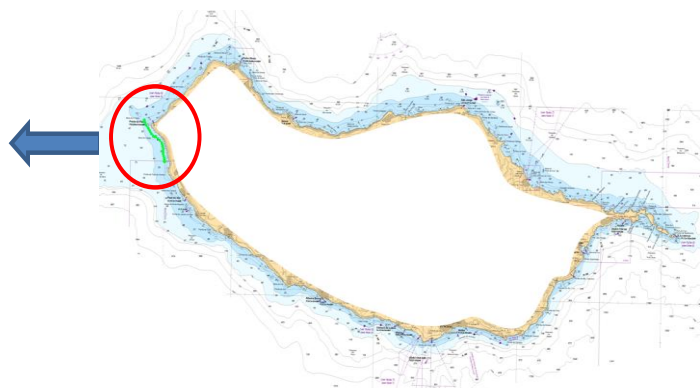
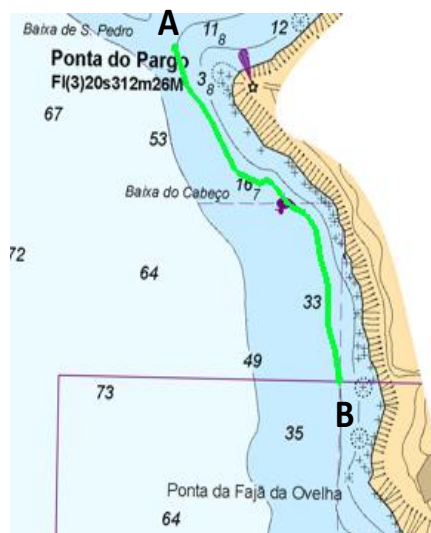
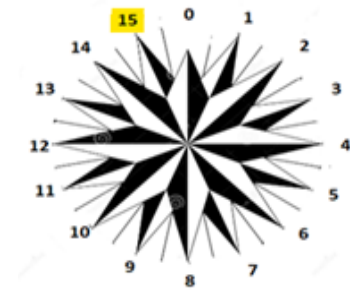


Figure 4.13, Madeira Island, Ponta do Pargo, Hs variation at 20 meters depth, simulation 2 (Hs=12 m, Tp=20 s, Dir=337,5°N).

The same goes for Calheta, where the values of Hs related to simulation 2 in the observation arc shown in Figure 4.14 slightly exceed 1.5 meters, almost always maintaining values close to zero.

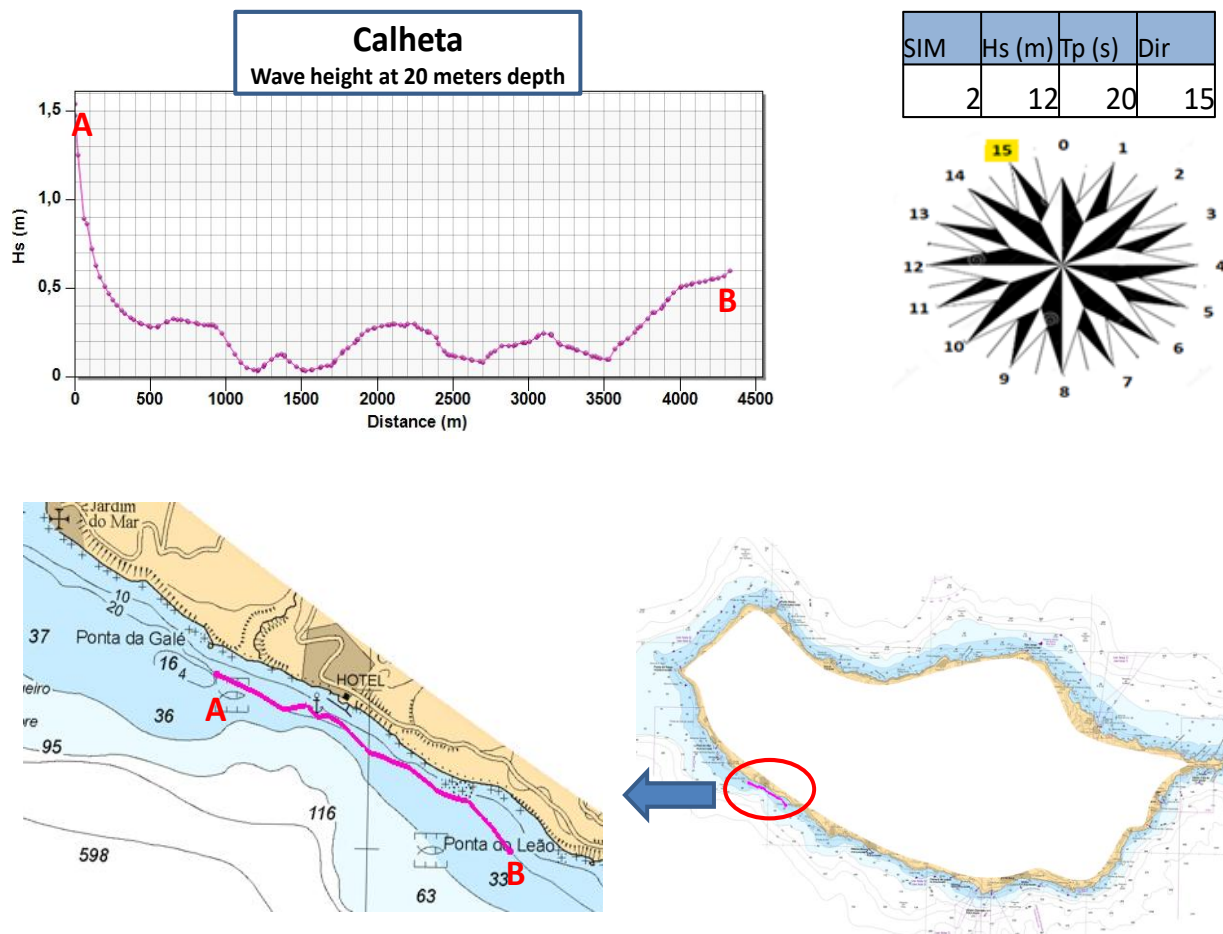


Figure 4.14, Madeira Island, Calheta, Hs variation at 20 meters depth, simulation 2 (Hs= 12 m, Tp= 20 s, Dir=337,5°N).

Simulation 3

After the results of simulations 1 and 2, where the Hs values decreased while changing the direction from 14 to 15, it is now expected to see the values of Hs increasing running simulation 3 (Hs 12 m, Tp 20 s, Dir=292,5 °N). The offshore direction is now WNW.

Nº SIMULATION	Hs (m)	Tp (s)	Dir	Dir (º N)
1	12	20	14	315
2	12	20	15	367,5
3	12	20	13	292,5
4	12	20	12	270
5	12	20	0	0
6	8	17	10	225
7	8	17	11	247,5
8	8	17	8	180
9	8	17	9	202,5

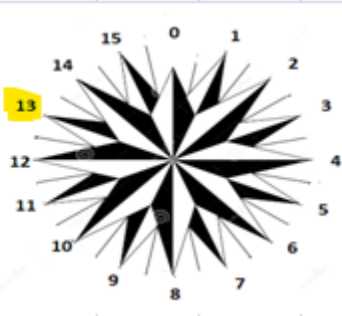


Table 4.11, simulations 3.

These expectations are already reflected in Figure 4.15, especially about the portion of the coast reached by higher values of Hs: it is evident that values of Hs clearly higher than in Figures 4.9 and 4.12 are observed in the central and southern part of the stretch of coast under study.

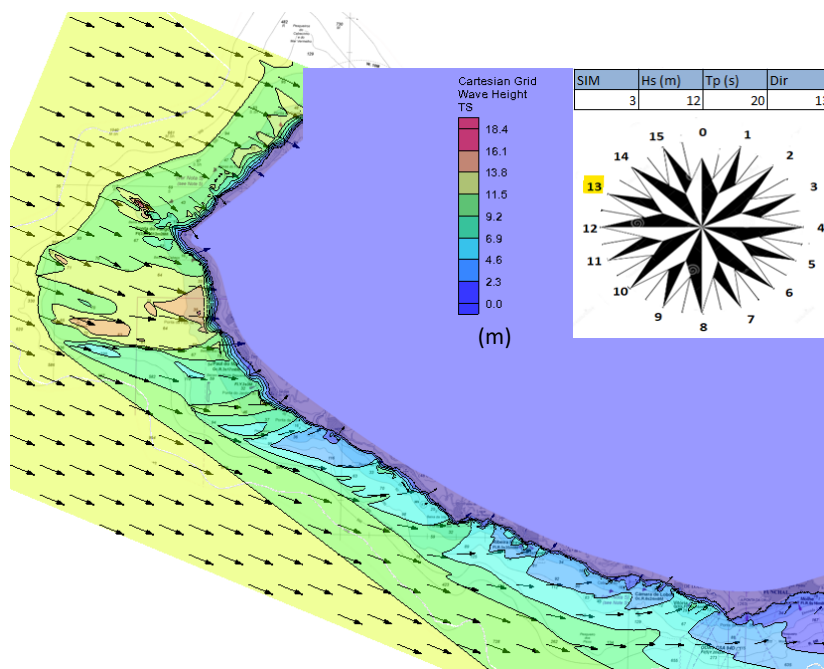
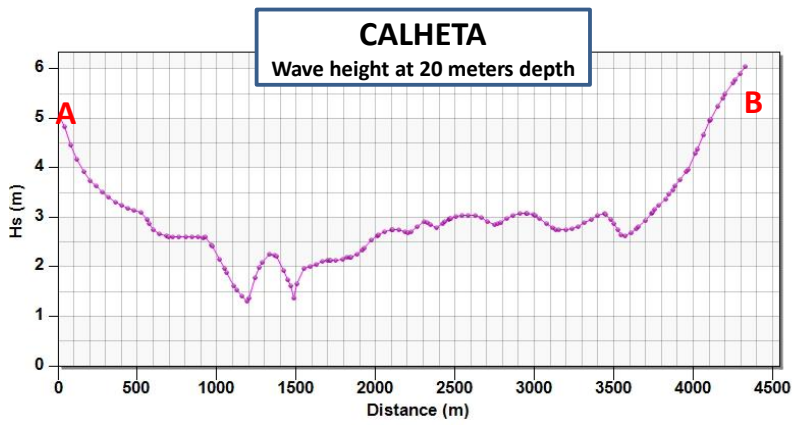


Figure 4.15, Madeira Island, South West part, Hs values and Dir, Simulation 3 (Hs= 12 m, Tp= 20 s, Dir=292,5 ºN).

This statement is also confirmed by Figure 4.16, where the trend of Hs in the observation arc in front of Calheta is showed. Comparing this figure with the analogous figures for simulations 1 and 2 (Figures 4.11 and 4.14), it is clear that the Hs has greater values on the whole arc, which exceeds 5 m in some parts of the arc.



SIM	Hs (m)	Tp (s)	Dir
3	12	20	13

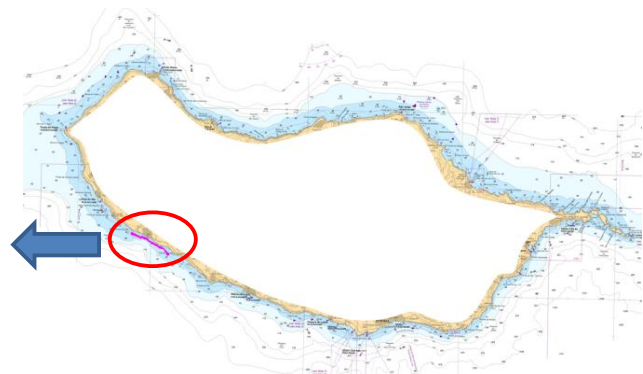
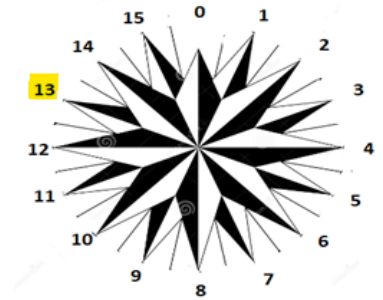


Figure 4.16, Madeira Island, Calheta, Hs variation at 20 meters depth, simulation 3 (Hs= 12 m, Tp= 20 s, Dir=292.5°N).

Moreover, even considering the observation arc in front of Lugar de Baixo, located further south, high values of Hs can be observed, with values greater than 8 m (Figure 4.17).

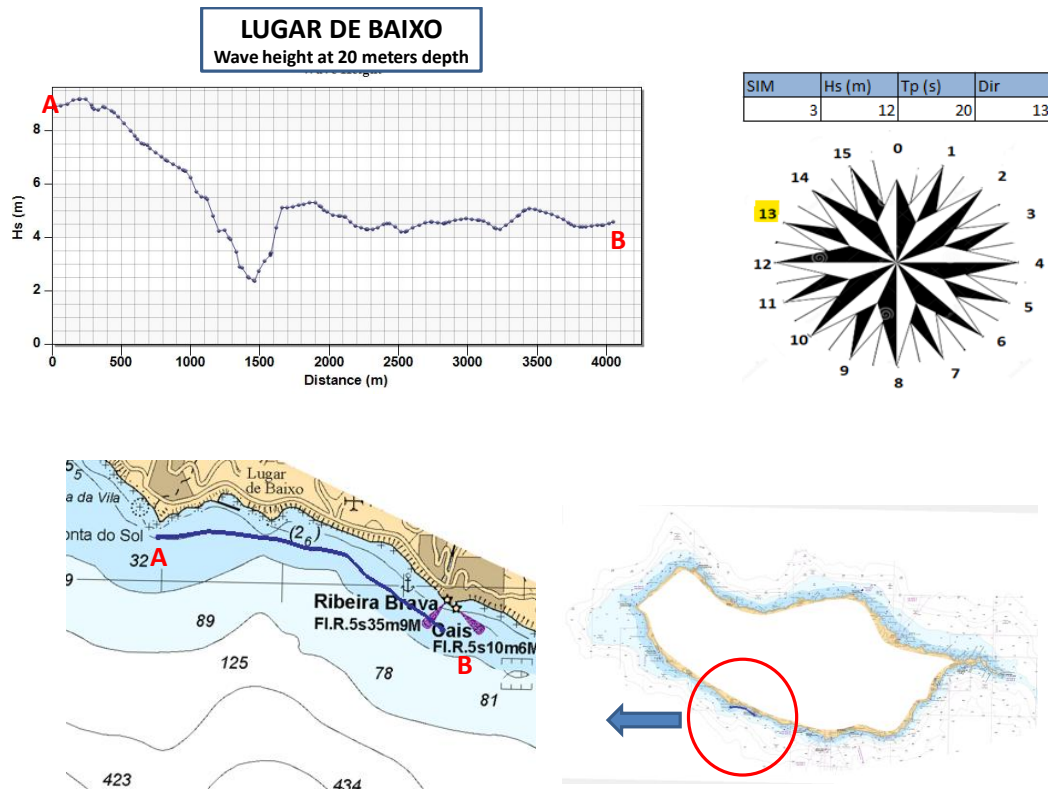
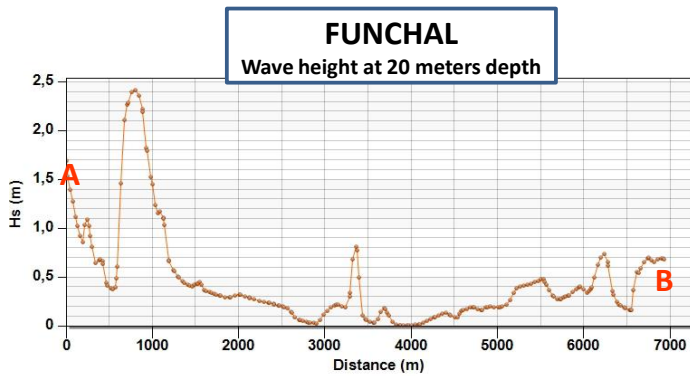


Figure 4.17, Madeira Island, Lugar de Baixo, Hs variation at 20 meters depth, simulation 3 (Hs= 12 m, Tp= 20 s, Dir=292,5°N).

The Hs observation arc in front of Funchal is also shown (Figure 4.18).



SIM	Hs (m)	Tp (s)	Dir
3	12	20	13

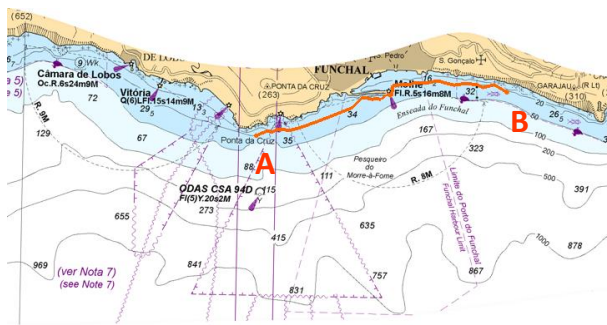
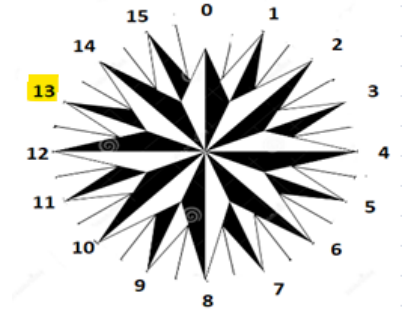


Figure 4.18, Madeira Island, Funchal, Hs variation at 20 meters depth, simulation 3 (Hs= 12 m, Tp= 20 s, Dir=292,5°N).

4.6.2 SIMULATION WITH WAVES COMING FROM SOUTH

After presenting the results for the simulations of waves coming from the northwest, the results of the simulations for waves coming from the south directions follow. As discussed earlier in Chapter 4.3 for all simulations propagating waves from the south, a different value of Hs is used. Three directions on the offshore boundary are considered: SW 225°N, WSW 247,5°N and S 180°N.

The results for simulation 6 (Hs= 8 m, Tp= 17 s, Dir=225°N, simulation 7 (Hs=8 m, Tp= 17 s, Dir=247,5°N) and simulation 8 (Hs 8 m, Tp 17 s, Dir=180°N) are presented.

Simulation 6

The results obtained regarding this simulation with waves from SW, as it will also be for simulations 7 and 8, follow perfectly what had been suggested by the analysis of the results in the monitoring points (Table 4.9).

Figure 4.19 shows Dir, Hs and the breaking area. Waves breaking occurs on the whole coast, from Ponta do Pargo to Funchal.

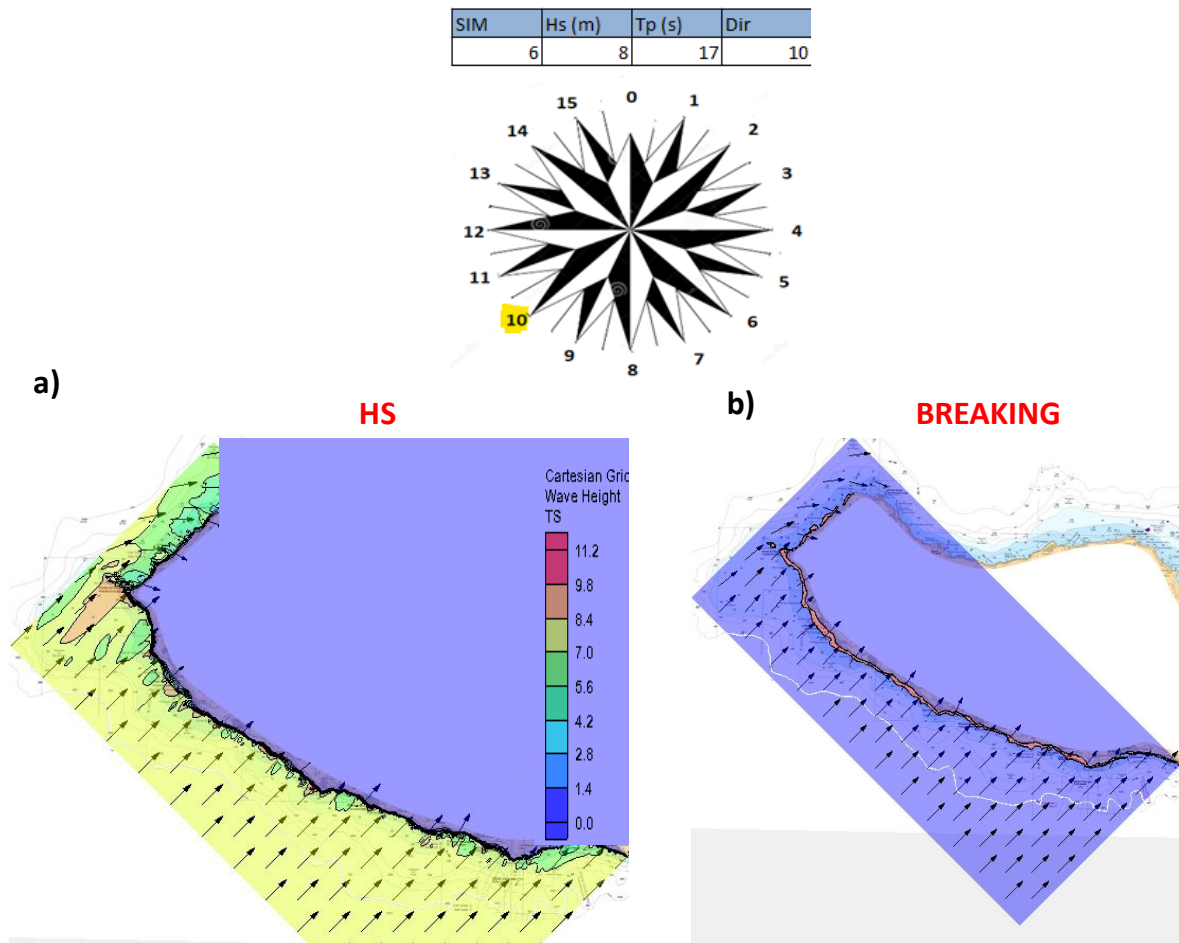


Figure 4.19, Madeira Island, South West part, simulation 6 (Hs 8= m, Tp= 17 s, Dir= 225 °N):

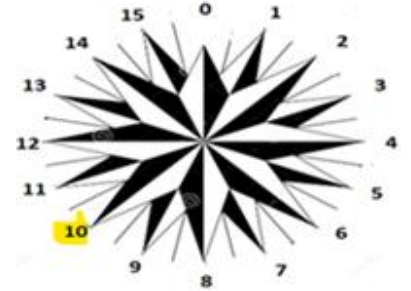
a) Hs values with Dir; b) Breaking

Figure 4.20 presents the Hs along all the four observation arc of Ponta do Pargo, Calheta, Lugar do Baixo and Funchal. Although it is always the Ponta do Pargo arc which presents the highest Hs values, in Ponta do Pargo Hs values are lower than those for the simulations that for waves coming from the Northwest directions (Package 1).

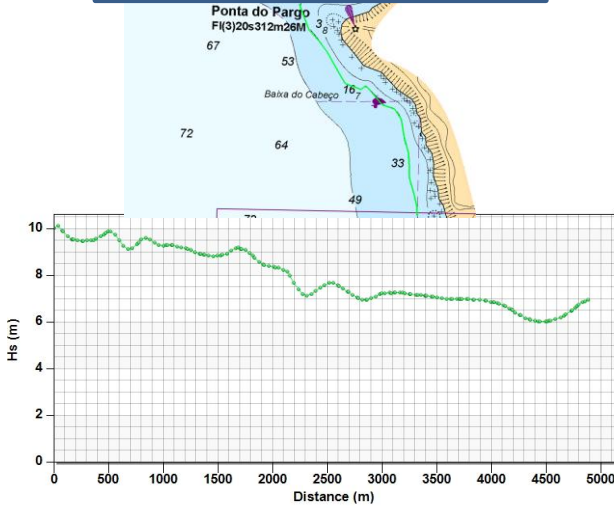
On the contrary, in all the other arcs (Calheta, Lugar de Baixo e Funchal) values are much higher than those obtained in the simulations of Package 1. In fact, Hs values are always close to 8 m, apart from the Funchal, where only a few points reach this value.



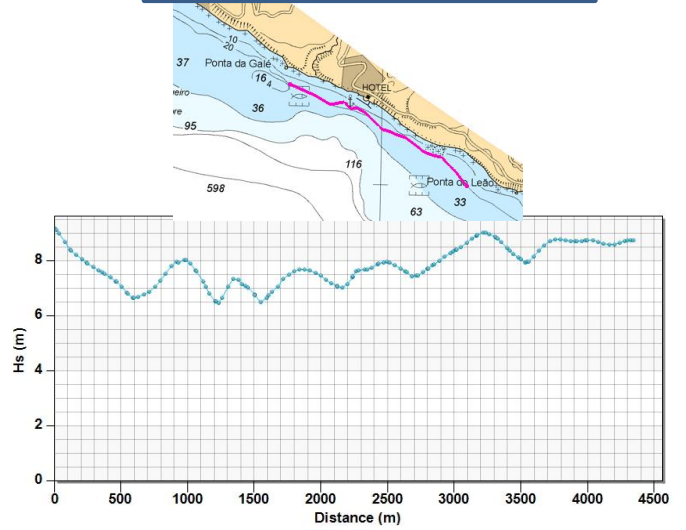
SIM	Hs (m)	Tp (s)	Dir
6	8	17	10



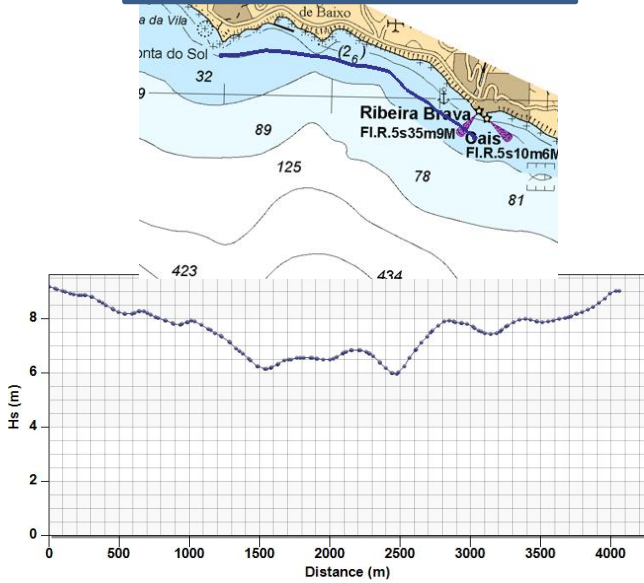
a) **PONTA DO PARGO**
Hs at 20 meters depth



b) **CALHETA**
Hs at 20 meters depth



c) **LUGAR DE BAIXO**
Hs at 20 meters depth



d) **FUNCHAL**
Hs at 20 meters depth

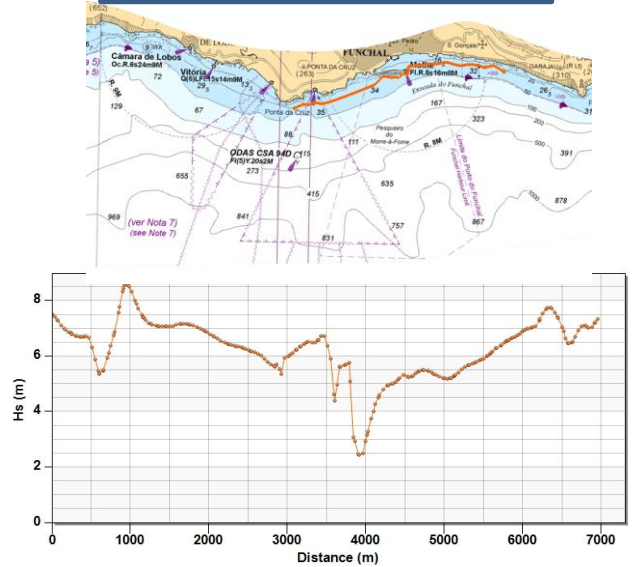


Figure 4.20, Hs at 20 meters depth, simulation 6 (Hs= 8 m, Tp= 17 s, Dir= 225 °N):

a) Ponta do Pargo; b) Calheta ; c) Lugar de Baixo ; d) Funchal

Simulation 7

The same comments made for simulation 6 (waves from SW) can be also be drawn for simulations 7 where the waves are coming from WSW on the offshore boundary (Hs 8 m, Tp 17 s, Dir 11, 247,5°N). However the constancy between Hs values on all the arcs is less evident, as was perfectly expectable because the waves for this simulation arrive from an angle of 22.5 degrees further west.

Figure 4.21 displaying Hs values on the whole area of interest and the respective breaking confirms the similarity between simulations 6 and 7.

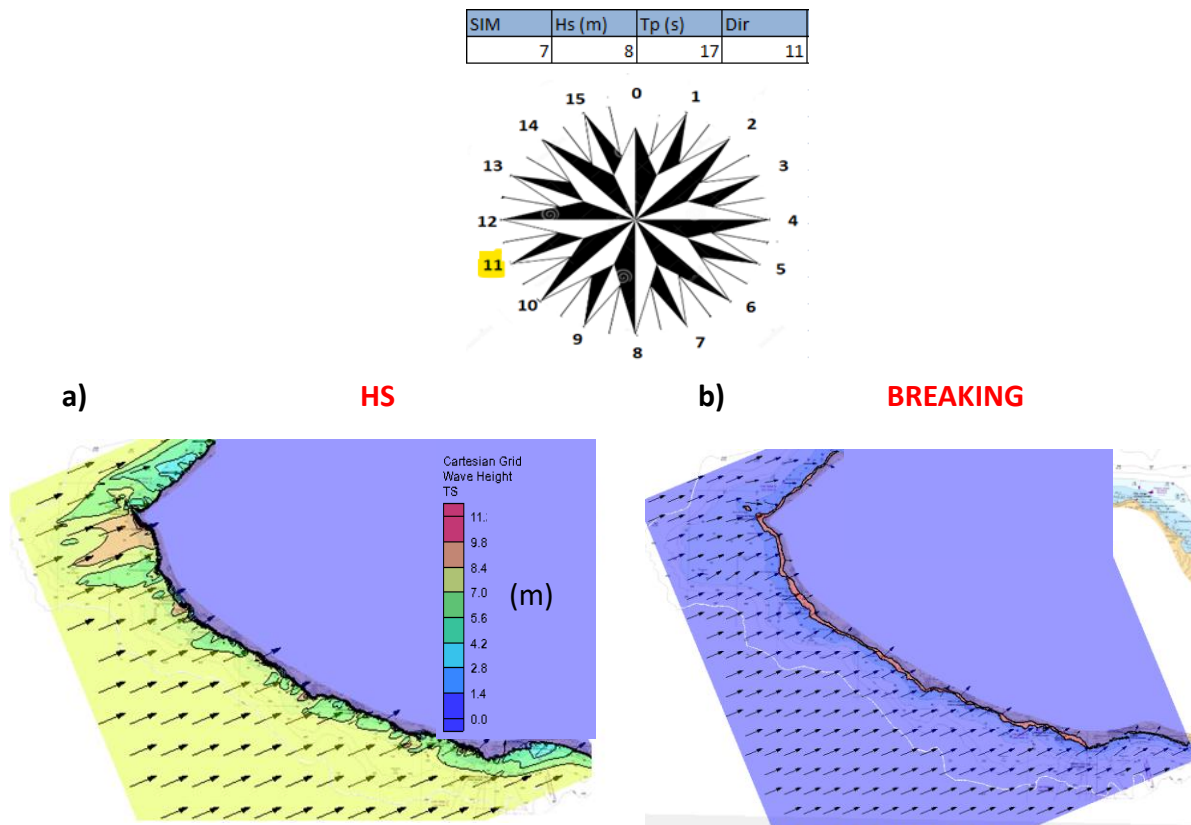


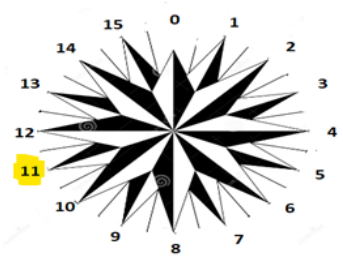
Figure 4.21, Madeira Island, South West part, simulation 7 (Hs= 8 m, Tp= 17 s, Dir=247.5 °N):

a) Hs values with Dir; b) Breaking

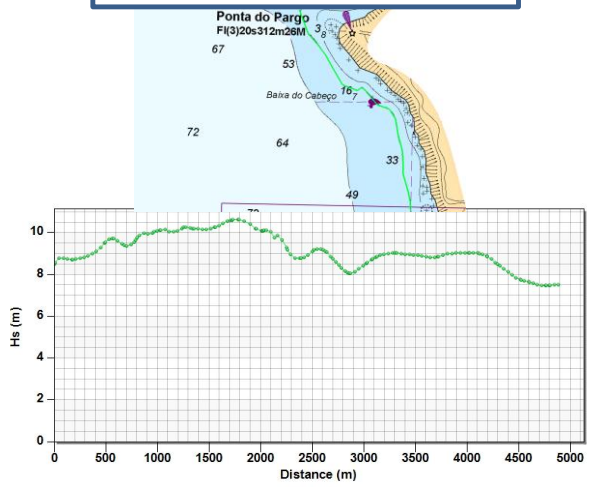
Finally, Figure 4.22 shows the Hs trend on the four observation arcs, confirming what already said for the analogous figure relative to simulation 6(Figure 4.20).



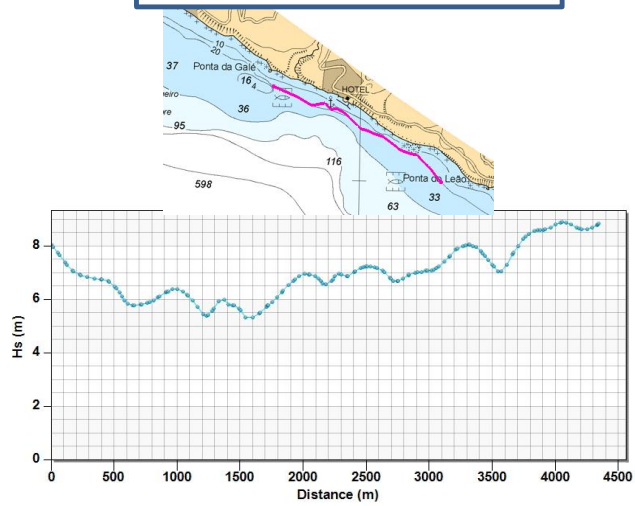
SIM	Hs (m)	Tp (s)	Dir
7	8	17	11



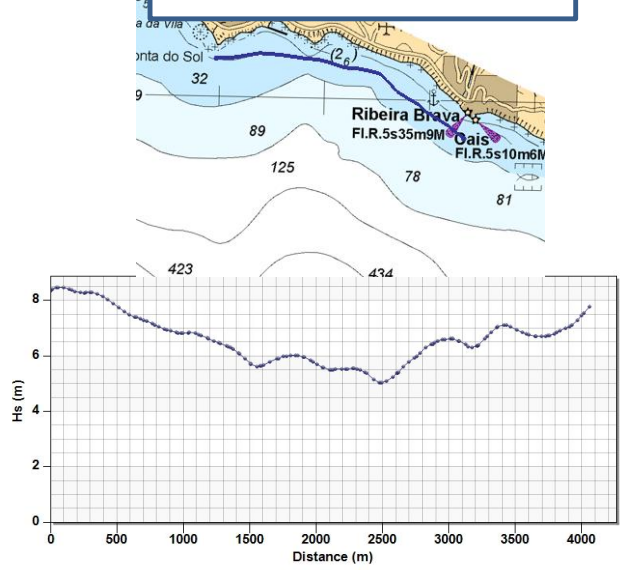
a) **PONTA DO PARCO**
Hs at 20 meters depth



b) **CALHETA**
Hs at 20 meters depth



c) **LUGAR DE BAIXO**
Hs at 20 meters depth



d) **FUNCHAL**
Hs at 20 meters depth

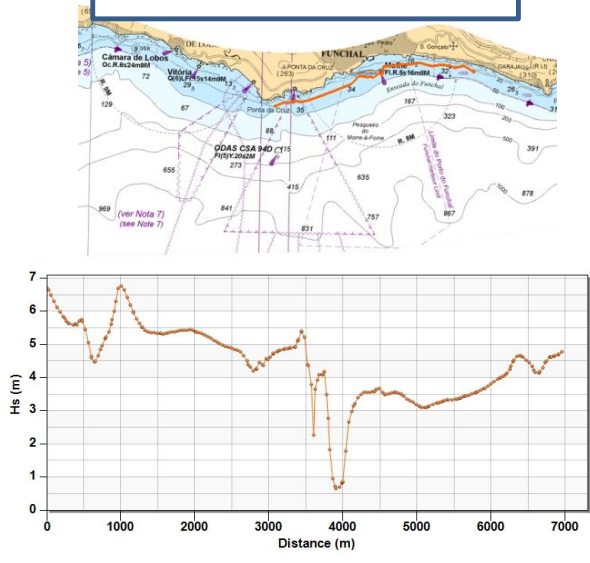


Figure 4.22, Hs at 20 meters depth, simulation 6 (Hs= 8 m, Tp= 17 s, Dir= 247.5 °N):

a) Ponta do Pargo; b) Calheta ; c) Lugar de Baixo ; d) Funchal

Simulation 8

After seeing the results of the previous simulations, it is expectable from simulation 8, waves coming from S, (Hs=8 m, Tp= 17 s, Dir 8, 180 ° N) that Hs values will be smaller in the northern part and greater in the southern part of the coastal stretch, and that Hs is more constant throughout. Figure 4.23, shows Hs values and the surf zone, and Figure 4.28, shows Hs on the four observation arcs.

Figure 4.23 shows, in fact, a more constant behaviour along the entire coast for Hs propagated with for waves coming from south.

SIM	Hs (m)	Tp (s)	Dir
8	8	17	8

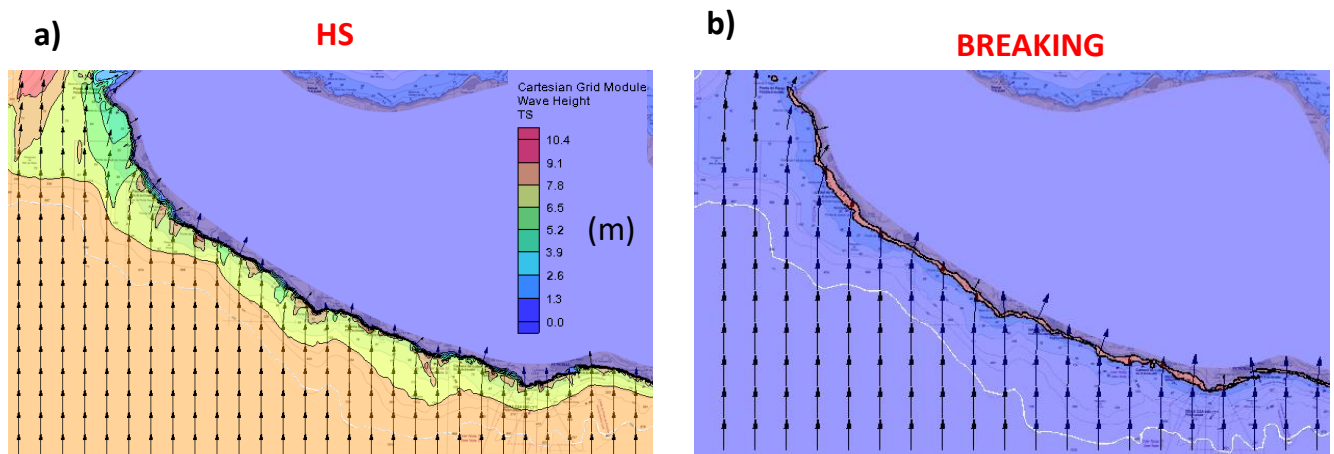
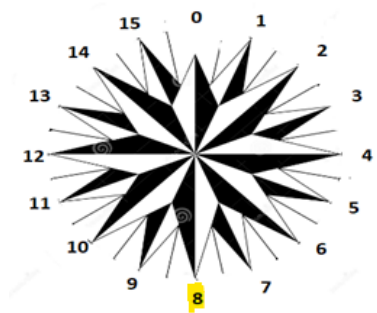


Figure 4.23, Madeira Island, South West part, simulation 8 (Hs= 8 m, Tp 17= s, Dir=180 °N):

a) Hs values with Dir; b) Breaking

Figure 4.24 shows the lowest H_s values observed in the observation arc of Ponta do Pargo and the highest values in the arc in front of Funchal, with Calheta and Lugar de Baixo maintaining approximately the same values observed in the analogous graphs for simulations 6 and 7.

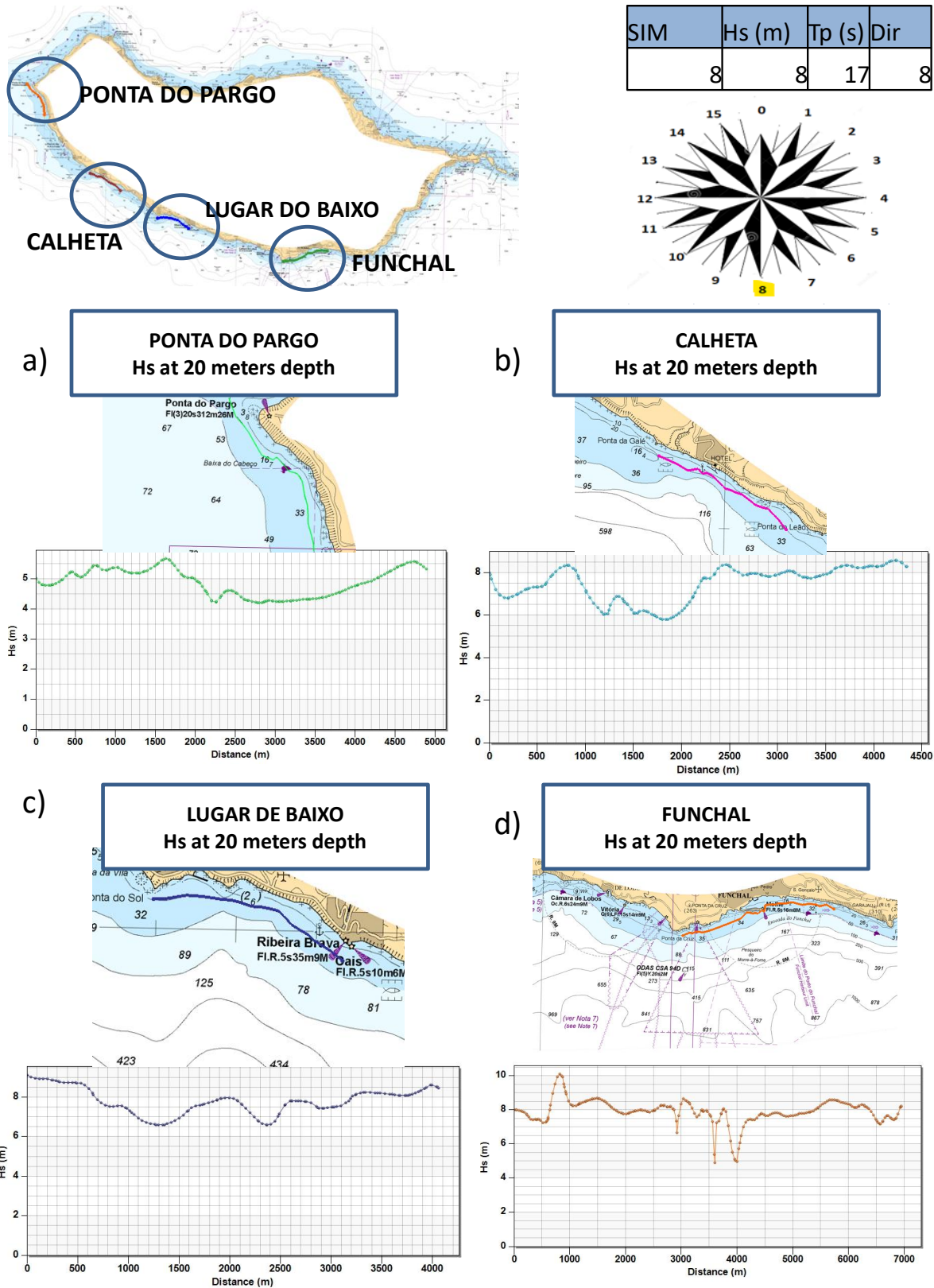


Figure 4.24, Hs at 20 m depth contour, simulation 6 (Hs= 8 m, Tp= 17 s, Dir=247.5 °N):

a) Ponta do Pargo; b) Calheta ; c) Lugar de Baixo ; d) Funchal

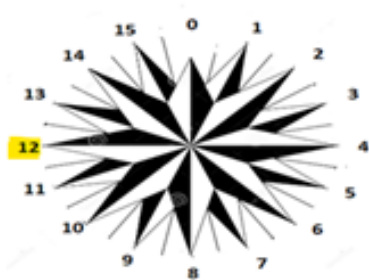
4.6.3 COMPARISON: SIMULATION 4 VS SIMULATION 9

After presenting the results of the simulations that consider waves coming from the northwest and simulations that consider waves coming from the south, the results of the simulation of package 1 that reported the most significant results, and the results of the simulation belonging to package 2 that showed the most important results are now presented.

So this paragraph compares the results for simulation 4, waves from W, (Hs= 12 m, Tp= 20 s, Dir=270 °N) and simulation 9, waves from SSW (Hs=8 m, Tp= 17 s, Dir= 202,5°N).

a)

SIM	Hs (m)	Tp (s)	Dir	Dir °N
4	12	20	12	270



b)

SIM	Hs (m)	Tp (s)	Dir	Dir °N
9	8	17	9	202,5

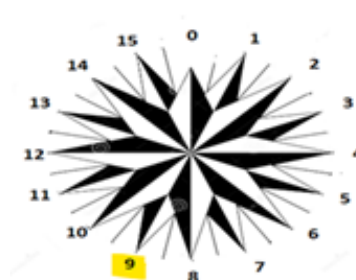


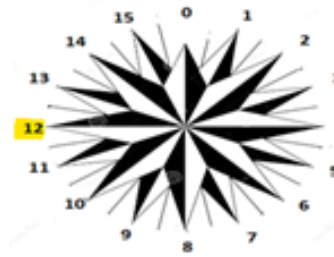
Figure 4.25, a) simulation 4 (Hs= 12 m, Tp= 20 s, Dir= 270 °N); b) Simulation 9 (Hs= 8 m, Tp= 17 s, Dir= 202.5 °N)

Figure 4.30 shows the Hs values and the respective Breaking for both simulations. The figure shows how simulation 4 corresponds to higher Hs values in the north-west part, while simulation 9

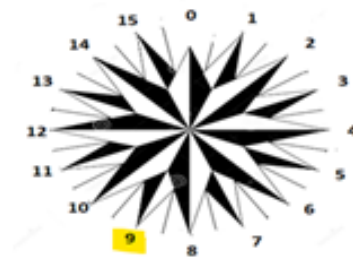
corresponds to H_s values that become more similar to those of simulation 4, up to exceed them even in some points, when moving towards Funchal.

However, although it is true that moving southwards there are more points where waves coming from SSW show higher H_s values than waves coming from W, these points are interspersed with points where waves come from W are more severe.

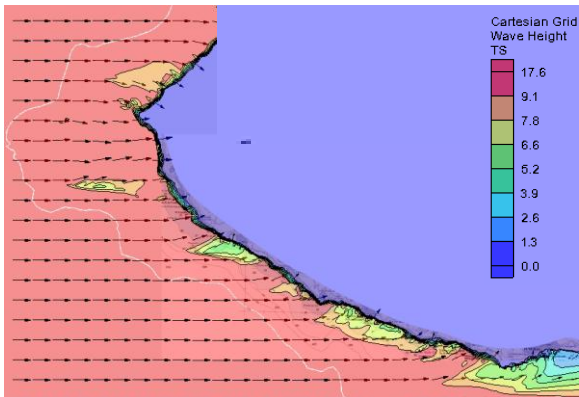
SIM	Hs (m)	Tp (s)	Dir	Dir (°N)
4	12	20	12	270



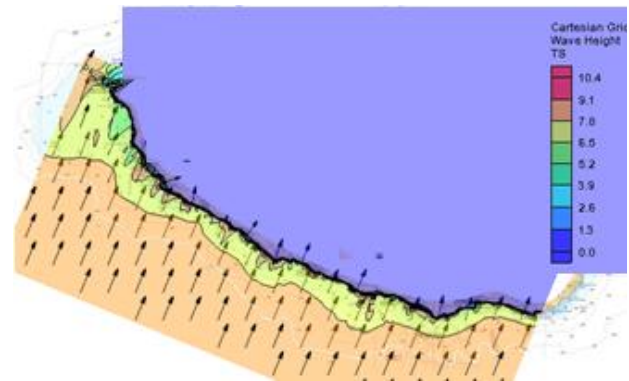
SIM	Hs (m)	Tp (s)	Dir	Dir (°N)
9	8	17	9	202,5



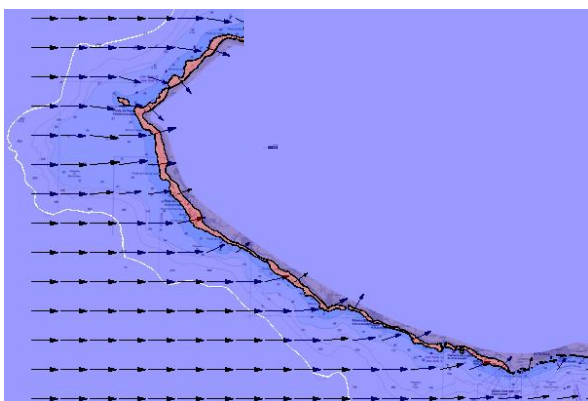
a) HS



b) HS



a.i) BREAKING



b.i) BREAKING

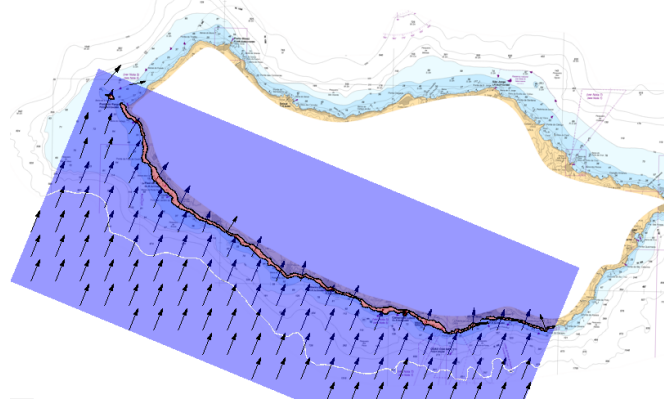
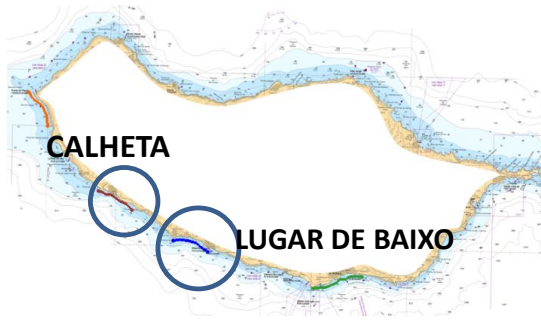
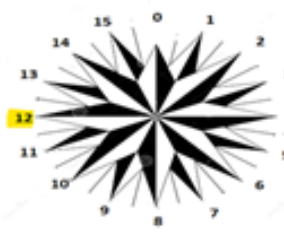


Figure 4.26, a) Hs and Dir, Simulation 4 (Hs= 12 m, Tp= 20 s, Dir= 270 °N); b) Hs and Dir, Simulation 9 (Hs= 8 m, Tp= 17 s, Dir= 202.5 °N); a.i) Breaking, Simulation 4 (Hs= 12 m, Tp= 20 s, Dir= 270 °N); b.i) Breaking, Simulation 9 (Hs 8= m, Tp= 17 s, Dir=202.5 °N)

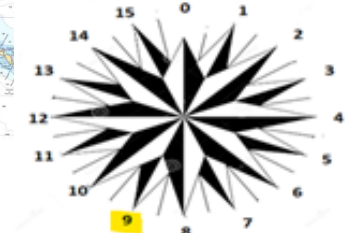
Figure 4.27 shows examples of this behaviour for Calheta and Lugar de Baixo.

This figure compares the trend of H_s in the observation arcs in front of the two locations, and it shows that in Calheta the biggest H_s are related to simulation 9, Figure 4.27 b, while for Lugar de Baixo the biggest values are related to simulation 4, Figure 4.27 c.

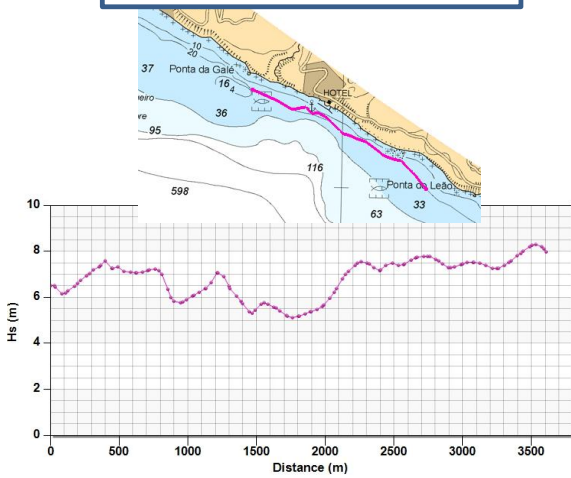
SIM	Hs (m)	Tp (s)	Dir
4	12	20	12



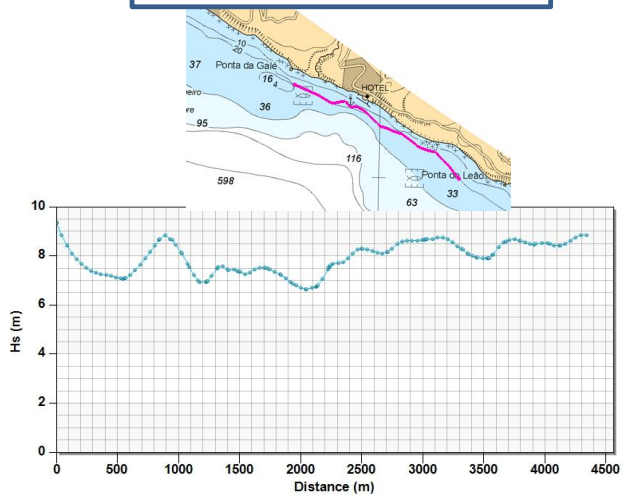
SIM	Hs (m)	Tp (s)	Dir
9	8	17	9



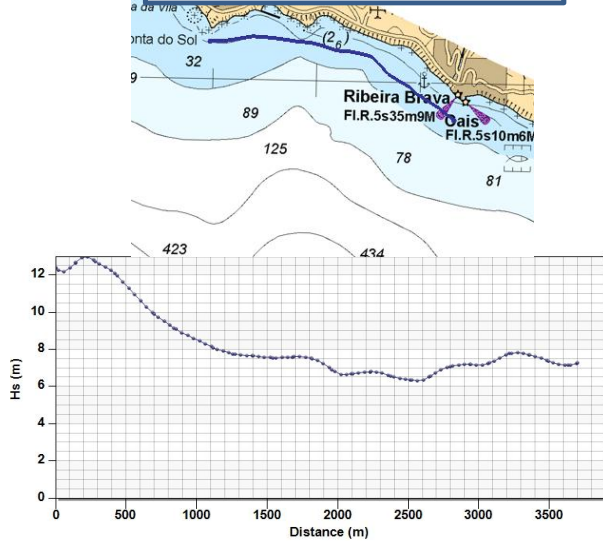
a) CALHETA
Hs at 20 meters depth



b) CALHETA
Hs at 20 meters depth



c) LUGAR DE BAIXO
Hs at 20 meters depth



d) LUGAR DE BAIXO
Hs at 20 meters depth

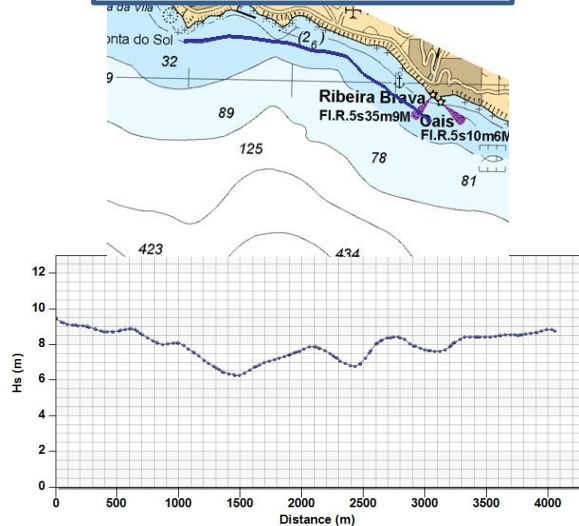


Figure 4.27, Hs at 20 meters depth: a) Calheta, Simulation 4 (Hs= 12 m, Tp= 20 s, Dir= 270 °N); b) Hs and Dir, Simulation 9 (Hs= 8 m, Tp= 17 s, Dir= 202.5 °N); a.i) Breaking, Simulation 4 (Hs= 12 m, Tp= 20 s, Dir= 270 °N); b.i) Breaking, Simulation 9 (Hs= 8 m, Tp= 17 s, Dir= 202.5 °N)

This fact is attributed to the phenomenon of refraction. In fact, it can be seen how the bathymetry off Calheta (Figure 4.28.a) and that off Lugar de Baixo (4.28.b) are extremely different from each other. This figure shows, in addition to the different bathymetries, the direction of the waves propagated in simulation 4.

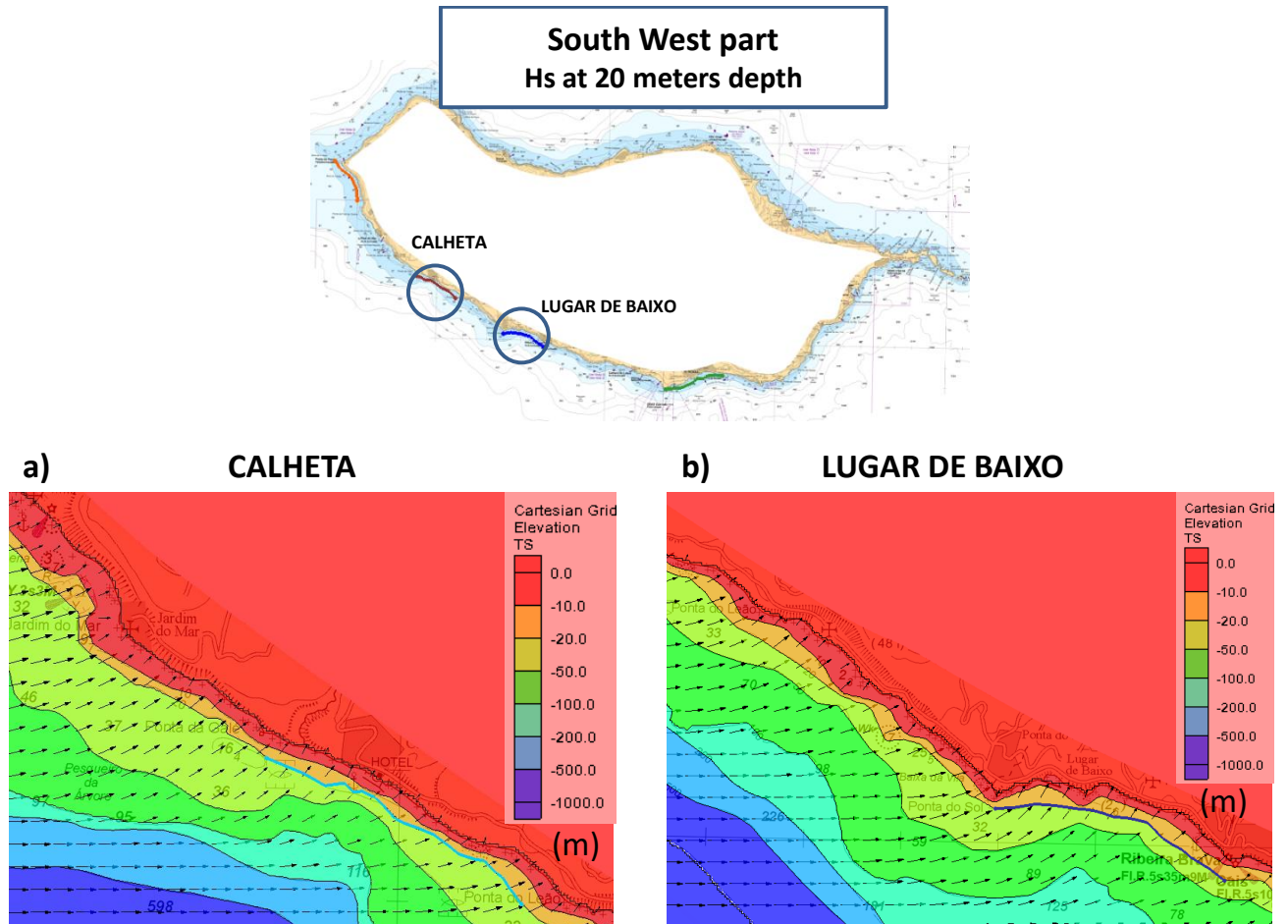


Figure 4.28, Madeira Island, Bathymetry with waves direction, Simulation 4 ($H_s= 12$ m, $T_p= 20$ s, $Dir= 270$ °N): a) Calheta; b) Lugar de Baixo

4.6.4 SIMULATION WITH WAVES COMING FROM NORTH: SIMULATION 5

Lastly, it has been run a simulation propagating waves coming straight from North, i.e. with direction 0 (0°N).

As previously mentioned, this was done to demonstrate the shadow effect already discussed in chapter 2.

Some outputs related to simulation 5 ($H_s = 12$ m, $T_p = 20$ s, $Dir = 0^\circ N$) are therefore presented specifically to highlight this shadow effect.

In particular, H_s trend on an observation arc covering the whole south west coast is showed (Figure 4.32 a), together with H_s values throughout the area where the waves were propagated (Figure 4.32.b).

Figure 4.32 as a whole shows how the waves coming from the North, after assuming values near Ponta do Pargo (northernmost part of the observation arc), are drastically reduced moving more and more towards the south, reaching and maintaining values close to zero throughout the arc.

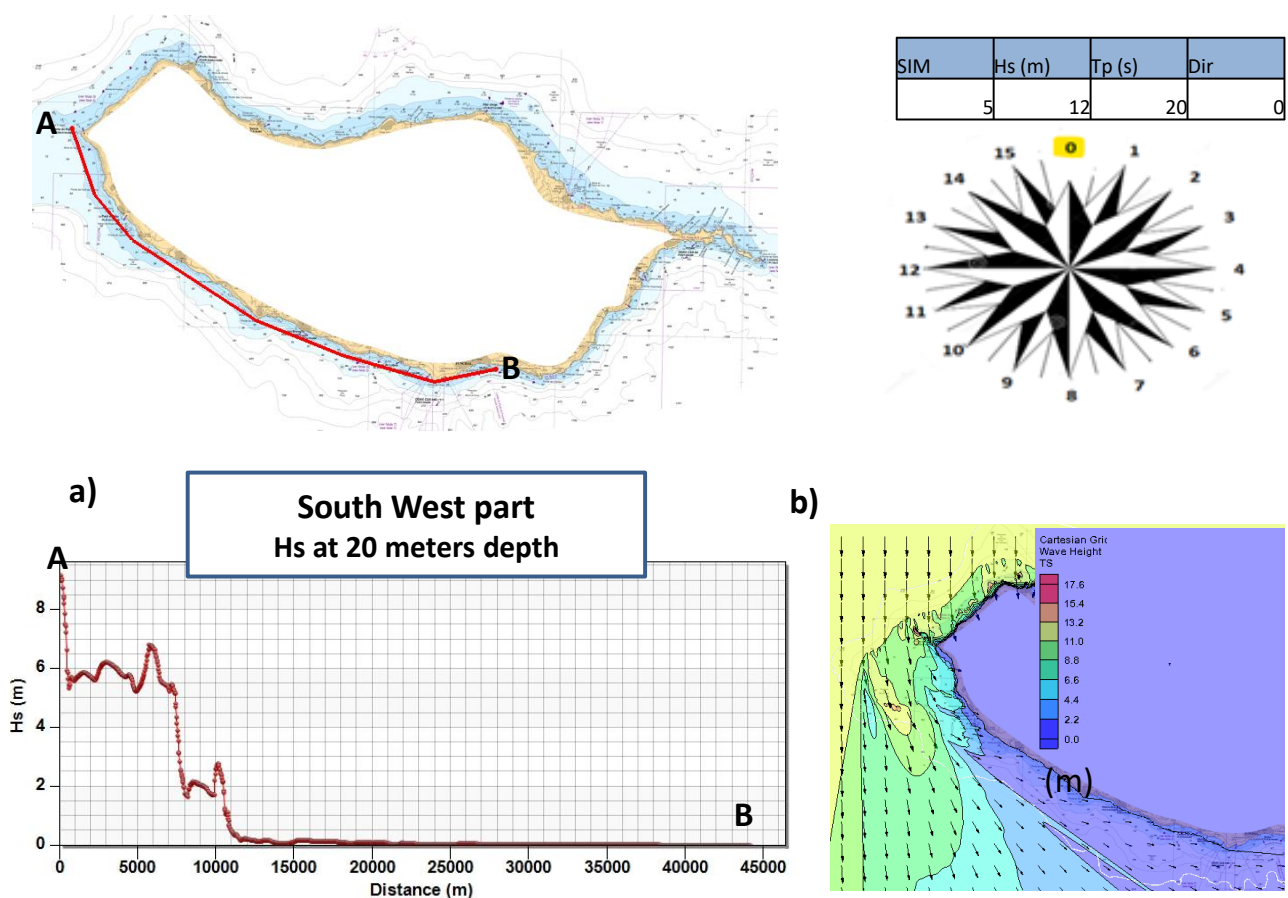


Figure 4.29, Madeira Island, South West part, Simulation 5 ($H_s = 12$ m, $T_p = 20$ s, $Dir = 0^\circ N$):

- a) H_s trend on the observation arc covering the whole South West coast at 20 meters depth; b) H_s values on the whole area of interest.

4.7 TIDE

This paragraph investigates the need to consider the action of the tides in this study. It should be mentioned that up to now all the simulations were done neglecting the contribution of the tide, or rather considering a tide height equal to 0.0 m, which corresponds approximately to low tide. In this paragraph, the results for selected simulations are compared to see the tide influence on the results. In particular, the results of simulation 4 (Hs 12 m, Tp 20 s, Dir 12, 270 °N) and simulation 9 (Hs 8 m, Tp 17 s, Dir 9, 202.5 °N) were compared.

According to the “ tabela de marés” delivered by Instituto “Hidrografico”) the highest tide observable in 2023 will be 2.6 m (Hidrografico), so simulations 4 and 9 were redone considering a tide of 2.6 m. The next two figures shows the differences in terms of Hs values for the whole South West area of Madeira island, for simulation 4, Figure 4.30 and simulation 9, Figure 4.31.

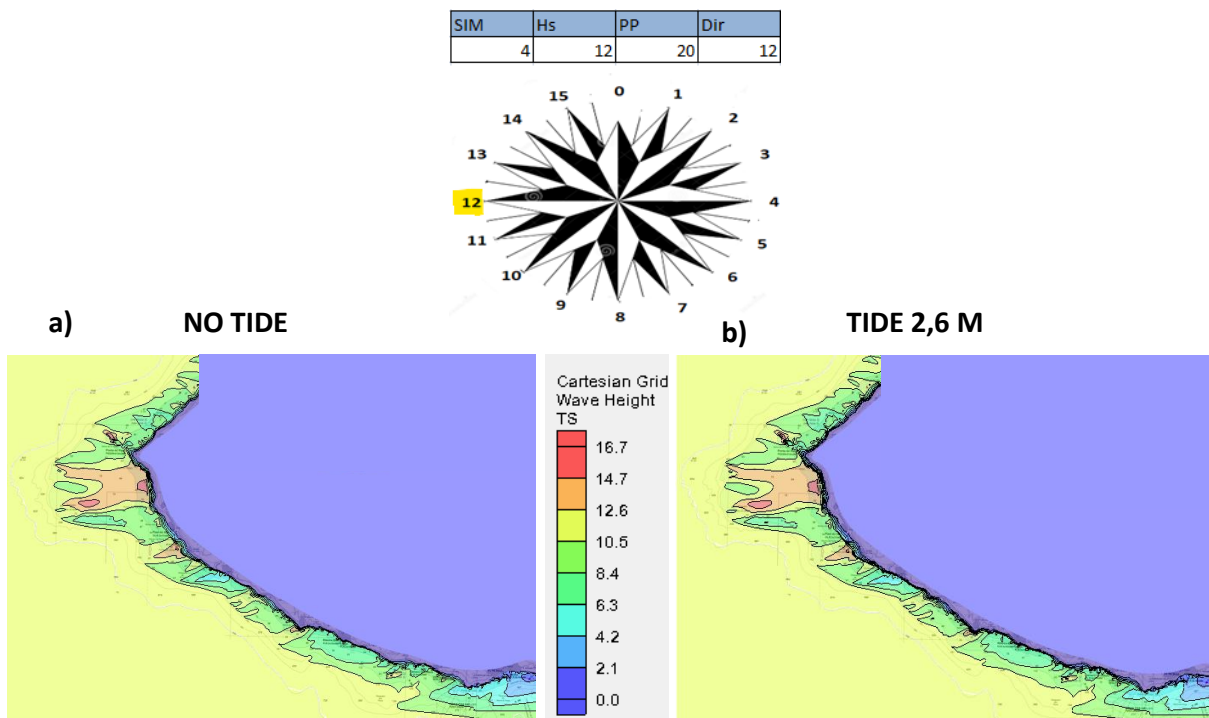


Figure 4.30, Madeira Island, South West part, simulation 4 (Hs= 12 m, Tp= 20 s, Dir= 270 °N):

a) Hs considering a 0 m tide; b)Hs considering a 2.6 m tide

SIM	Hs	PP	Dir
9	8	20	9

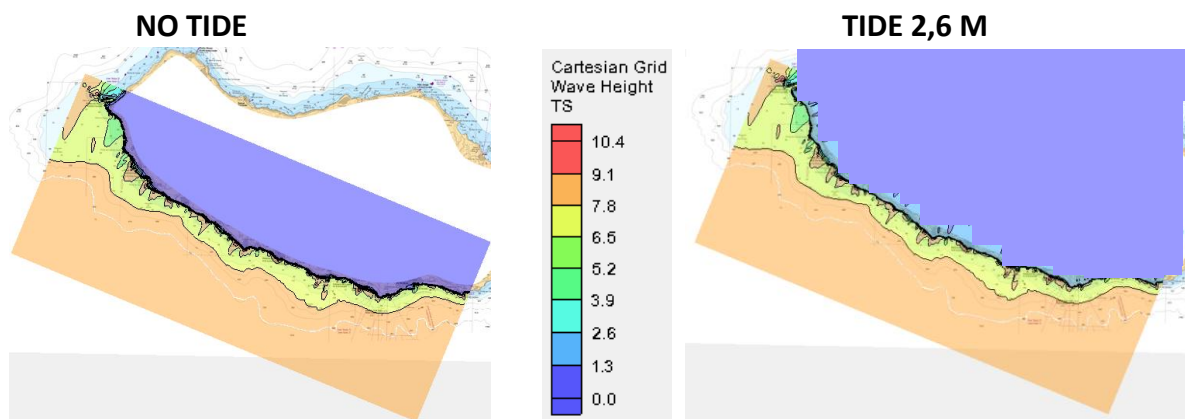
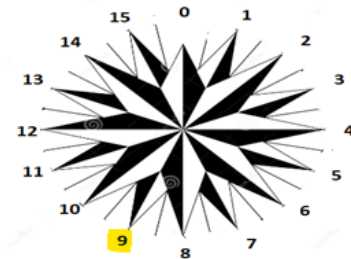


Figure 4.31, Madeira Island, South West part, simulation 9 (Hs= 8 m, Tp= 17 s, Dir= 247.5 °N):

a) Hs considering a 0 m tide; b)Hs considering a 2.6 m tide

These two figures suggest that the differences that occur in the two cases in the value of Hs are small. To confirm this fact, the values of Hs obtained in the monitoring points were compared. Table 4.12 shows that the relative difference (i.e. expressed as a percentage) remains below 10% .

LOCATION	N° SIM	4 no tide	4 tide2,6m	% differences	9 no tide	9 tide2,6m	% differences
Ponta do Pargo	11	11,38	11,38	3,34%	7,75	7,03	10,24%
Ponta do Foja Ovelja	11,47	11,47	11,48	0,09%	7,68	7,47	2,81%
Hotel (Calheta)	5,12	5,12	5,19	1,35%	6,96	7,01	0,71%
Lugar De Baixo	7,28	7,28	7,35	0,95%	6,15	6,15	0,00%
Cabo Girao	8,7	8,7	8,52	2,11%	8,45	8,31	1,68%
Funchal	4,68	4,68	3,99	17,29%	5,54	6,14	9,77%

Table 4.12, Hs with no tide and tide of 2,6m tide, simulations 4 and 9.

4.8 SUMMARY

In this chapter, the analyses carried out in the previous chapters were useful for conducting 9 simulations (see Table 4.8) using the STWAVE software on SMS. By inputting information related to bathymetry (see paragraph 4.4), which relies on a specific computational grid (see paragraph 4.5), waves with certain Hs (see paragraph 4.3.1), Tp (see paragraph 4.3.2), and Dir (see paragraph 4.3.3) were propagated from offshore to shore.

From the results of these simulations, it was possible to draw important conclusions regarding which offshore wave conditions led to the most significant Hs values near the southwest coast of the island of Madeira.

In particular, the aspects that are most important to emphasize are as follows:

- The highest Hs values near almost the entire southwest coast were obtained downstream of the simulation in which waves with a direction of 270°N , i.e., directly from the west, were propagated (simulation 4).
- Some sections of the coast reported the highest Hs values downstream of simulation 9 (Hs = 8 m, Tp = 17 s, Dir = 202.5°N).
- Particular attention should be given to the fact that the locations of Calheta and Lugar de Baixo, which are very close to each other (see Figure 4.28), did not record the highest Hs values downstream of the same simulation: while for Calheta, these values were obtained downstream of simulation 9 (Hs = 8 m, Tp = 17 s, Dir = 202.5°N), for Lugar de Baixo, they were obtained downstream of simulation 4 (Hs = 12 m, Tp = 20 s, Dir = 270°N). This phenomenon has been attributed to the refraction phenomenon (see discussion in paragraph 4.6.3).
- Paragraph 4.7 has demonstrated that the tidal effect can be neglected within this study, see Table 4.12.

5 COMPARISON BETWEEN DIFFERENT BATHYMETRIES

Bathymetry map versus Bathymetry web versus Bathymetry survey scatter set

5.1 INTRODUCTION

On the previous chapter, a series of simulations were done, each one using different boundary conditions in order to study wave propagation. The research done shows what are the extreme waves that can reach the southwest part of Madeira Island.

While for the establishment of the boundary conditions, i.e. H_s , T_p and Dir in the offshore of the island, some remarks were made in Chapter 2 and 3, further investigation needs to be done about the bathymetry used to perform these simulations. The bathymetry is the main factor influencing wave propagation towards the coast (Venturi, J et al, 2023. “On the influence of the bathymetry on wave propagation”).

The simulations presented in Chapter 4 were obtained, as previously mentioned, using Bathymetry Map, a bathymetry created manually by digitizing on screen. In this way a scatter set was created from a digital image of a Navigation Map. The mathematical model needs the bathymetric information in each grid cell. The bathymetry is imported to the computational grid from a scatter set. A scatter set is a cloud of points randomly distributed in space and triangulated (the same as a TIN – Triangular Irregular Network).

The source of bathymetry that is readily available are the navigation maps published by the hydrographic institutes in different countries. Those maps are published for navigation purposes. They usually exhibit more detail close to ports and harbours. On the open coast the maps have usually very large scales of the order of magnitude 1:100000.

The goal of this chapter is to show how the wave propagation results could be influenced by the source for the bathymetry.

This chapter will present the already introduced “Bathymetry Web” and the “Bathymetry Survey Scatter” set in detail, showing the main differences between them and the “Bathymetry Map”.

The differences will be first assessed using values on the same point for different bathymetries, initially across the entire area and then specifically for the locations of Calheta and Lugar de Baixo. This exercise compares bottom elevations in the same point.

Subsequently, the focus will shift to the differences that occur when performing wave propagation with the same boundary conditions but using different bathymetries as a basis. The computational grid remains the same with a cell size constant of 40 m.

5.2 BATHYMETRY WEB

As mentioned, a website was used (Gridded Bathymetry data), where it is possible to download bathymetries from all over the world in several types of format. After downloading the GeoTiff file showed in Figure 4.4, the accuracy of this bathymetry had to be established. To accomplish this, the GeoTiff file was converted from a raster image to a scatter in SMS. The pixel size is 400m as shown in Figure 5.1. This means that the bottom elevation is known every 400m in both directions.

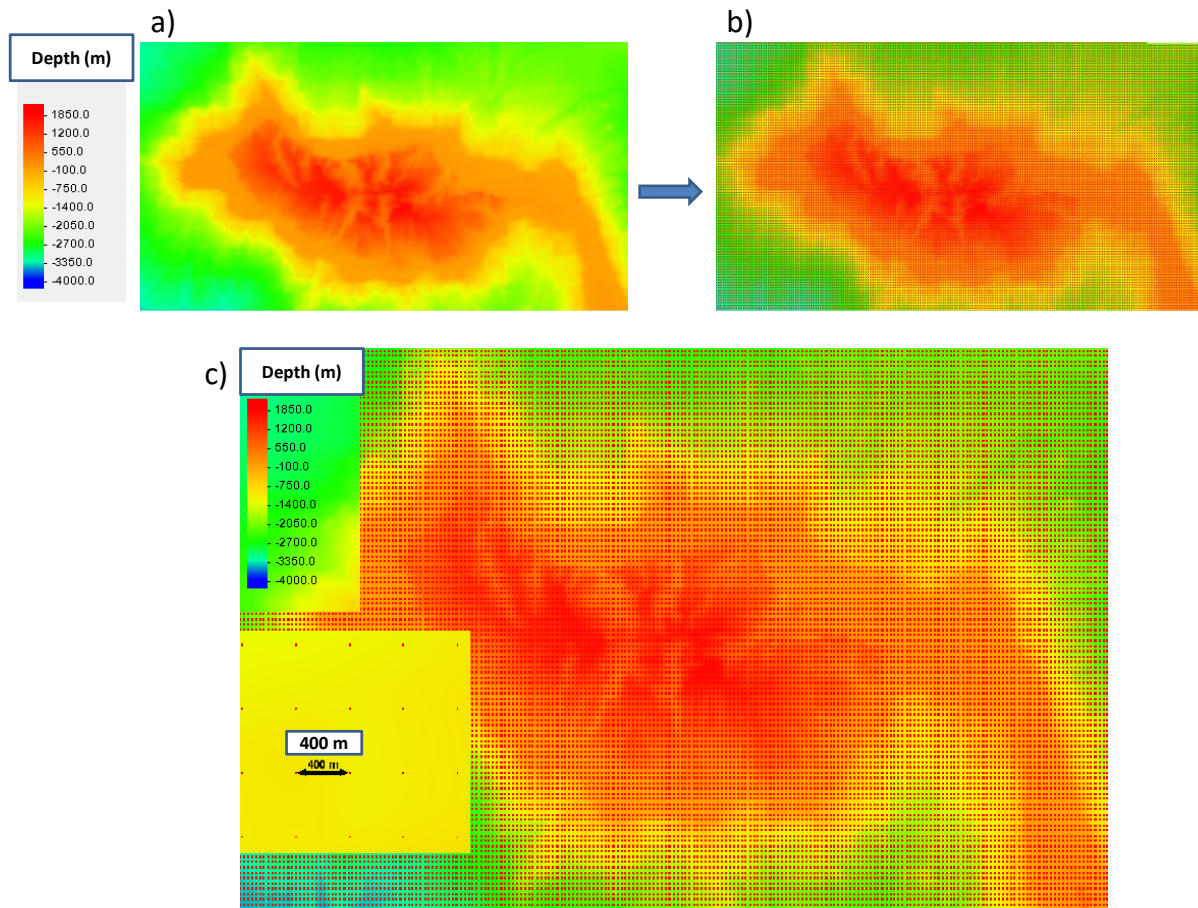


Figure 5.1, a) GeoTiff file of bathymetry downloaded from the Web; b) GeoTiff file converted to scatter set; c) scatter set showing 400 meters distance between elevation points

Based on the procedure performed while using Bathymetry map, i.e. importing the scatter created to a 40 m cells Grid, it can be concluded that the resolution of “Bathymetry Map” and the resolution of “Bathymetry Web” are not even comparable; in fact, recalling the conclusion reached in paragraph 4.5, namely that it was reasonable to attribute an accuracy of at least 40 meters to the "Bathymetry map" (see Figure 4.6), the fact that the points containing the depth information on Figure 5.1 are 400 meters apart, leads to the conclusion that the web provides bathymetry having a degree of precision lower than that obtained from the navigation map of approximately an order of magnitude (400 m versus 40 m).

Further analyses will follow to support the thesis about the discrepancy between Bathymetry map and Bathymetry web.

5.2.1 BATHYMETRY MAP versus BATHYMETRY WEB

To show the differences between the two bathymetries, both were imported to a Cartesian grid of 40 m. Figures 5.2 and 5.3 shows Bathymetry Map and Bathymetry Web imported to Cartesian grids, both in 2D and 3D.

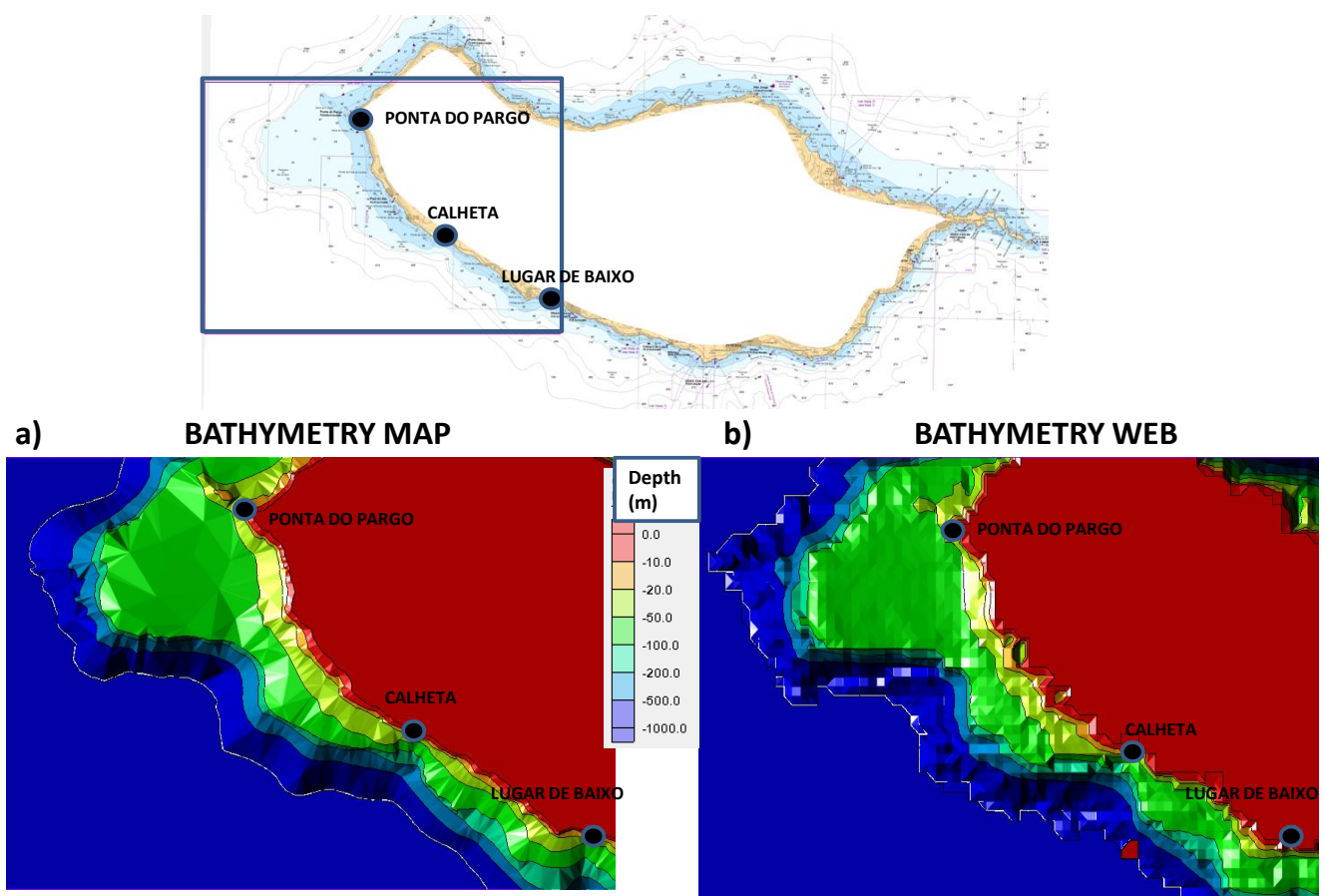


Figure 5.2, Madeira Island, area from Ponta do Pargo to Lugar de Baixo. Bathymetry imported to a 40 m rectangular grid (2D) from: a) Bathymetry Map ; b) Bathymetry Web

From this first comparison It is already possible to observe some significant differences between the two bathymetries. It is evident that the pixels in the Bathymetry Web are still visible. This suggests a very low density of points with depth information that lead to the same value of depth being applied to a large area, while the Bathymetry map displays lines that seem more natural and realistic.

Furthermore, it can be said that there are disparities in values at the same points; in fact, the shape of the bathymetry lines is different between Figure 5.2.a and 5.2.b and between 5.3.a and 5.3.b.

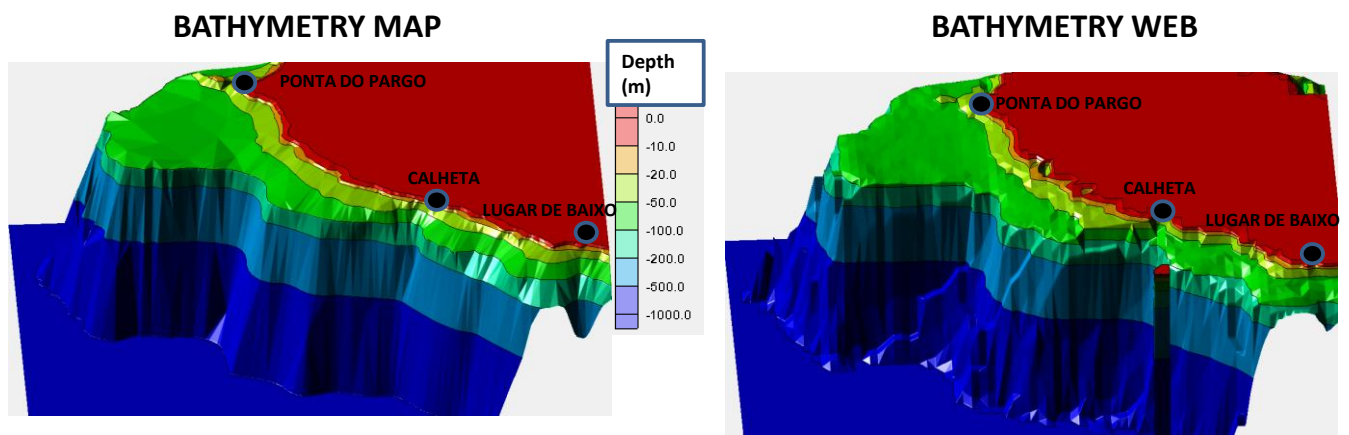
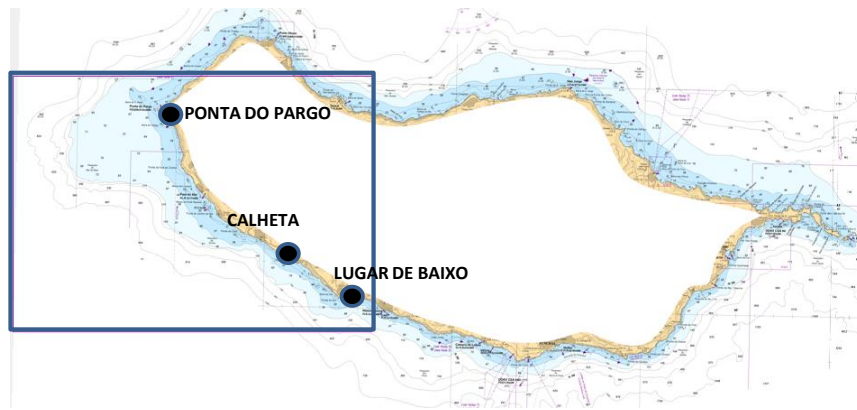


Figure 5.3, Madeira Island, area from Ponta do Pargo to Lugar de Baixo, Bathymetry imported to a 40 m rectangular grid (3D) from: a) Bathymetry Map ; b) Bathymetry Web

To analyse the differences, three variables are now introduced:

- d_{map} is the depth in each cell of the grid for Bathymetry map
- d_{web} is the depth in each cell of the grid for Bathymetry web
- d_{scatter} is the depth in each cell of the grid for Bathymetry survey scatter

In Figure 5.4, $|d_{\text{map}} - d_{\text{web}}|$ is represented in a Cartesian grid with 40 m cell size.

In the whole area of interest significant differences occur, frequently reaching 50 m with some values surpassing 100 or even 200 m.

BATHYMETRY LINES

Bathymetry web on navigation map

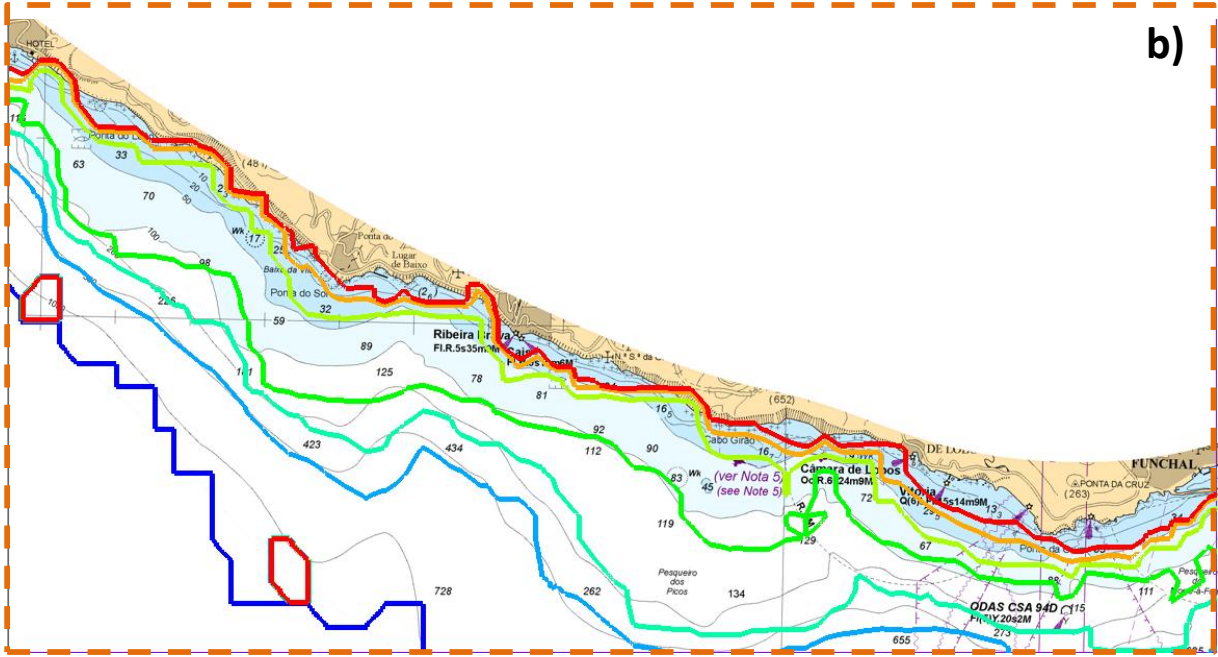
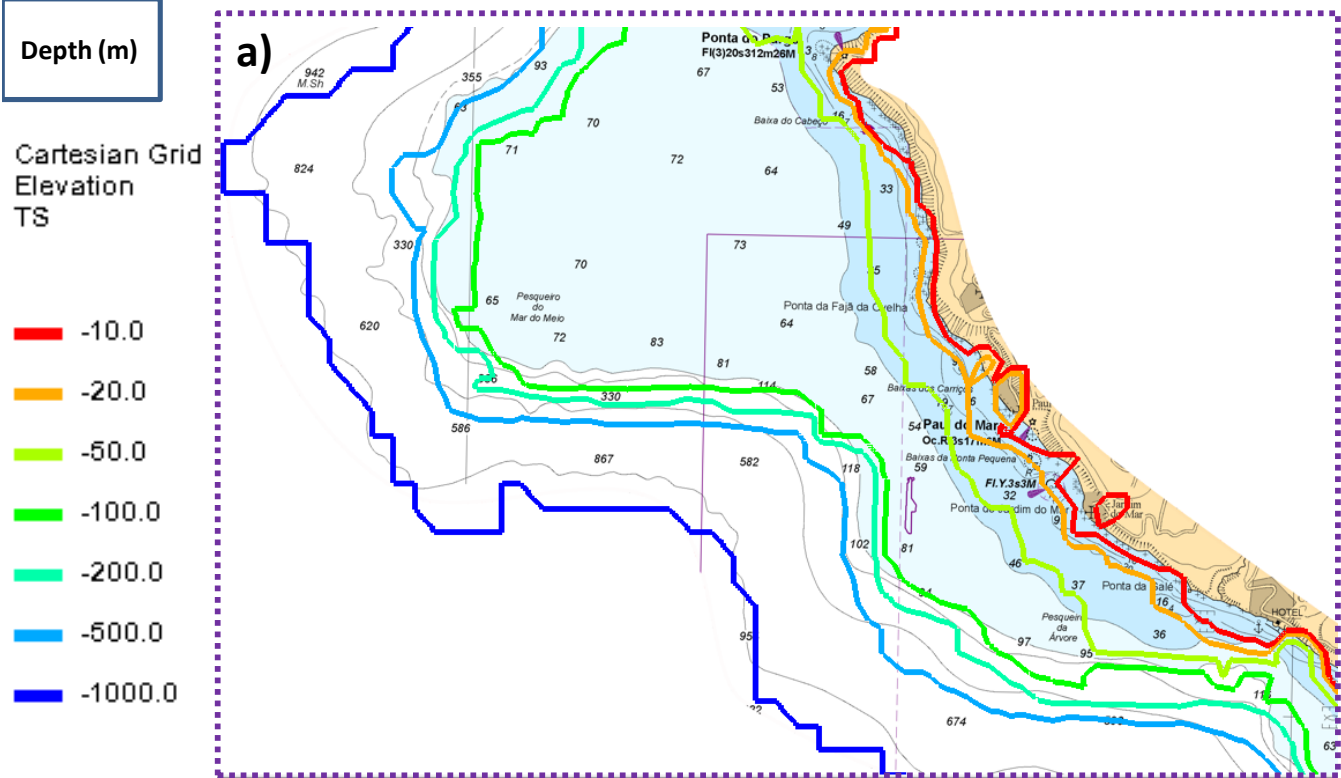


Figure 5.6, Madeira Island, Bathymetry lines from Bathymetry web above navigation map used to create Bathymetry map:
a) top left portion displayed in Figure 6; b) bottom right portion displayed in Figure 6

Figures 5.7 and 5.8 show the differences between Bathymetry map and Bathymetry web in Calheta and Lugar De Baixo.

The bathymetry in front of Lugar de Baixo allow for the waves coming from the west a greater refraction than in Calheta, this highlights the importance of using bathymetries with a minimum resolution in wave propagation models.

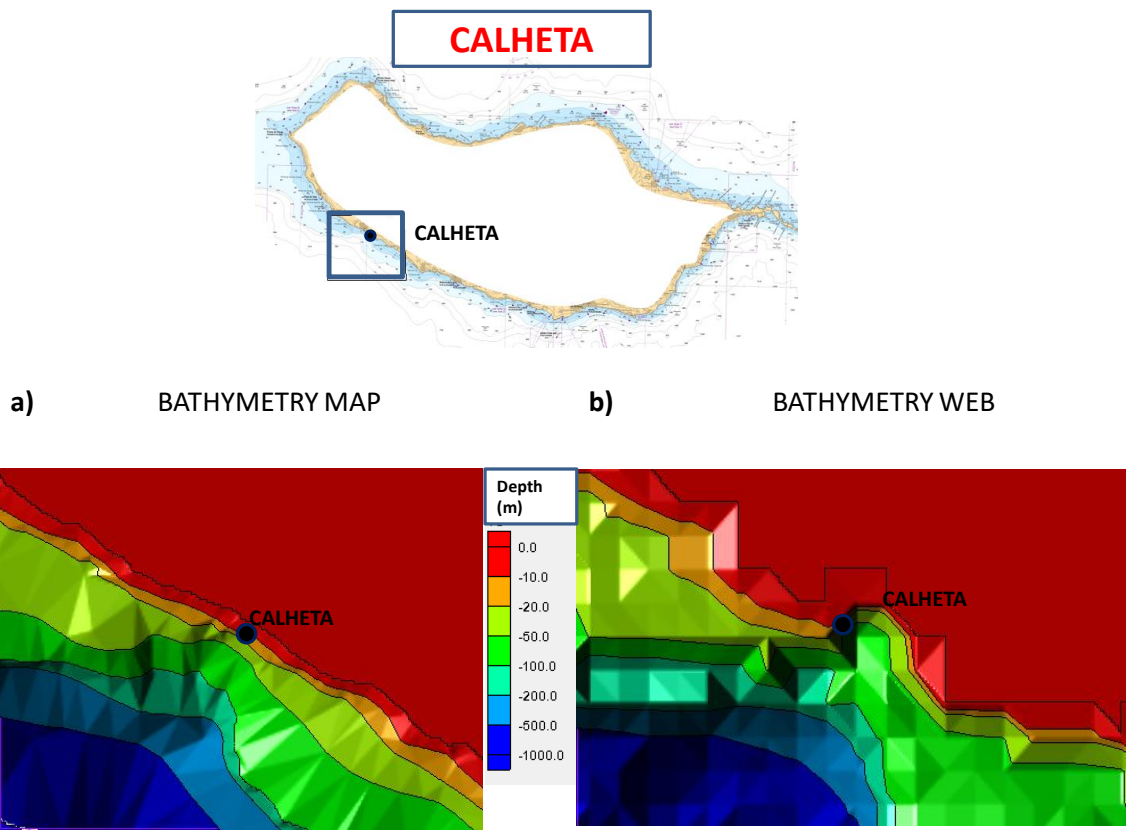


Figure 5.7, Madeira Island, Calheta: a) Bathymetry map; b) Bathymetry web

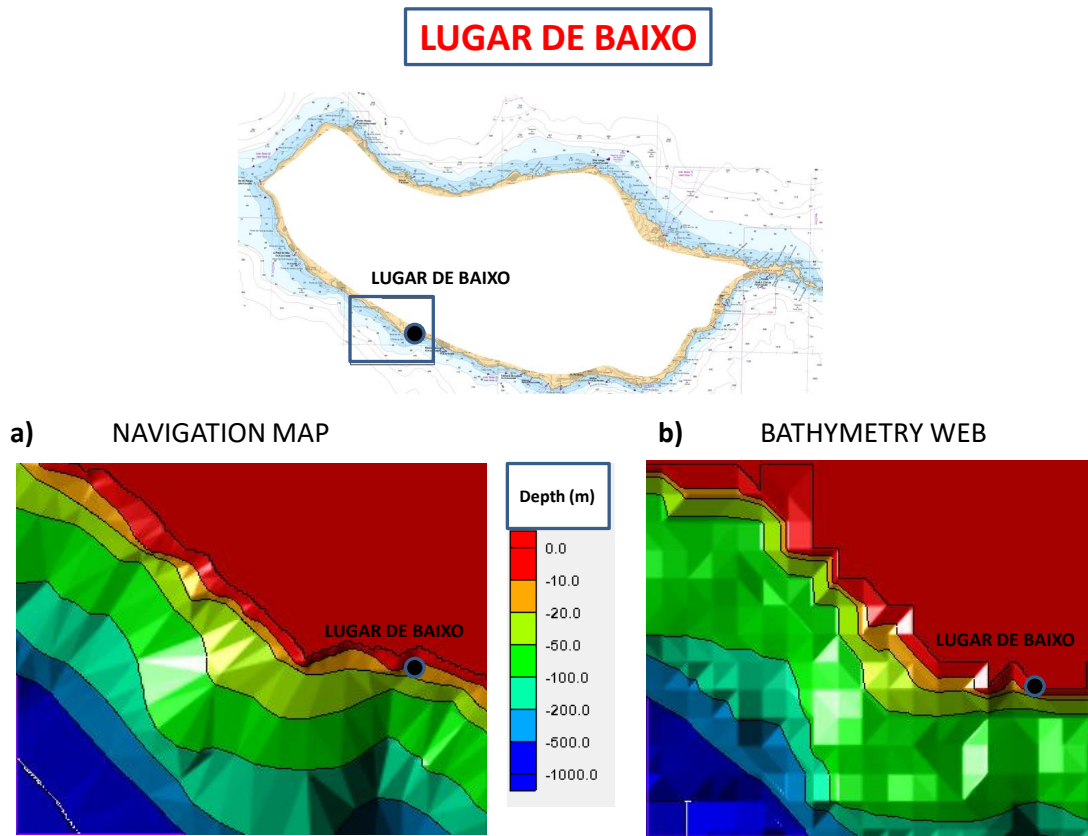


Figure 5.8, Madeira Island, Lugar de Baixo: a) Bathymetry map; b) Bathymetry web

The question is: how different would the wave propagation results of Chapter 3 be if the Bathymetry web was used instead of Bathymetry map?

To answer this question, simulations 4 ($H_s=12$ m, $T_p=20$ s, $Dir=270^\circ N$), waves from W, and simulation 9 ($H_s=8$ m, $T_p=17$ s, $Dir=202.5^\circ N$) waves from SSW, were re-launched, and the results using Bathymetry map and Bathymetry web compared. These events were selected because, as mentioned in Chapter 3, they showed the highest H_s values for various parts of the coast under consideration.

All simulations using different bathymetries as the basis were launched using a Cartesian grid composed of 40-meter cells. However, as explained in Chapter 3, the GeoTiff file used to create Bathymetry Web consists of points that are 400 meters apart. It may seem unnecessary to run simulations with bathymetries of this level of resolution on a grid with such small cells, considering that depth information is only available every 400 m, and the grid cells are 10 times smaller.

Three new variables are introduced to identify the value of H_s in each cell of the Cartesian grid obtained as a result of simulations with different types of bathymetry:

- $H_{s_{map}}$ is H_s in each cell of the grid computed with “Bathymetry Map”

- $H_{s_{web}}$ is H_s in each cell of the grid computed with “Bathymetry Web”
- $H_{s_{scatter}}$ is H_s in each cell of the grid computed with “Bathymetry survey scatter”

5.2.2 SIMULATION 4 ($H_s= 12$ m, $T_p= 20$ s, $Dir= 270^\circ N$)

Figure 5.9 shows a Cartesian grid of 40 m cell size where in each cell is computed $|H_{s_{map}} - H_{s_{web}}|$ for simulation 4 ($H_s= 12$ m, $T_p= 20$ s, $Dir= 270^\circ N$). Significant differences can be observed across the analysed area, with values of $|H_{s_{map}} - H_{s_{web}}|$ ranging from an average of 4 to 10 m. There are extremes exceeding 14 m, in the area of Ponta do Pargo.

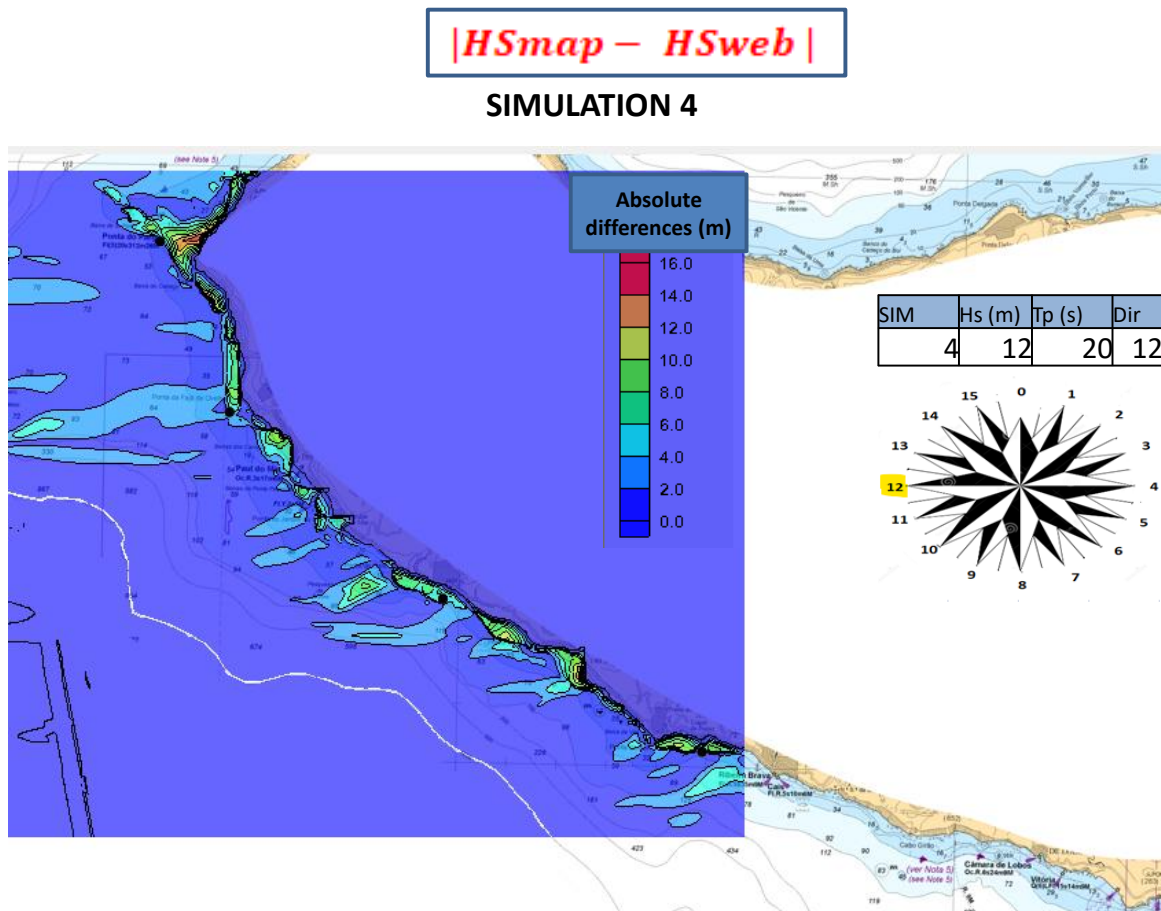
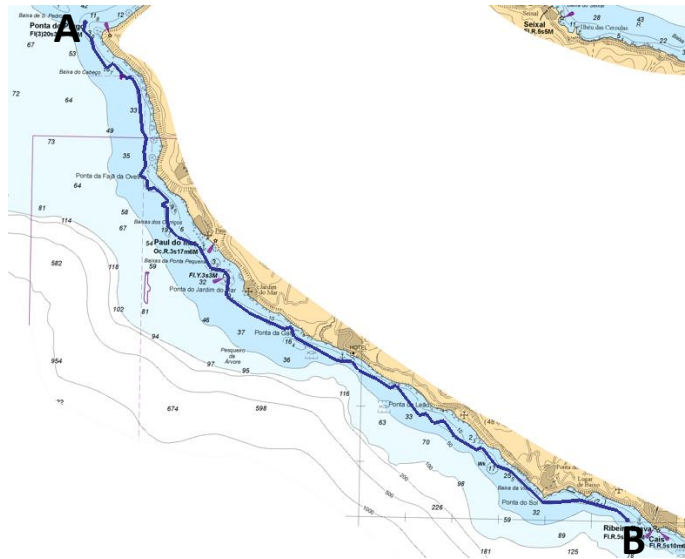
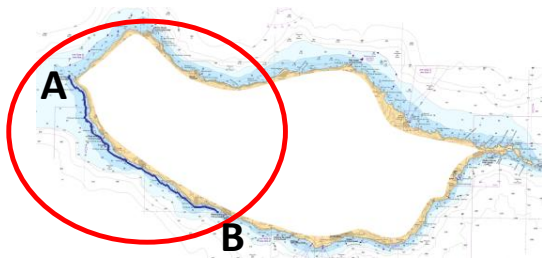


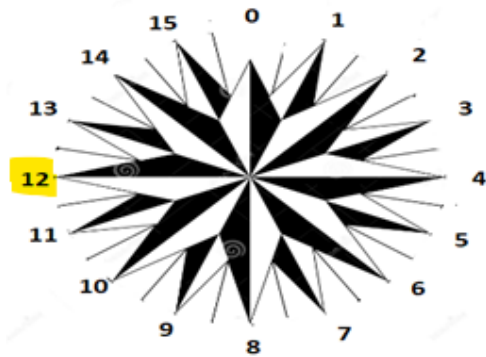
Figure 5.9, Madeira Island, area from Ponta do Pargo to Lugar de Baixo, $|H_{s_{map}} - H_{s_{web}}|$ on a Cartesian grid with 40 meters cell size, simulation 4 ($H_s= 12$ m, $T_p= 20$ s, $Dir= 270^\circ N$).

Figure 5.10 shows the values of $H_{s_{map}}$ and $H_{s_{web}}$ in the observation arc that goes from Ponta do Pargo to Lugar de Baixo, approximately along the 20 m depth contour (because the bathymetry is different).

There is a consistent deviation between the simulated Hs values using different bathymetries, with very few points where $H_{s_{\text{map}}}$ and $H_{s_{\text{web}}}$ are the same.



SIM	Hs (m)	Tp (s)	Dir
4	12	20	12



Hs

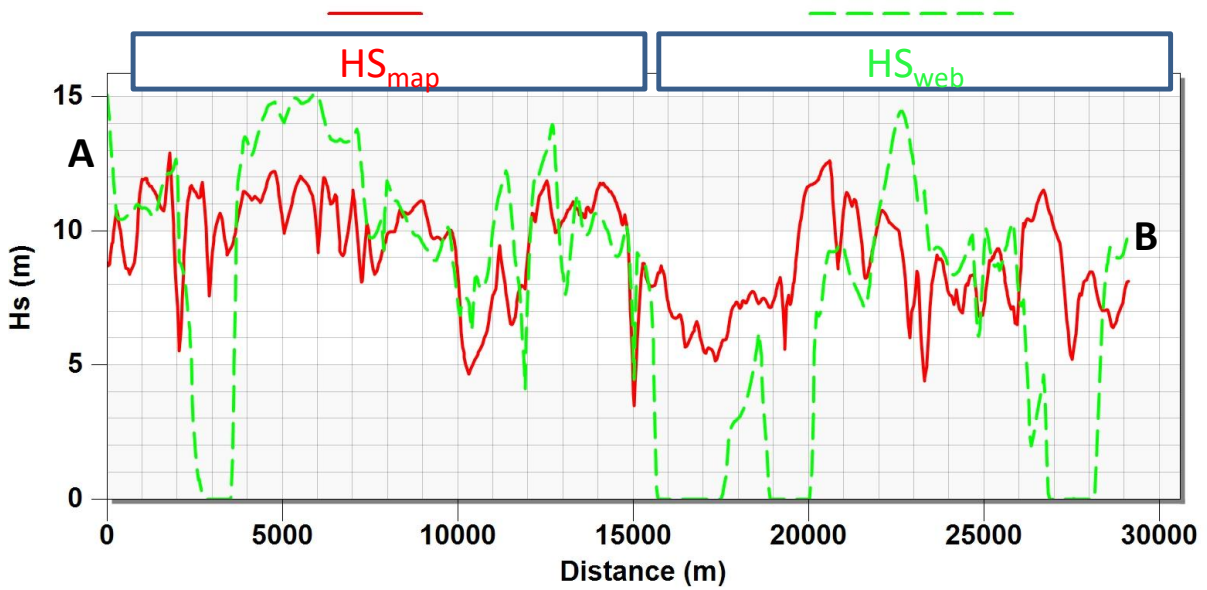
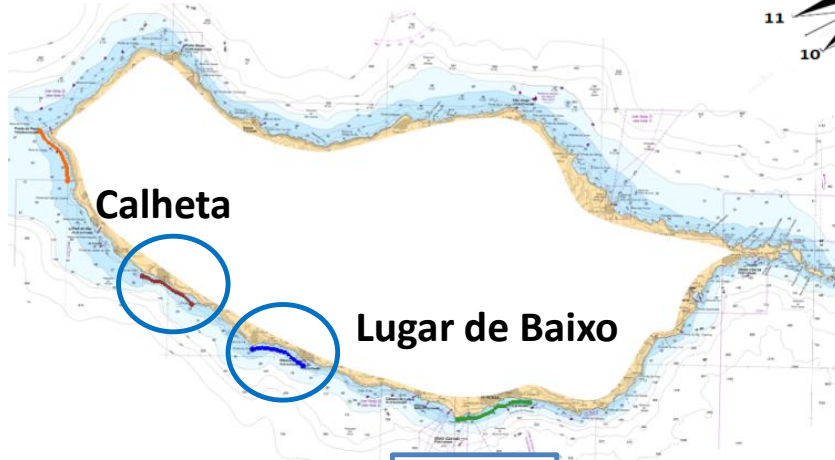
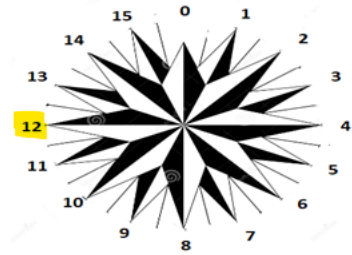


Figure 5.10, Madeira Island, observation arc along the 20m depth contour from Ponta do Pargo to Lugar de Baixo, $H_{s_{map}}$ and $H_{s_{web}}$, simulation 4 ($H_s=12$ m, $T_p=20$ s, $Dir=270$ °N).

Figure 5.11 presents the comparison made for H_s on the observation arc at approximately 20 m depth, but referring to the specific location of Calheta (Figure5.11.a) and Lugar de Baixo (Figure 5.11.b).

SIM	Hs (m)	Tp (s)	Dir
4	12	20	12



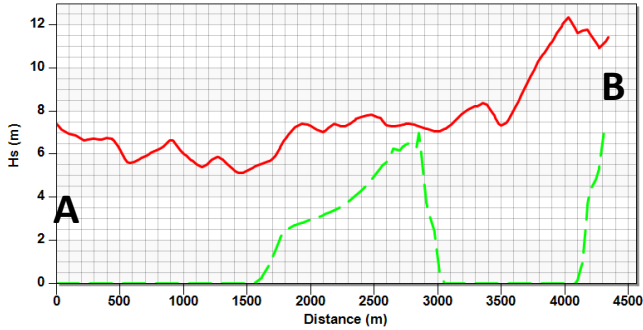
Hs

HS_{map}

HS_{web}

a)

CALHETA



b)

LUGAR DE BAIXO

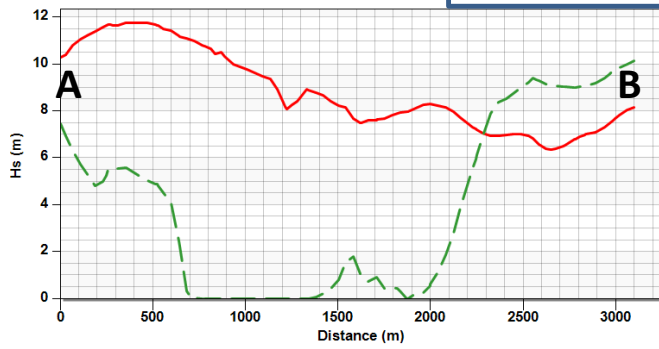


Figure 5.11, Madeira Island, HS_{map} and HS_{web} , simulation 4 ($H_s= 12$ m, $T_p= 20$ s, $Dir = 270$ °N): a) Calheta; b) Lugar de Baixo

5.2.3 SIMULATION 9 ($H_s = 8$ m, $T_p = 17$ s, $Dir = 202.5^\circ N$), waves from SSW.

Figure 5.12 displays the values of $|H_{s_{map}} - H_{s_{web}}|$ on a 40 m cells Cartesian grid.

Similarly to figure 5.9, great values of $|H_{s_{map}} - H_{s_{web}}|$ are present on the whole coast, with the difference exceeding 5 m in many cells. Ponta do Pargo shows the greatest differences.

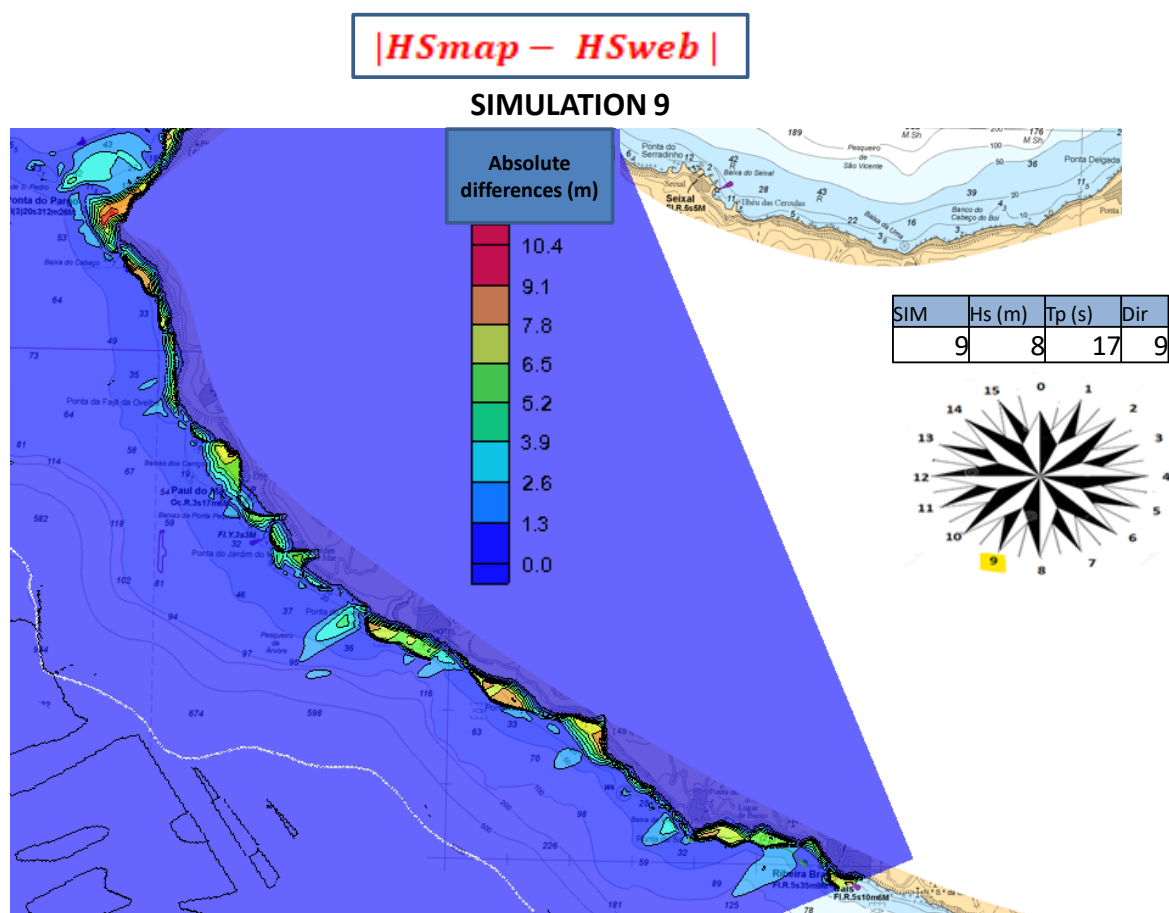
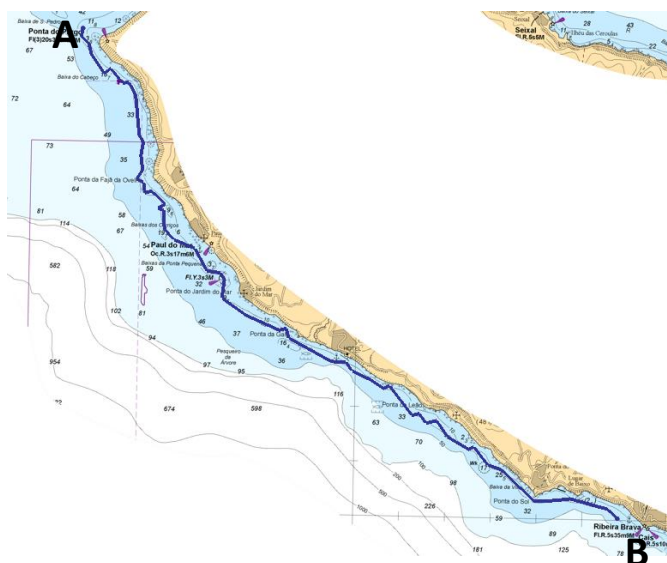
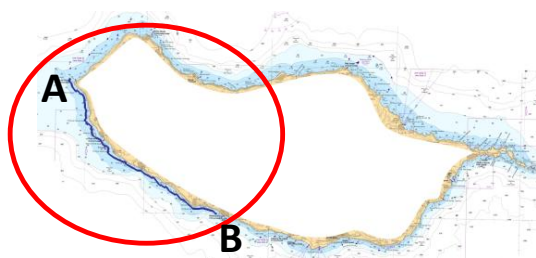


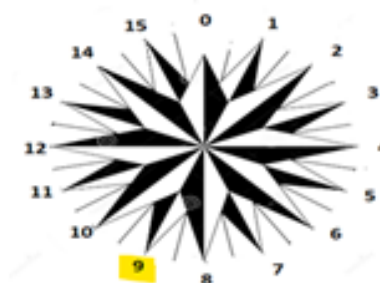
Figure 5.12, Madeira Island, area from Ponta do Pargo to Lugar de Baixo, $|H_{s_{map}} - H_{s_{web}}|$ on a cartesian grid with 40 m cell size, simulation 9 ($H_s = 8$ m, $T_p = 17$ s, $Dir = 202.5^\circ N$).

The significance is confirmed in Figure 5.13, where $H_{s_{map}}$ and $H_{s_{web}}$ on the observation arc from Ponta do Pargo to Lugar de Baixo at approximately 20 m depth are displayed.

Few points where the two curves intercept are displayed, with some $H_{s_{web}}$ values that reach 0, probably due to the fact that the observation arc stands in a land cell in these points.



SIM	Hs (m)	Tp (s)	Dir
9	8	17	9



Hs

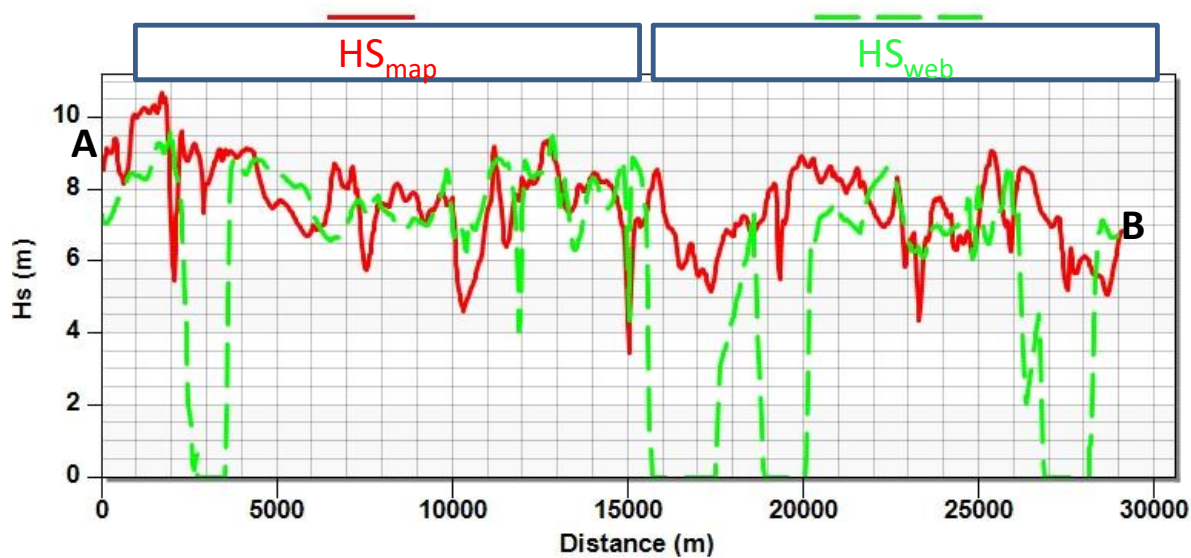
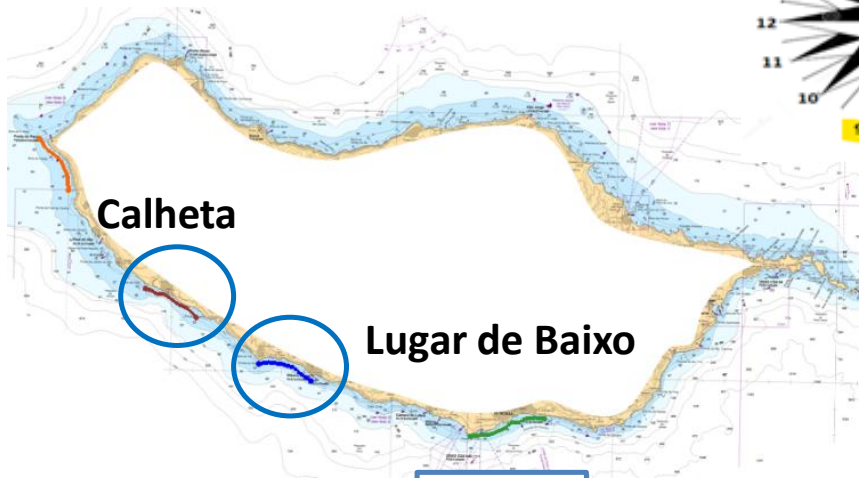
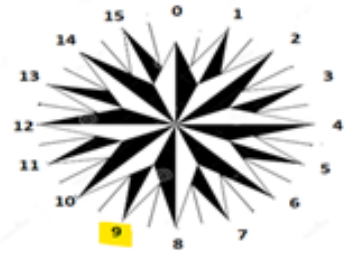


Figure 5.13, Madeira Island, observation arc from Ponta do Pargo to Lugar de Baixo, HS_{map} and HS_{web} , simulation 9 ($H_s=8$ m, $T_p=17$ s, $Dir=202,5^\circ N$).

Figure 5.14 represents Hs_{map} and Hs_{web} on the observation arcs in front of Calheta (Figure 14.a) and Lugar de Baixo (Figure 14.b).

This, along with the consistent distance between the two lines, which is usually at least 2 meters and can reach 6-7 m, provides very strong evidence of the discrepancy between the results obtained using the two different bathymetries for the simulations.

SIM	Hs (m)	Tp (s)	Dir
9	8	17	9



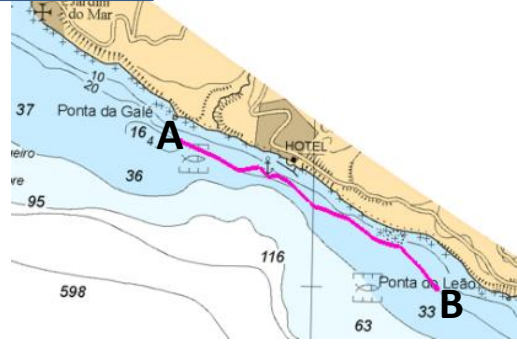
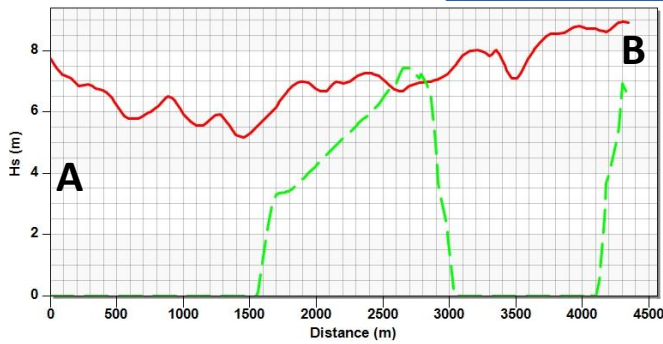
Hs

HS_{map}

HS_{web}

a)

CALHETA



b)

LUGAR DE BAIXO

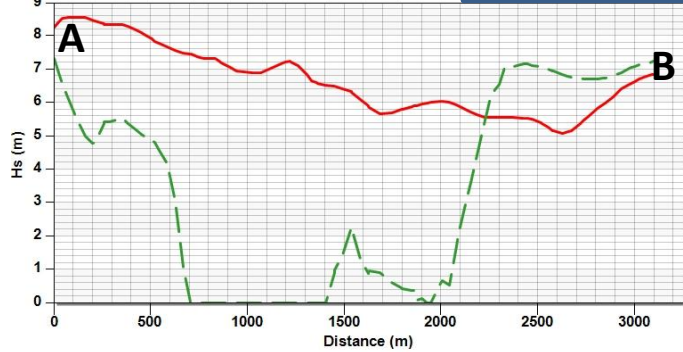


Figure 5.14, Madeira Island, HS_{map} and HS_{web} , simulation 9 ($H_s = 8$ m, $T_p = 17$ s, $Dir = 9^\circ N$): a) Calheta; b) Lugar de Baixo

5.3 BATHYMETRY SURVEY SCATTERSET

After focusing on the comparison between Bathymetry map and a less detailed bathymetry, i.e. Bathymetry web, and the results of the respective simulations, a similar comparison has been conducted between Bathymetry map and a more detailed bathymetry, i.e. Bathymetry survey scatter set.

This bathymetry was obtained by combining points from detailed survey close to the coast from Ponta do Pargo to Lugar de Baixo, with points from the Bathymetry Map, as it has already been explained in chapter 4, see Figure 4.5.

While the comparison made between Bathymetry map and Bathymetry web was completely unequal in terms of accuracy in favour of Bathymetry map, the comparison carried out in this paragraph has revealed to be more fair.

5.3.1 BATHYMETRY SURVEY SCATTERSET versus BATHYMETRY MAP

Figures 5.15 and 5.16 show the differences between the two bathymetries first in 2D and then in 3D. The bathymetries look similar, however the Bathymetry survey scatter set is based on a cloud of points and the Bathymetry Map is based mainly on the values of the bathymetric lines present on the original navigation map. Points in between were interpolated linearly (Figures 5.15.b and 5.16.b). This linear interpolation is clearly visible on the form of triangular faces modelling the bottom. Even small morphological features of the bottom (mounds) may influence wave propagation.

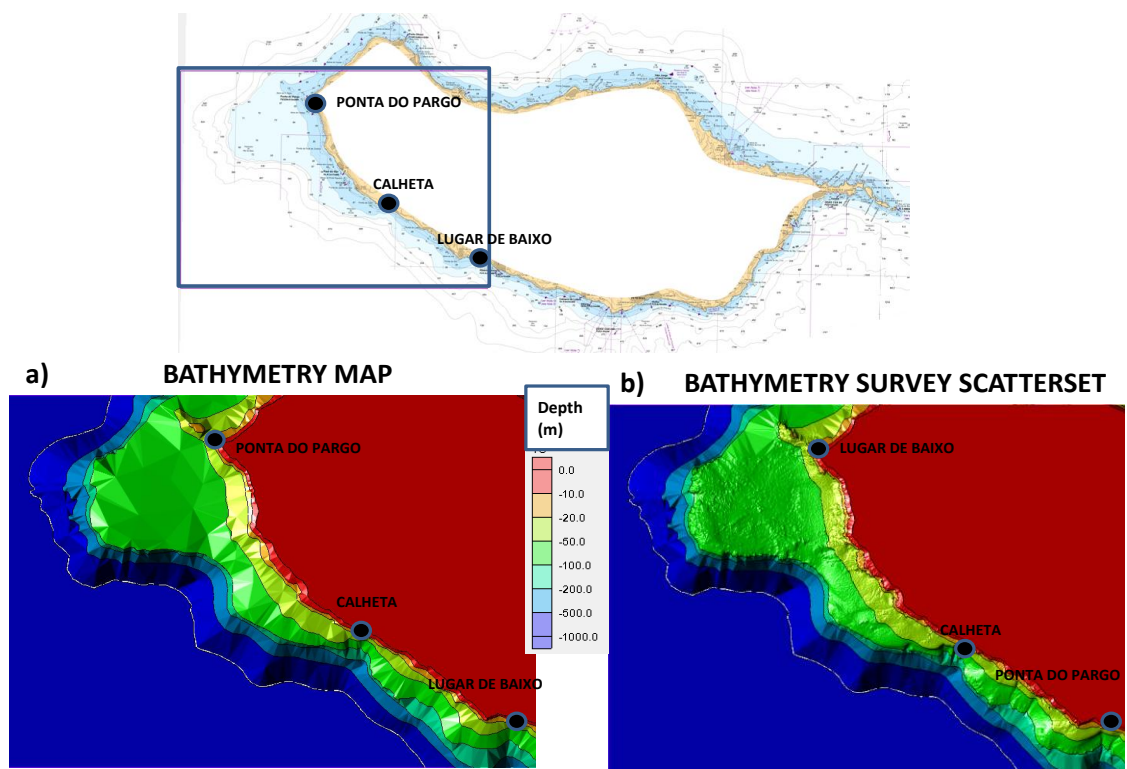


Figure 5.15, Madeira Island, area from Ponta do Pargo to Lugar de Baixo, Bathymetry on 40 m rectangular grid (2D) from:
 a) Bathymetry Map ; b) Bathymetry survey scatter set

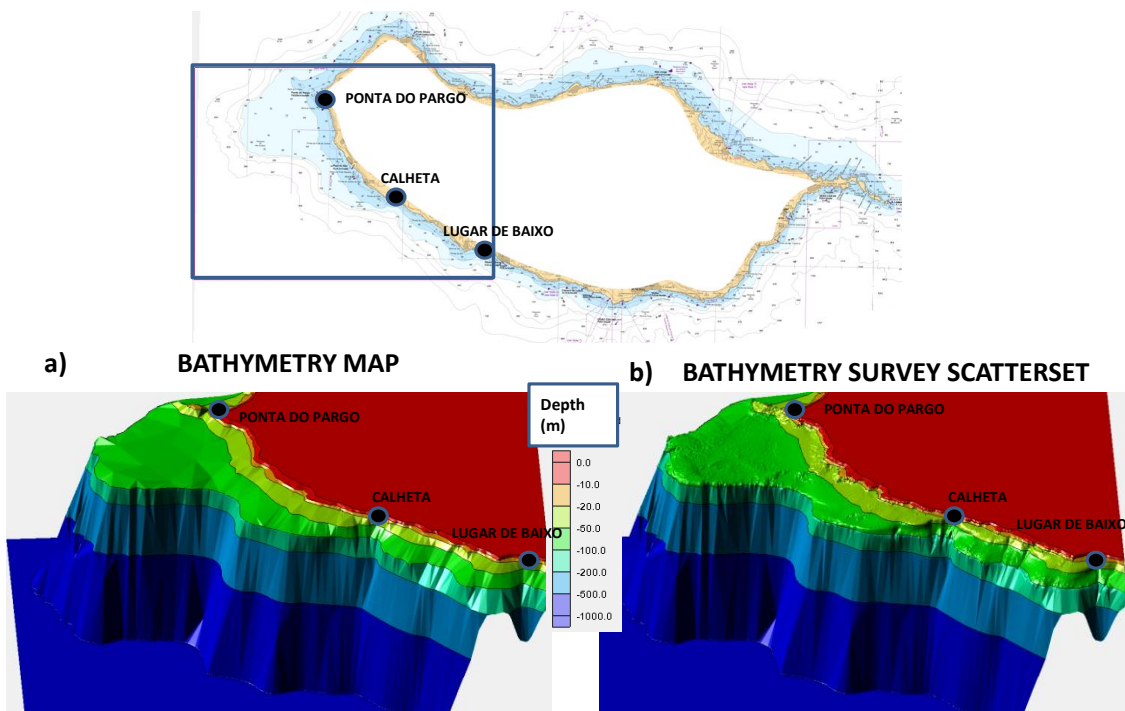
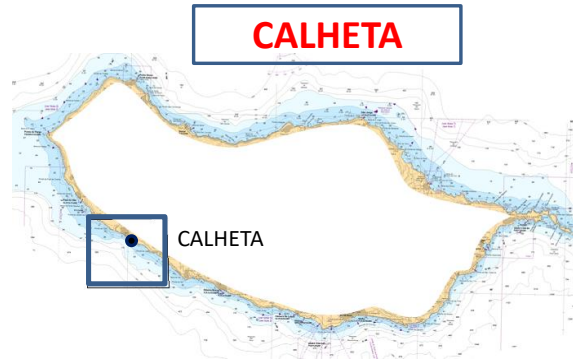
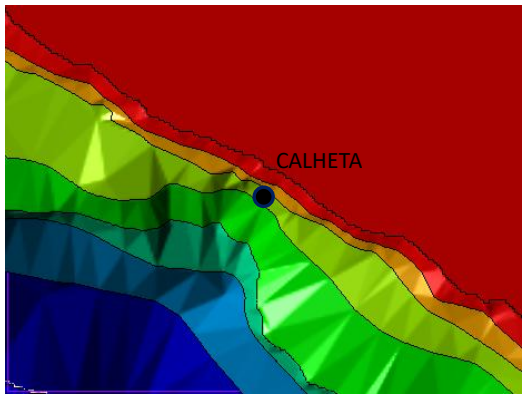


Figure 5.16, Madeira Island, area from Ponta do Pargo to Lugar de Baixo, Bathymetry imported to a 40 m rectangular grid (3D) from: a) Bathymetry Map ; b) Bathymetry survey scatter set

The same conclusion can be drawn comparing the two different bathymetries in front of Calheta (Figure5.17) and Lugar de Baixo (Figure 5.18).



a) BATHYMETRY MAP



b) BATHYMETRY SURVEY SCATTERSET

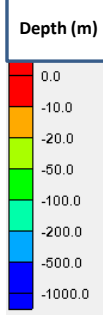
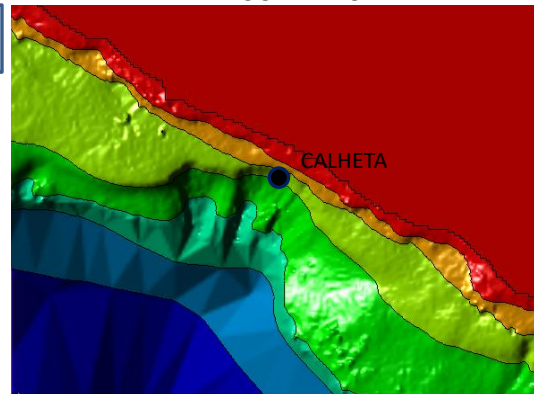
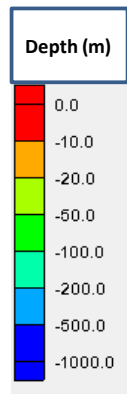


Figure 5.17, Madeira Island, Calheta: a) Bathymetry map; b) Bathymetry survey scatter set

LUGAR DE BAIXO



a) NAVIGATION MAP



b) BATHYMETRY SURVEY SCATTERSET



Figure 5.18, Madeira Island, Lugar de Baixo: a) Bathymetry map; b) Bathymetry web

Lastly, Figure 19 shows the depth differences in each cell of the grid in terms of absolute values, i.e. $|d_{\text{scatter}} - d_{\text{map}}|$.

The values of $|d_{\text{scatter}} - d_{\text{map}}|$ displayed in Figure 5.19, compared to the ones of Figure 5.4, where the values $|d_{\text{map}} - d_{\text{web}}|$ were displayed, show smaller absolute differences, with the huge majority of the cells that presents values of $|d_{\text{scatter}} - d_{\text{map}}|$ smaller than 10 m.

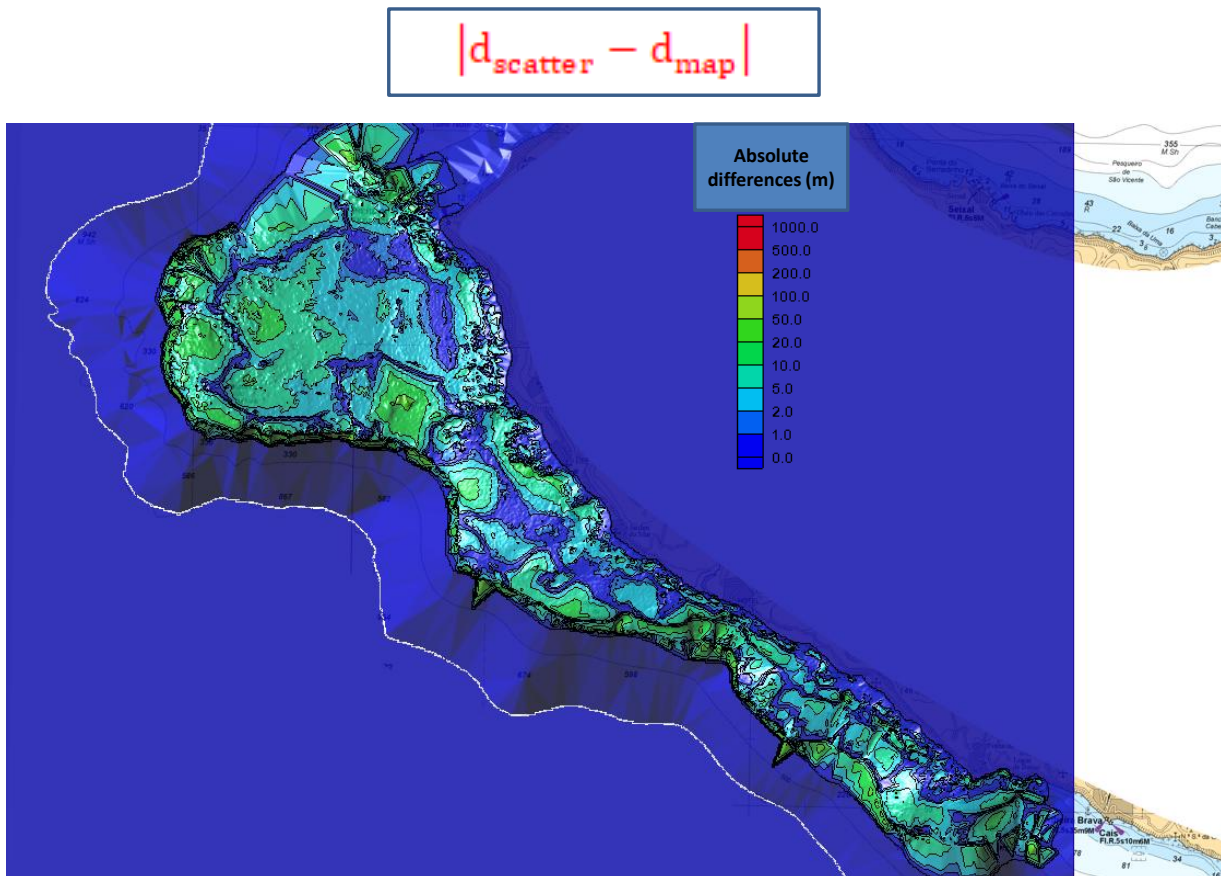


Figure 5.19, Madeira Island, area from Ponta do Pargo to Lugar de Baixo, $|d_{\text{scatter}} - d_{\text{map}}|$ on a Cartesian grid with 40 meters cell size

In order to see if running simulations using Bathymetry map and Bathymetry survey scatter set could actually lead to differences, the simulation 4 ($H_s= 12$ m, $T_p= 20$ s, $Dir=270^\circ N$) and simulation 9 ($H_s= 8$ m, $T_p= 17$ s, $Dir= 202,5^\circ N$) were re-launched with Bathymetry survey scatter.

5.3.2 SIMULATION 4 ($H_s= 12$ m, $T_p= 20$ s, $Dir= 270^\circ N$) waves from W

Figure 5.20 shows the results from Ponta do Pargo to Lugar de Baixo where $|H_{s_{scatter}} - H_{s_{map}}|$.

Following what one might expect after the analyses made in the last paragraph where the values of $|d_{scatter} - d_{map}|$ were presented and compared to the values of $|d_{web} - d_{map}|$, Figure 5.20 shows that the values of $|H_{s_{scatter}} - H_{s_{map}}|$ are smaller than the ones observed for $|H_{s_{web}} - H_{s_{map}}|$.

Some points of the figure, $H_{s_{map}}$ and $H_{s_{scatter}}$ values differ by more than 5 m, reaching the peak of 6,4 m.

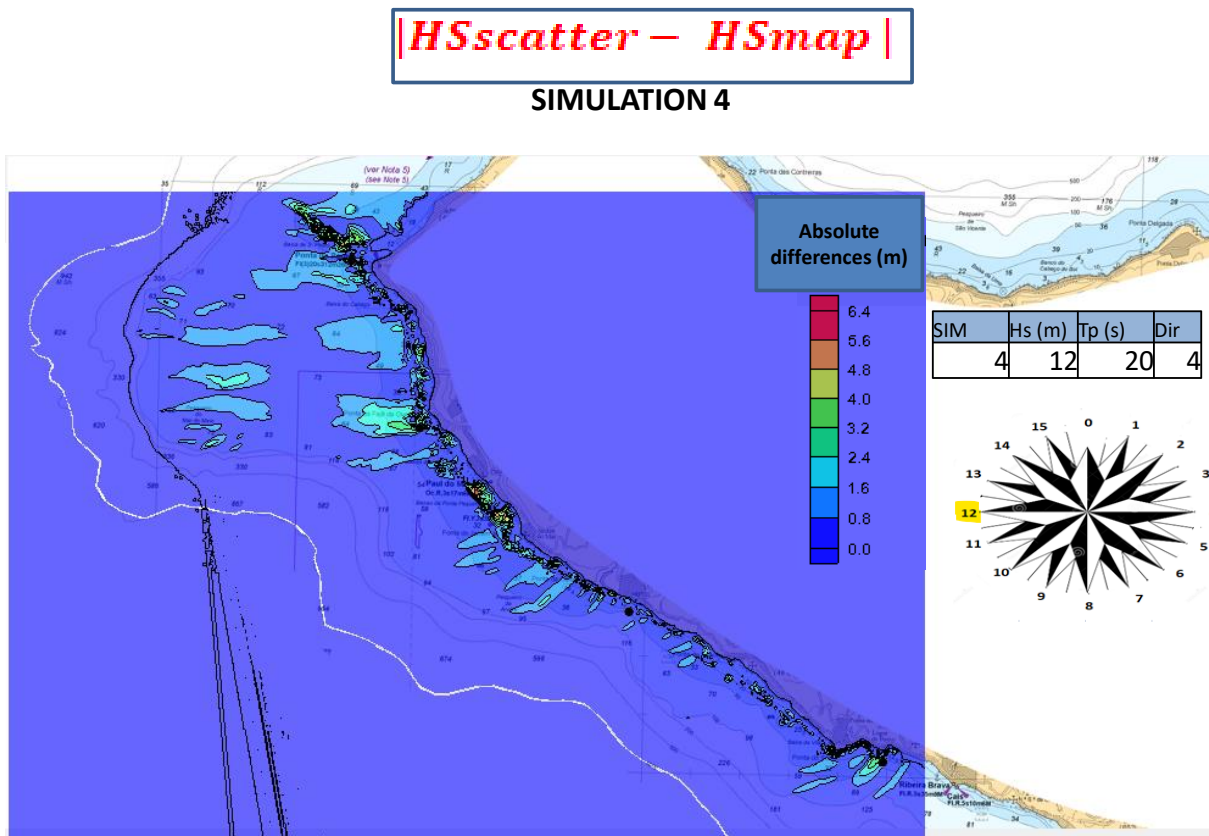
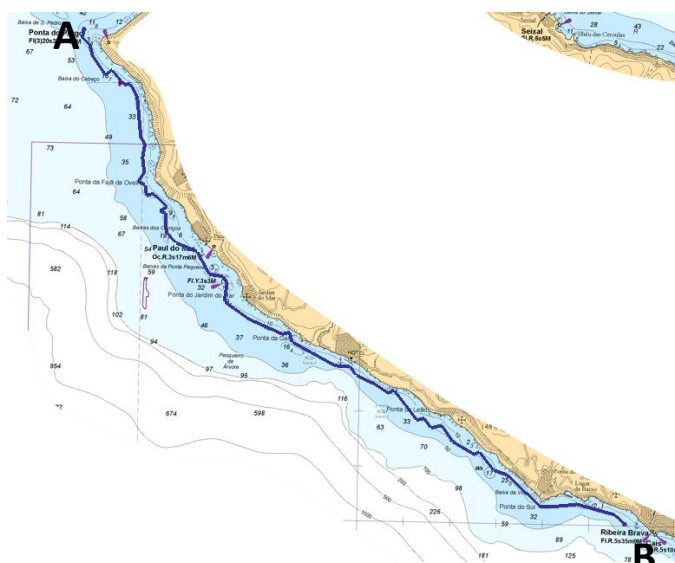
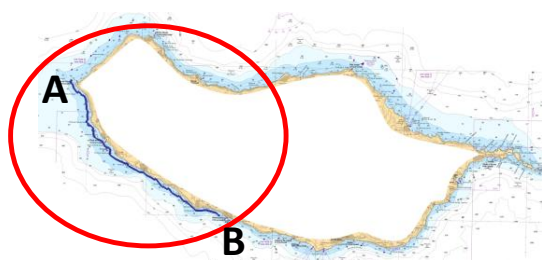


Figure 5.20, Madeira Island, from Ponta do Pargo to Lugar de Baixo, $|H_{s_{scatter}} - H_{s_{map}}|$ on a grid with 40 m cell size, simulation 4 ($H_s 12$ m, $T_p 20$ s, $Dir 12, 270^\circ N$)

These conclusions are confirmed by Figures 5.21 which show the values of $H_{s_{scatter}}$ and $H_{s_{map}}$ (Figure 5.21) on the observation arc from Ponta do Pargo to Lugar de Baixo. Even if Figure 5.21 shows that it is evident that the discrepancy between $H_{s_{map}}$ and $H_{s_{scatter}}$ along the observation arc is not as important as between $H_{s_{map}}$ and $H_{s_{web}}$ on figure 5.10, some points where significant differences occur can be noticed.



SIM	Hs (m)	Tp (s)	Dir
4	12	20	12

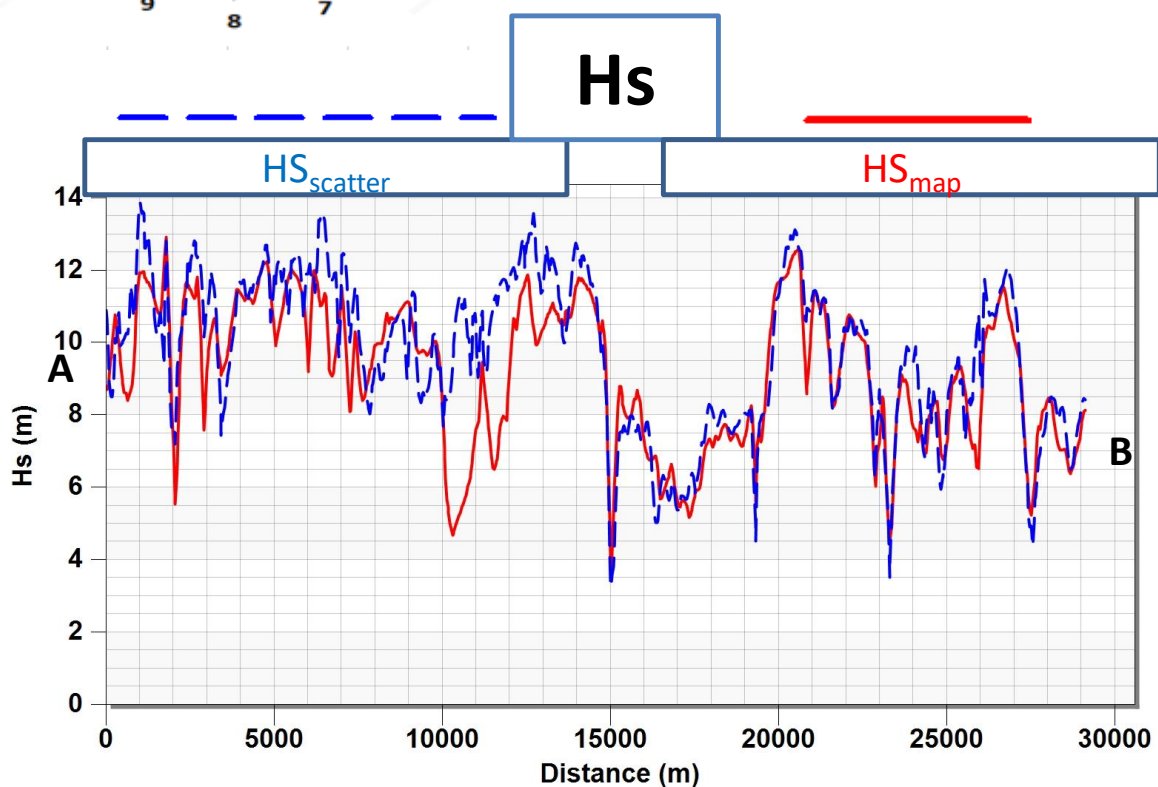
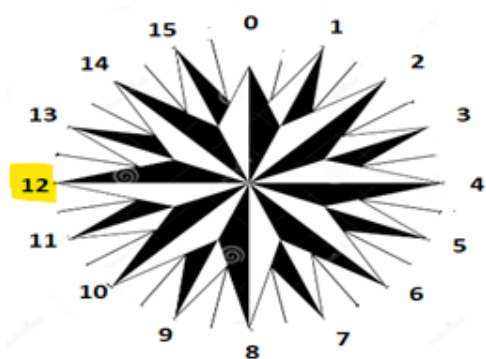
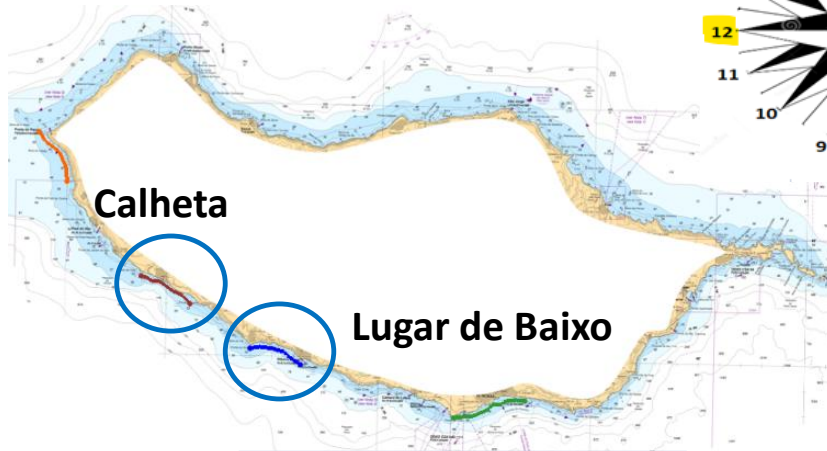
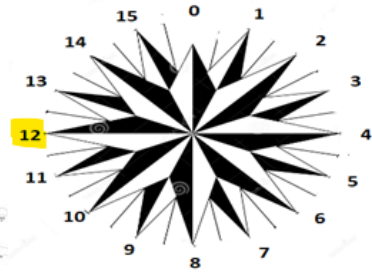


Figure 5.21, Madeira Island, observation arc from Ponta do Pargo to Lugar de Baixo, $HS_{scatter}$ and HS_{map} , simulation 4 ($H_s=12$ m, $T_p=20$ s, $Dir=270$ °N)

Analogous statements follow the comparison between $H_{s_{\text{map}}}$ and $H_{s_{\text{scatter}}}$ in the observation arc in front of Calheta and Lugar de Baixo, displayed in Figure 5.22.

The discrepancy between the curves representing $H_{s_{\text{map}}}$ and $H_{s_{\text{scatter}}}$ is not as evident as it was showed in Figure 5.11 for $H_{s_{\text{map}}}$ and $H_{s_{\text{web}}}$, but still, especially in Lugar e Baixo, discrepancies of more than 2 m can be observed.

SIM	Hs (m)	Tp (s)	Dir
4	12	20	12



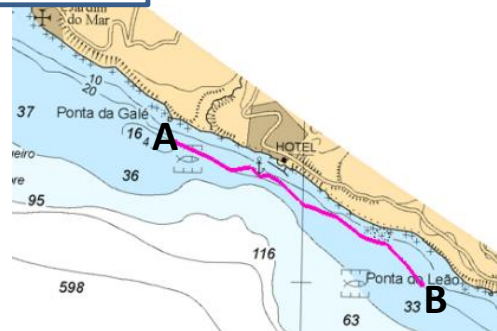
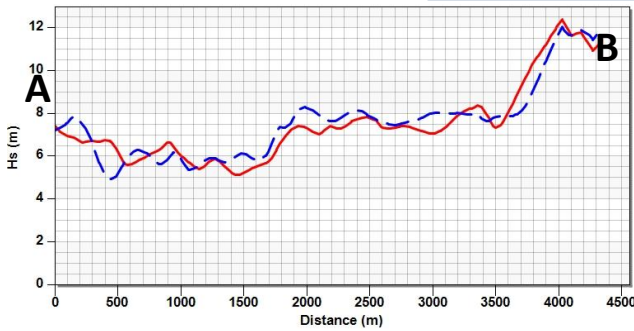
Hs on observation arc

$HS_{scatter}$

HS_{map}

a)

CALHETA



b)

LUGAR DE BAIXO

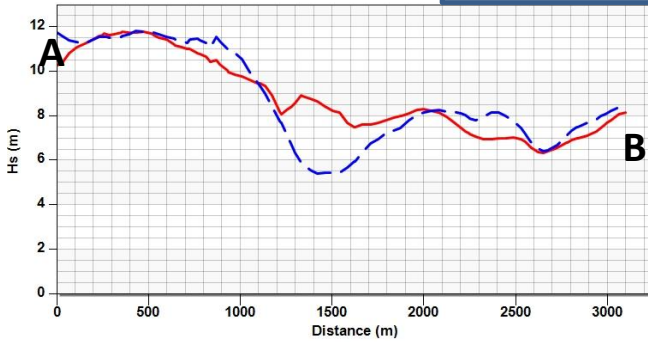


Figure 5.22, Madeira Island, $HS_{scatter}$ and HS_{map} , simulation 4 ($H_s= 12$ m, $T_p= 20$ s, $Dir= 270$ °N): a) Calheta; b) Lugar de Baixo

5.3.3 SIMULATION 9 ($H_s = 8$ m, $T_p = 17$ s, $Dir = 202,5^\circ N$)

Figure 5.23 shows the values of $|H_{s_{scatter}} - H_{s_{map}}|$ on a Cartesian grid having 40 m cells covering the area from Ponta do Pargo do Lugar de Baixo.

These values happen to be even smaller than the ones observed in Figure 5.20 in average.

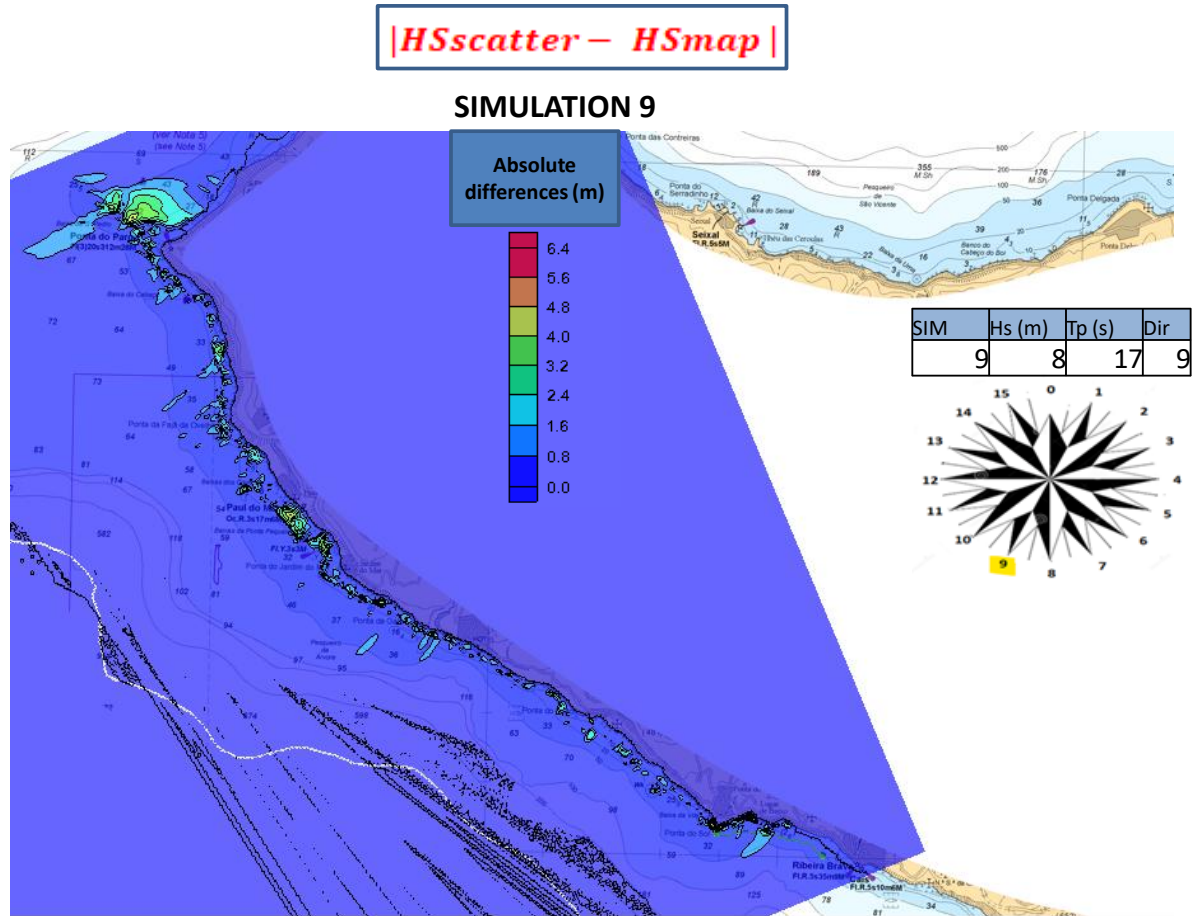
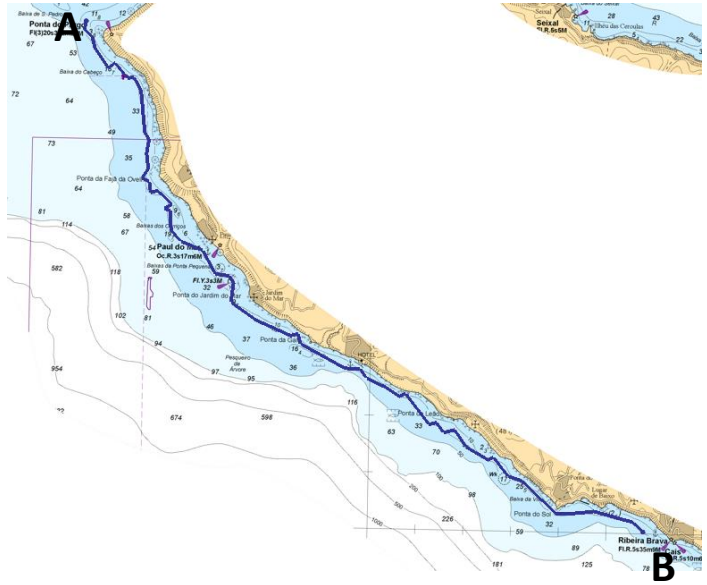
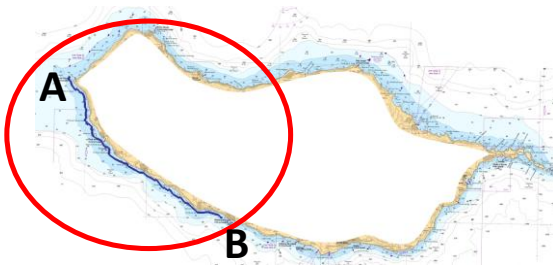
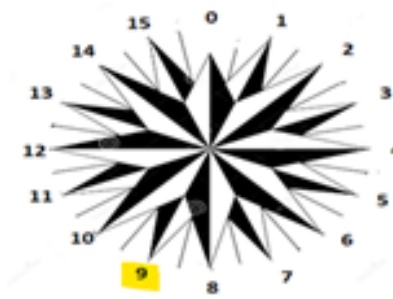


Figure 5.23, Madeira Island, area from Ponta do Pargo to Lugar de Baixo, $|H_{s_{scatter}} - H_{s_{map}}|$ on a Cartesian grid with 40 meters cell size, simulation 9 ($H_s = 8$ m, $T_p = 17$ s, $Dir = 202,5^\circ N$)

Figure 5.24 shows the trend of $H_{s_{scatter}}$ and $H_{s_{map}}$ on the observation arc going from Ponta do Pargo to Lugar de Baixo.



SIM	Hs (m)	Tp (s)	Dir
9	8	17	9



Hs

$HS_{scatter}$

HS_{map}

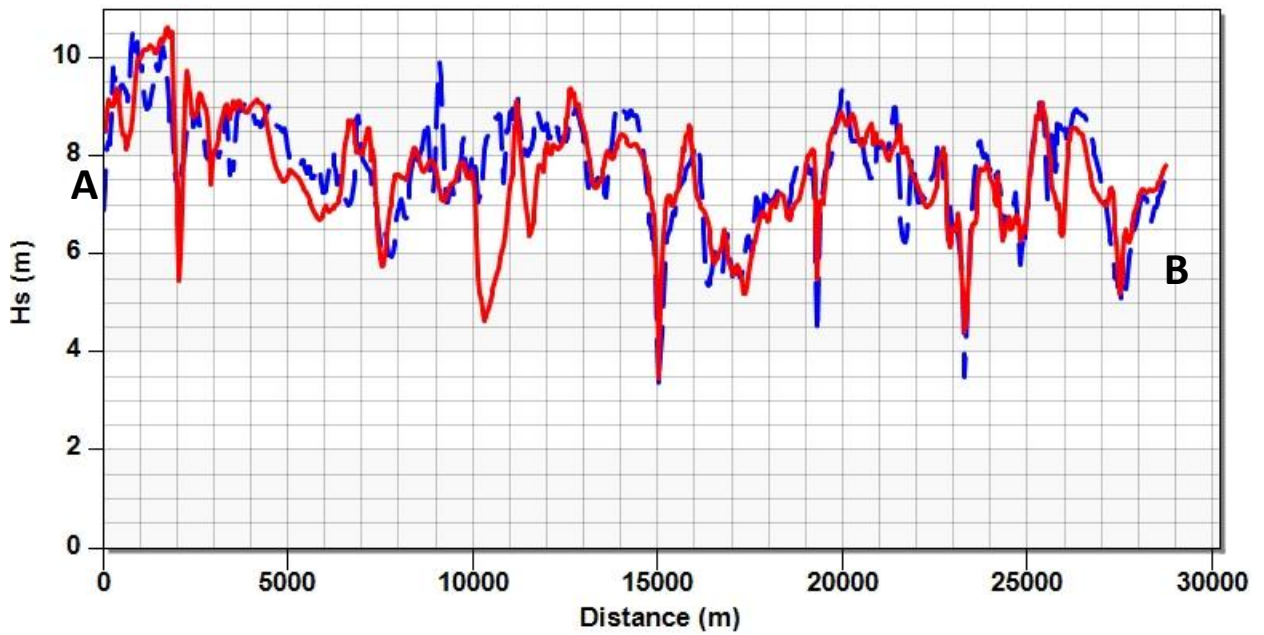
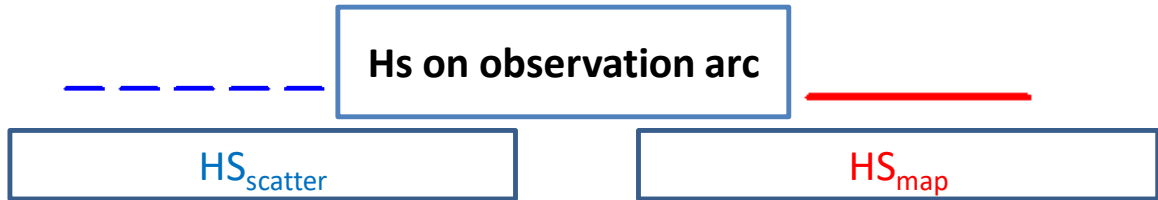
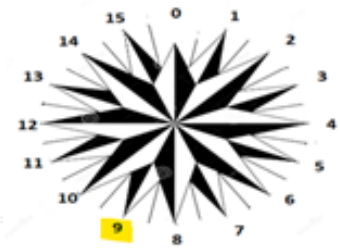


Figure 5.24, Madeira Island, from Ponta do Pargo to Lugar de Baixo, $Hs_{scatter}$ and Hs_{map} , simulation 9 ($Hs= 8$ m, $Tp= 17$ s, $Dir= 202,5$ °N)

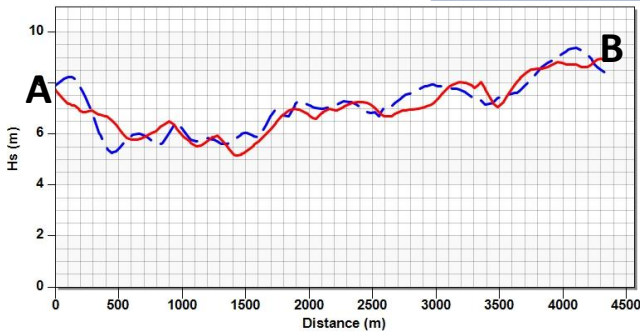
Lastly, Figure 5.25 shows the values of $Hs_{scatter}$ and Hs_{map} along the observation arcs in front of Calheta and Lugar de Baixo.

As in Figure 5.22, the trend of the curves is quite similar, except for a portion on the observation arc in front of Lugar de Baixo where Hs values are consistently different.

SIM	Hs (m)	Tp (s)	Dir
9	8	17	9



CALHETA



LUGAR DE BAIXO

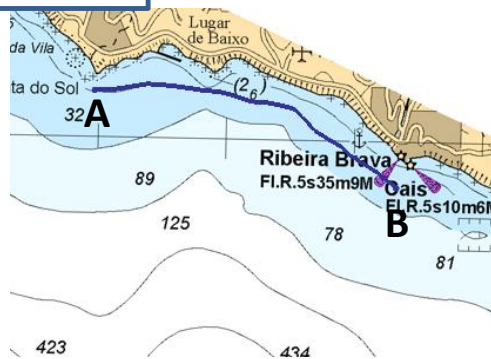
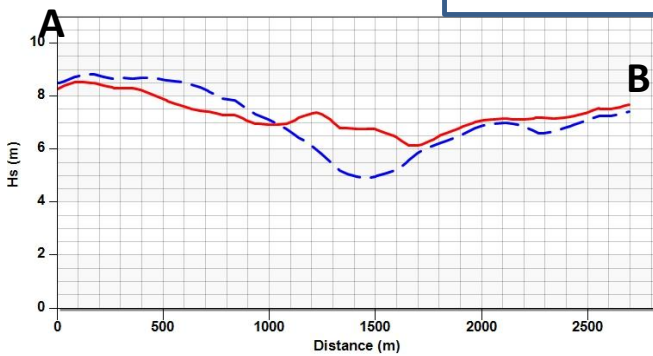


Figure 5.25, Madeira Island, $HS_{scatter}$ and HS_{map} , simulation 9 ($H_s=8$ m, $T_p=17$ s, $Dir=202,5^\circ N$): a) Calheta; b) Lugar de Baixo

5.4 SUMMARY

In this chapter, particular attention has been given to the type of bathymetry that can be used as a basis for simulations, such as those carried out in Chapter 4. After presenting the main differences between the three available bathymetries in the context of this study, it was demonstrated how the results of the simulations could vary significantly depending on the choice of one bathymetry over another. Below are listed the most noteworthy conclusions related to this chapter.

- The bathymetry map used for simulations in Chapter 4 appears to have a good level of precision and reliability, following the discussed in paragraph 5.2.1, particularly in Figure 5.2. However, after comparing it with the Bathymetry Survey Scatter Set, it is evident that further improvements in bathymetry precision and accuracy can lead to results that differ even from a highly accurate study like the one conducted in Chapter 5.
- Bathymetry Web exhibits precision and accuracy that can be considered entirely inadequate for conducting studies like the one carried out in this thesis (see figures 5.10 and 5.13 in particular).
- Considering all the results presented, it can be concluded that a lack of attention in the bathymetry selection phase can lead to misleading outcomes in the evaluation of design conditions for structures aimed at coastal protection from wave power.

6 CONCLUSIONS

In this thesis work, a study was conducted on the wave climate near the island of Madeira. This study was divided into three main parts: the first, in which the climate conditions in the waters off the island were defined, was developed in Chapters 2 and 3; the second, developed in Chapter 4, assessed the propagation of wave conditions from offshore to the coast, particularly the southwest coast of the island. Chapter 5 conducted an analysis regarding the influence of bathymetry in works similar to those in Chapter 4.

In the first part, starting from Hindcast data provided near specific points offshore of the Madeira island, the wave climate conditions were first analyzed on various sides of the island, with special attention to the southwest coast. It was observed how considering one side of the island over another could lead to significant differences in wave climate.

Conditions could vary, first of all, in terms of the absolute H_s value. It was noted that values of H_s were significantly higher in the points to the north and west of the island compared to those observed in the southern points. Differences were also noticeable concerning Dir.

These two conclusions drew attention to the presence of the island's shadow effect. While it was mentioned in the introduction that one would expect wave conditions to not vary much over the ocean surface in the absence of obstacles, what was observed in Chapter 2 leads to the conclusion that the island of Madeira represents a significant obstacle in the propagation of wave conditions.

Subsequently, in Chapter 3, data from the three points closest to the southwest coast of the island were examined, and a study was conducted on the relationship between H_s and T_p , the variability of conditions in different months, and extreme values. The study of variability in different months is particularly interesting to determine the best time of the year for activities requiring calm conditions. Variations too pronounced in the observed data may suggest avoiding such interventions during that period of the year.

Regarding the relationship between H_s and T_p and the extreme values, they served as the basis for the wave propagation study conducted in Chapter 4, where certain wave conditions were propagated from offshore to the southwest coast using the STWAVE software. The decision about which conditions to propagate was based on the study of extreme values and the relationship between H_s and T_p . A reference wave with a return period of 100 years was chosen, corresponding to an H_s value of 12 m and a T_p value of 20 s for waves coming from the west, and an H_s of 8 m and a T_p of 17 s for waves coming from the south.

In the second part of the thesis, simulations were carried out with STWAVE to propagate these waves towards the coast. The main objective of this section was to determine which waves were more important to consider in different portions of the southwest coast. Particularly offshore of the islands, bathymetry is very irregular, and it was shown how, due to the phenomenon of refraction, wave conditions could propagate nonlinearly and reach very close portions of the coast in different ways.

The last part of the thesis is based on a question that arises following the conclusions of the second part: if bathymetry conditions can influence wave propagation so much, how much can the results of such studies vary using different sources of bathymetric information as a basis? Chapter 5 presents a comparison between the simulations carried out in chapter 4 and the same simulations conducted with different bathymetry sources.

What emerged from this comparison is that the results vary significantly. Even a carefully conducted study like the one in this thesis can lead to significantly different results compared to those obtained from a study with different bathymetry sources. This highlights the importance of carefully choosing, in relation to the type of study being conducted, the elements on which the analysis is based, starting from the choice of Hindcast data, through the mode of extreme value analysis, and the choice of simulation boundary conditions, ending with the most appropriate selection of bathymetry.

7 LIST OF FIGURES

Figure 2.1, Madeira Island, location of the five points where Hindcast data have been analysed: North East, North, North West, South West, and South.....	7
---	---

Figure 2.2, Madeira Island, location of the North West point.....	9
Figure 2.3, Classification of data into 16 directions for analysis.	10
Figure 2.4, Polar diagram of Hs, North West point.....	11
Figure 2.5, Polar Diagram for Tp, North West point.....	13
Figure 2.6, Comparison of Polar Diagram for Hs between Winter and Summer, North West point	14
Figure 2.7, comparison of Polar Diagram for Tp between Winter and Summer, North West point.....	15
Figure 2.8, North West point, comparison of minimum, maximum, and average Hs values for each direction between: a) Winter; b) Summer.....	16
Figure 2.9, North West point, comparison of minimum, maximum, and average Tp values for each direction between: a) Winter; b) Summer.....	17
Figure 2.10, Madeira Island, location of the North West point and the South West point.....	18
Figure 2.11, comparison of Polar Diagrams with Hs between the North West point and the South West point.	19
Figure 2.12, Madeira Island, location of the North point and the South point	20
Figure 2.13, comparison polar diagrams with Hs values between the North point and the South point.	21
Figure 2.14, Madeira Island, location of the North point and the North East point	22
Figure 2.15, Comparison of direction distribution with Hs values between the North point and the North East point.....	23
Figure 2.16, location of the North East point.	24
Figure 2.17, Madeira Island, location of the South West and the South point	24
Figure 2.18, comparison of direction distribution with Hs values between the South West point and the South point.....	25
Figure 2.19, Madeira Island, location of 11 points from Copernicus dataset	Errore. Il segnalibro non è definito.
Figure 3.1, Madeira Island, South West coast, area of interest from Ponta do Pargo to Funchal.	27
Figure 3.2, Madeira Island, closest points to South West coast where Hindcast data were available: North West, South West and South	28
Figure 3.3, Joint distribution Tp and Hs, North West point.	30
Figure 3.4, Histogram of Tp and the percentage of Hs. Colours representing intervals of Hs. North West point.....	31
Figure 3.5, Joint distribution Tp and Hs, North West point, direction 0 (0°N).	Errore. Il segnalibro non è definito.
Figure 3.6 Histogram of Tp and the percentage of Hs. Colours representing intervals of Hs. North West point, direction 0 (0°N).....	Errore. Il segnalibro non è definito.
Figure 3.7, Joint distribution Tp and Hs, North West point, direction 1 (22,5°N).	Errore. Il segnalibro non è definito.
Figure 3.8, Joint distribution Tp and Hs, North West point, direction 15 (337,5°N).	Errore. Il segnalibro non è definito.
Figure 3.9, Joint distribution Tp and Hs, North West point, direction 15 (337,5°N).	Errore. Il segnalibro non è definito.
Figure 3.10, Histogram of Tp and the percentage of Hs. Colours representing intervals of Hs. North West point,.....	Errore. Il segnalibro non è definito.
Figure 3.11, Joint distribution Tp and Hs, North West point, direction 14(315 °N).	Errore. Il segnalibro non è definito.
Figure 3.12, Histogram of Tp and the percentage of Hs. Colours representing intervals of Hs. North West point, direction 14 (315 °N).....	Errore. Il segnalibro non è definito.
Figure 3.13, Joint distribution Tp and Hs, North West point, direction 13 (292,5 °N).	Errore. Il segnalibro non è definito.

Figure 3.14, Histogram of T_p and the percentage of H_s . Colours representing intervals of H_s . North West point, direction 13 ($292,5^\circ N$).....	Errore. Il segnalibro non è definito.
Figure 3.15, Box plot showing the monthly variability in terms of H_s . Red points: outliers; Black lines: “whiskers”, Blue lines: median; upper side of the box: 75 th percentile; lower side of the box: 25 th percentile. North West point.	35
Figure 3.16, Plot comparing frequency distribution relative to the sample of data under consideration with both the Gumbel and Weibull curves to determine which curve provides a better fit to the data.	41
Figure 3.17, Plot comparing the CDFs fitted to the data sample using both MLE method and MM , in order to determine which method provides better parameters for fitting the data. Errore. Il segnalibro non è definito.	
Figure 4.1, Madeira Island, Package 1 of simulations with waves coming from 12 to 15 direction, and 0. ...	49
Figure 4.2, Madeira island, Package 2 of simulations with waves coming from 8 to 11 direction	52
Figure 4.3, Madeira Island, navigation map used to manually create the scatter set with the depth.....	55
Figure 4.4, Madeira Island, Bathymetry downloaded from the Web, GeoTiff file.	56
Figure 4.5, Madeira Island, survey scatter set merged with points of the Bathymetry Map in order to create the Bathymetry survey scatter set.	56
Figure 4.6, comparison of results obtained with 10, 40, 60 and 100 meters cells grid, Ponta do Pargo.	58
Figure 4.7, Madeira Island, 6 monitoring points: Ponta do Pargo, Ponta do Foja do Ovelja, Hotel (Calheta), Lugar de Baixo, Cabo Girao and Funchal.	59
Figure 4.8 - Madeira Island. Observation arcs at 20 m depth contour: Ponta do Pargo, Calheta, Lugar de Baixo and Funchal.....	61
Figure 4.9 - Madeira Island. South West part, H_s values and Dir, Simulation 1 ($H_s=12$ m, $T_p=20$ s, Dir = $315^\circ N$).	62
Figure 4.10 - Madeira Island, Ponta do Pargo, H_s at 20 m depth, simulation 1 ($H_s=12$ m, $T_p= 20$ s, Dir= $315^\circ N$).	63
Figure 4.11 - Madeira Island, Calheta, H_s variation at 20 meters depth, simulation 1 (H_s 12 m, T_p 20 s, Dir = $315^\circ N$).....	64
Figure 4.12 - Madeira Island, South West part, H_s values and Dir, Simulation 2 (H_s =12 m, T_p =20 s, Dir= $337,5^\circ N$).	65
Figure 4.13 - Madeira Island, Ponta do Pargo, H_s variation at 20 meters depth, simulation 2 ($H_s=12$ m, $T_p=20$ s, Dir= $337,5^\circ N$).	66
Figure 4.14 - Madeira Island, Calheta, H_s variation at 20 meters depth, simulation 2 ($H_s= 12$ m, $T_p= 20$ s, Dir= $337,5^\circ N$).....	67
Figure 4.15 - Madeira Island, South West part, H_s values and Dir, Simulation 3 ($H_s= 12$ m, $T_p= 20$ s, Dir= $292,5^\circ N$).....	68
Figure 4.16 - Madeira Island, Calheta, H_s variation at 20 meters depth, simulation 3 ($H_s= 12$ m, $T_p= 20$ s, Dir= $292,5^\circ N$).....	69
Figure 4.17 - Madeira Island, Lugar de Baixo, H_s variation at 20 meters depth, simulation 3 ($H_s= 12$ m, $T_p= 20$ s, Dir= $292,5^\circ N$).	70
Figure 4.18 - Madeira Island, Funchal, H_s variation at 20 meters depth, simulation 3 ($H_s= 12$ m, $T_p= 20$ s, Dir= $292,5^\circ N$).....	71
Figure 4.19 - Madeira Island, South West part, simulation 6 (H_s 8= m, $T_p= 17$ s, Dir= $225^\circ N$):	72
Figure 4.20 - H_s at 20 meters depth, simulation 6 ($H_s= 8$ m, $T_p= 17$ s, Dir= $225^\circ N$):	74
Figure 4.21 - Madeira Island, South West part, simulation 7 ($H_s= 8$ m, $T_p= 17$ s, Dir= $247,5^\circ N$):	74
Figure 4.22 -, H_s at 20 meters depth, simulation 6 ($H_s= 8$ m, $T_p= 17$ s, Dir= $247,5^\circ N$):	76
Figure 4.23 - Madeira Island, South West part, simulation 8 ($H_s= 8$ m, T_p 17= s, Dir= $180^\circ N$):	76
Figure 4.24 - H_s at 20 m depth contour, simulation 6 ($H_s= 8$ m, $T_p= 17$ s, Dir= $247,5^\circ N$):	78
Figure 4.25 - a) simulation 4 ($H_s= 12$ m, $T_p= 20$ s, Dir= $270^\circ N$); b) Simulation 9 ($H_s= 8$ m, $T_p= 17$ s, Dir= $202,5^\circ N$)	78

Figure 4.26 - a) Hs and Dir, Simulation 4 (Hs= 12 m, Tp= 20 s, Dir= 270 °N); b) Hs and Dir, Simulation 9 (Hs= 8 m, Tp= 17 s, Dir= 202,5 °N); a.i) Breaking, Simulation 4 (Hs= 12 m, Tp= 20 s, Dir= 270 °N); b.i) Breaking, Simulation 9 (Hs 8= m, Tp= 17 s, Dir=270 °N)	80
Figure 4.27 - Hs at 20 meters depth: a)Calheta, Simulation 4 (Hs= 12 m, Tp= 20 s, Dir= 270 °N); b) Hs and Dir, Simulation 9 (Hs= 8 m, Tp= 17 s, Dir= 202,5 °N); a.i) Breaking, Simulation 4 (Hs= 12 m, Tp= 20 s, Dir= 270 °N); b.i) Breaking, Simulation 9 (Hs 8= m, Tp= 17 s, Dir=270 °N)	82
Figure 4.28 - Madeira Island, Bathymetry with waves direction: a) Calheta; b) Lugar de Baixo.....	83
Figure 4.33 - Madeira Island, South West part, Simulation 5 (Hs= 12 m, Tp= 20 s, Dir= 0 °N):	84
Figure 4.30 - Madeira Island, South West part, simulation 4 (Hs= 12 m, Tp= 20 s, Dir= 270 °N):	85
Figure 4.31 - Madeira Island, South West part, simulation 9 (Hs= 8 m, Tp= 17 s, Dir= 247,5 °N):	86
Figure 5.1, a) GeoTiff file of bathymetry downloaded from the Web; b) GeoTiff file converted to scatter set; c)scatter set showing 400 meters distance between elevation points	89
Figure 5.2, Madeira Island, area from Ponta do Pargo to Lugar de Baixo. Bathymetry imported to a 40 m rectangular grid (2D) from: a) Bathymetry Map ; b) Bathymetry Web	90
Figure 5.3, Madeira Island, area from Ponta do Pargo to Lugar de Baixo, Bathymetry imported to a 40 m rectangular grid (3D) from: a) Bathymetry Map ; b) Bathymetry Web	91
Figure 5.4, Madeira Island, South West part, dmap – dweb on a Cartesian grid with 40 m cell size.	92
Figure 5.6, Madeira Island, South West part, Bathymetry lines from Bathymetry web above navigation map used to create Bathymetry map	93
Figure 5.7, Madeira Island, Bathymetry lines from Bathymetry web above navigation map used to create Bathymetry map: a) top left portion displayed in Figure 6; b) bottom right portion displayed in Figure 6....	95
Figure 5.7, Madeira Island, Calheta: a) Bathymetry map; b) Bathymetry web.....	95
Figure 5.8, Madeira Island, Lugar de Baixo: a) Bathymetry map; b) Bathymetry web	96
Figure 5.9, Madeira Island, area from Ponta do Pargo to Lugar de Baixo, HSmap – HSweb on a Cartesian grid with 40 meters cell size, simulation 4 (Hs= 12 m, Tp= 20 s, Dir= 270 °N).....	97
Figure 5.10, Madeira Island, observation arc along the 20m depth contour from Ponta do Pargo to Lugar de Baixo, HSmap and HSweb , simulation 4 (Hs= 12 m, Tp= 20 s, Dir= 270 °N).	99
Figure 5.11, Madeira Island, HSmap and HSweb , simulation 4 (Hs= 12 m, Tp= 20 s, Dir = 270 °N): a) Calheta; b) Lugar de Baixo.....	101
Figure 5.12, Madeira Island, area from Ponta do Pargo to Lugar de Baixo, HSmap – HSweb on a cartesian grid with 40 m cell size, simulation 9 (Hs= 8 m, Tp= 17 s, Dir= 202,5 °N).	102
Figure 5.13, Madeira Island, observation arc from Ponta do Pargo to Lugar de Baixo, HSmap and HSweb , simulation 9 (Hs= 8 m, Tp= 17 s, Dir= 202,5 °N).....	103
Figure 5.14, Madeira Island, HSmap and HSweb , simulation 9 (Hs= 8 m, Tp= 17 s, Dir= 9= °N): a) Calheta; b) Lugar de Baixo.....	105
Figure 5.15, Madeira Island, area from Ponta do Pargo to Lugar de Baixo, Bathymetry on 40 m rectangular grid (2D) from: a) Bathymetry Map ; b) Bathymetry survey scatter set	107
Figure 5.16, Madeira Island, area from Ponta do Pargo to Lugar de Baixo, Bathymetry imported to a 40 m rectangular grid (3D) from: a) Bathymetry Map ; b) Bathymetry survey scatter set	108
Figure 5.17, Madeira Island, Calheta: a) Bathymetry map; b) Bathymetry survey scatter set.....	109
Figure 5.18, Madeira Island, Lugar de Baixo: a) Bathymetry map; b) Bathymetry web	110
Figure 5.19, Madeira Island, area from Ponta do Pargo to Lugar de Baixo, dscatter – dmap on a Cartesian grid with 40 meters cell size	111
Figure 5.20, Madeira Island, from Ponta do Pargo to Lugar de Baixo, HSscatter – HSmap on a grid with 40 m cell size, simulation 4 (Hs 12 m, Tp 20 s, Dir 12, 270 °N)	112
Figure 5.21, Madeira Island, observation arc from Ponta do Pargo to Lugar de Baixo, HSscatter and HSmap , simulation 4 (Hs= 12 m, Tp= 20 s, Dir= 270 °N).....	113
Figure 5.22, Madeira Island, HSmap and HSweb , simulation 4 (Hs= 12 m, Tp= 20 s, Dir= 270 °N): a) Calheta; b) Lugar de Baixo.....	115

Figure 5.23, Madeira Island, area from Ponta do Pargo to Lugar de Baixo, <i>HSscatter – HSmap</i> a Cartesian grid with 40 meters cell size, simulation 9 (Hs= 8 m, Tp= 17 s, Dir= 202,5 °N).....	116
Figure 5.24, Madeira Island, from Ponta do Pargo to Lugar de Baixo, <i>HSmap</i> and <i>HSweb</i> , simulation 9 (Hs= 8 m, Tp= 17 s, Dir= 202,5 °N).....	118
Figure 5.25, Madeira Island, <i>HSscatter</i> and <i>HSmap</i> , simulation 9 (Hs= 8 m, Tp= 17 s, Dir= 202,5 °N): a) Calheta; b) Lugar de Baixo.....	119

8 LIST OF TABLES

Table 2.1, Hindcast data (Dir, Tp, Hs) available at 3-hours intervals, North point.....	8
Table 2.2, Hs versus Dir, North West point.	12
Table 2.3, wave count in Tp classes, North West point.	14
Table 3.1, % of data per each direction, North West point.	32
Table 3.2, Maximum Hs values for every year from 1979 to 2022, North West point.	39
Table 3.3, yearly maximum values arranged in descending order, with their respective order number "i"	40
Table 3.4, Gumbel and Weibull parameters obtained using MLE and MM	40
Table 3.5, CDF used with relative parameters and equation to calculate the Hs values corresponding to a given Return Period.....	43
Table 3.6, Hs values corresponding to return periods of 10, 20, 50, and 100 years, calculated using the Gumbel distribution, with parameters determined using MLE method.	43
Table 3.7, Hs values corresponding to 1, 5, 10, 50 and 100 years of Return Period reported on MetoceanView website.	44
Table 4.1 direction distribution, North West point.....	50
Table 4.2, direction distribution, South West point.....	51
Table 4.3 Hs for 10,20, 50 and 100 years of return period, North West point	51
Table 4.4, Hs for 10,20, 50 and 100 years of return period, South West point	51
Table 4.5, Hs for 10,20, 50 and 100 years of return period, South point.	52
Table 4.6, direction distribution, South point.....	53
Table 4.7, Hs for 10, 20, 50 and 100 years of return period, obtained from extreme values analyse using only waves coming from 4 to 12 direction.....	53
Table 4.8, simulation with respective Hs, Tp and Dir	54
Table 4.9, Hs for every simulation in each of the monitoring points	59
Table 4.10, simulations 1 and 2.....	61
Table 4.11, simulations 3.....	68
Table 4.12, Hs with no tide and tide of 2,6m tide, simulations 4 and 9.	87

9 BIBLIOGRAPHY

Acquaveo. (s.d.). Tratto da Acquaveo - Water Resources Software & Engineering Services

Acquaveo. *STWAVE: Steady-State Spectral Wavv Model User's Manual for STWAVE, version 6.0.*

delf hydraulics, W. (2007). *estudo do clima de agitacao maritima ao longo da costa sudoeste da Madeira.*

Gridded Bathymetry data. (s.d.). Tratto da GEBCO data download

Hidrografico, I. (s.d.). *Instituto Hidrografico.* Tratto da https://loja.hidrografico.pt/In/web/wp-content/uploads/2022/08/TabMares_I_2023.pdf

Holthuijsen, L. (2007). *Waves in Oceanic and Coastal Waters.* Delf: Delf University of Tecnology and UNESCO-IHE.

MetoceanView. (s.d.). Tratto da MetOceanView.

MetOceanView. (s.d.). Tratto da Metoceanview: MetOcean Solutions

MetOceanView. (2023). *Hs verification metrics against satellite estimates from 1991-2017.*

Rita Esteves, J. P. *ANÁLISE CLIMATOLÓGICA DA AGITAÇÃO MARÍTIMA.* Lisbon: Instituto Hidrographico.

Rstudio. (s.d.). Tratto da Rstudio: <https://www.rstudio.com/>

Venturi, J. (2023). *On the influence of the bathymetry on wave propagation.*

WindRoses PRO . (s.d.). Tratto da Windroses PRO: Enviroware - WindRose PRO3

Y.Goda. (2000). *Random seas and design of maritime structures.* Yokohama National University.